The copyright of this thesis vests in the author. No quotation from it or information derived from it is to be published without full acknowledgement of the source. The thesis is to be used for private study or non-commercial research purposes only.

Published by the University of Cape Town (UCT) in terms of the non-exclusive license granted to UCT by the author.

University of Cape Town

Quality Control of Astronomical CCD Observations

Thapelo Obed Tshenye, Bsc(Hons), University of Cape Town

Supervised by :

Dr. P. A. Woudt,
University of Cape Town
and
Dr. L. A. Balona,
South African Astonomical Observatory

University of Cape Town

May 2007

Submitted to the University of Cape Town in partial fulfilment for the degree of Master of Science in Astrophysics and Space Science.

Acknowledgements

I would like to thank both my supervisors Dr. Luis Balona at South African Astronomical Observatory (SAAO) and Dr. Patrick Woudt at the University of Cape Town (UCT) for the time they have dedicated on helping me through this project. For the many times I had to walk into their offices without appointments and they listened and offered me help all the time. I am grateful to Dr. Balona, for seeing me through the project, his patience and for the many times he had to read and correct my mistakes sometimes more than once. I would like to thank Dave Carter (SAAO) for the help he offered me during the early stage of the project. I would also like to thank Assoc. Prof. Bruce Bassett (University of Portsmouth) for the helpful comments and the suggestions. I am also grateful to the SAAO for allowing me to use their facilities.

Ke leboga batsadi ba ka Matlhodi le Chimane, bonnake Tumelo, Tshepang le Dineo le kgaitsadi wa ka Manare, gore ba bo ba nnile le tshepo, le tshegetso, le tshusumetso e ntsi mo goreng ke digele dithutong tsa ka. Ke sa lebale go leboga Borra-Tshenye le Borra-Kgosiemang. Modimo le Badimo ba me go ntshireletsa go fitlha janonng.

I would also love to thank Zingisa Hobo for everything that she has done for me (I will always love you).

I would like to thank all my friends Lesego Moitsheki, Keobakile Sedupane, Olebogeng Ramatlhodi, Malete Diale, the late Zacharia Mhlophe, bo-Sere, Rre Makinta and those that I did not mention for cheering me up every time I was down and for the positive influences.

I acknowledge the bursaries from UCT Council, Daimler-Benz, K. W. Johnston, Ford Foundation, NRF grant-holder, National Astrophysics and Space Science Programme (NASSP). The staff at the Postgraduate Funding Office (PGFO) for being helpful at all times.

University of Cape Town

Abstract

The Southern African Large Telescope (SALT) has recently been completed and is currently in the instrumentation commissioning phase. One of the things that must be ensured is that the imaging data that come from SALT are within specifications and that any faults are picked up as soon as possible. To do this, a procedure must be instituted every night (or even several times a night) to check the performance of the detector, Charge Coupled Device (CCD) cameras. A key design requirement is that we need to monitor the bias during the night. This allows us to quantify the change in the signal due to the CCD itself. Finally, a quick reduction process must be made to check if the signal-to-noise ratio of a given observation is within specification.

In this thesis a review of CCDs and their characteristics, the SALT Imaging Camera (SALTICAM), Flexible Image Transport System (FITS) and photometry is provided. Bias frames were obtained for several days using SALTICAM at Sutherland, using three binning factors (i.e. the unbinned (1×1), and binnings of 4×4 and 9×9 pixels). The variations of the intensity of the overscan and the bias regions as a function of time were determined from these bias frames. The variations were correlated with the CCD temperatures and a pattern in the bias was determined. The effect of aperture size on photometry was checked using the IRAF/DAOPHOT package on the artificial frames. The fiducial magnitude of artificial stars was compared with magnitude determined from aperture photometry and profile-fitting.

University of Cape Town

Contents

Acknowledgements i

Abstract ii

Table of Contents iii

List of Figures vi

List of Tables x

1 Introduction 1

I Background 3

2 Charge Coupled Device (CCD) 4

2.1 Introduction . . . 4

2.1.1 Operation of CCDs . . . 5

2.2 Bias Level . . . 5

2.2.1 Overscan and Prescan . . . 6

2.2.2 Bias frame . . . 6

2.2.3 Bias-corrected frame . . . 6

2.3 Dark Current . . . 7

2.3.1 Master Dark Frame . . . 8

2.3.2 Dark Current Noise Contributions . . . 9

2.3.3 Dark current subtraction . . . 10

2.4 Flat Fields . . . 10

2.4.1 Types of Flat Fields . . . 11

2.4.2 Flat fielding . . . 12

2.5 Readout noise and the Gain . . . 12

2.5.1 Readout Noise . . . 12

2.5.2 CCD Gain . . . 13

University of Cape Town

3 SALTICAM **15**
3.1 Introduction 15
3.2 SALTICAM Software Overview 16
3.3 SALTICAM Modes 18
3.4 SALTICAM Readout Speeds and Gain Settings 19

4 The Flexible Image Transport System **20**
4.1 Introduction 20
4.2 Primary Header Records 21
4.3 Extension Header Records 23
4.4 The Image Data Model 24
4.4.1 Binning 27
4.4.2 Deriving the Transformation Coefficients 28

5 Photometry **29**
5.1 Introduction 29
5.2 Aperture Photometry 30
5.3 Photometric errors 31
5.4 The Point Spread Function 32
5.4.1 Photometry using the PSF 32
5.5 Profile Fitting programs 34
5.5.1 DoPhot 34
5.5.2 The Image Reduction and Analysis Facility (IRAF) 37
5.5.3 Other IRAF packages 39
5.5.4 DAOPHOT 40
5.5.5 Using DAOPHOT on SALTICAM Data 41

II Tests and Applications **43**

6 Characterisation of the SALTICAM CCD Bias **44**
6.1 Introduction 44
6.2 The Intensity of the Bias Frame as a Function of Time 45
6.2.1 Windows Created on the Bias Frame 45
6.2.2 Results and Discussion 46
6.3 CCD Temperatures as a Function of Time 49
6.4 Correlation of Bias Level with Temperature 52
6.4.1 Results and Discussion 54
6.5 Investigation of bias variation in individual CCD Channels 58
6.5.1 Results using a 1×1 binning 58
6.5.2 Results and Discussion 59
6.5.3 Results using a 4×4 Binning Factor 66
6.5.4 Results and Discussion 66

University of Cape Town

6.5.5 Results using a 9 × 9 Binning Factor 69
6.5.6 Analysis of contribution of the bias 71
6.6 Conclusion 72

7 The Effect of Aperture Size on Photometry **75**
7.1 Introduction 75
7.2 Results and Discussions 77
7.2.1 Aperture Magnitude vs True magnitude 77
7.2.2 Aperture Magnitude vs Profile Fitting Magnitude 81
7.2.3 Comparing the Profile Fitting and the True magnitude 85
7.2.4 The Error Associated with Magnitude Measurement 86
7.3 Conclusion 88

Conclusion and Recommendations **88**

Appendices **90**

A Calculating the Readout Noise and the Gain of SALTICAM **91**

B The Least Squares Method **94**

C Examples of Coordinates Transformation **97**

D Example of FITS Primary and Extension Data Header **101**

E MatLab code for binning data **103**

F FORTRAN Code for calculating magnitude differences **106**

Bibliography **110**

University of Cape Town

List of Figures

3.1 The SALTICAM optics layout (O' Donoghue 2000). The CCDs are at the lower right. Light emerges from the exit pupil via the fold mirror to SALTICAM. If the fold mirror is out of the beam, light will go straight to PFIS. 16

3.2 A screenshot of the 'Man-Machine Interface'. This diagram shows the interface software used for operating SALTICAM. 17

3.3 A screenshot of the SALTICAM interface that is displayed on a large monitor. It displays an image of the part of the sky at which the telescope is pointing. The buttons at the bottom of the window are clickable to change the scale of the image, to allow zooming, for creating windows on the image, etc. 18

6.1 A schematic diagram showing the SALTICAM CCDs. The labels A,B,C and D show the amplifier in each channel and the arrows show the readout direction of each amplifier. The prescan regions are clearly identified. 46

6.2 Mean bias level (ADU counts) plotted against time (UT). The biases measured from the image region and the prescan region of the CCDs are shown in the left and right panels respectively. The readout speed of the camera was set to **fast readout mode**. The error bars shown are 100σ error bars to ensure visibility. 47

6.3 Mean bias level (ADU counts) plotted against time (UT). The biases measured from the image region and the prescan region of the CCDs are shown on the left and right panels respectively. The readout speed of the camera was set to **slow readout mode**. The error bars shown are 100σ error bars to ensure visibility. 48

6.4 Plots of the temperature of the SDSU, Cold Box (both in degrees Celsius), Cold End and CCD (both in Kelvin) (from the top panel to the bottom panel as shown in the figure) against time (UT). These data were obtained at the same time as data of the bias level. **Fast readout mode** was used. 50

University of Cape Town

6.5 Plots of the temperature of the the SDSU, Cold Box (both in degrees Celsius), Cold End and CCD (both in Kelvin)(from the top panel to the bottom panel as shown in the figure) against time (UT). These data were obtained at the same time as data of the bias level. **Slow readout mode** was used. 51
6.6 The top panel shows the time-dependence of the SDSU temperature (Celsius) while the bottom panel shows the time-dependence of the bias level (ADU counts). This is for **fast readout mode**. Note the similarity in the shape of both curves indicating the strong correlation between the bias level and the temperature. 52
6.7 The top panel shows the time-dependence of the SDSU temperature (Celsius) while the bottom panel shows the time-dependence of the bias level (ADU counts). This is for **slow readout mode**. Note the similarity in the shape of both curves indicating the strong correlation between the bias level and the temperature. 53
6.8 The bias level plotted against the SDSU temperature for the **fast readout mode**. The best linear fit to the data of the declining temperature. The values of the coefficients are shown in Table 6.3 54
6.9 The bias level plotted against the SDSU temperature for the **fast readout mode**. The best cubic fit to the data of the increasing temperature. The values of the coefficients are shown in Table 6.3 55
6.10 The bias level plotted against the SDSU temperature for the **slow readout mode**. The plot shows three different cases of the temperature represented by different points. The line (marked by A) represents the best fit to the data of the initial rapid decline in temperature. The values of the coefficients are shown in Table 6.4 56
6.11 The plots show a zoom in section in Figure 6.10. The lines (marked by B and C) represent the best fit to the data, where B is for the gradually declining temperature and C is for the increasing temperature. The values of the coefficients are shown in Table 6.4 57
6.12 The difference in the mean bias level measured in the prescan and image regions (ADU counts) plotted against time (UT) for the first and the second channels of the **first CCD** (channel 1 and 2), respectively, for **fast readout mode**. The numbers 1, 2, 3 and 4 indicate the windows created in each individual image and the prescan region of the CCD (see Table 6.5). The error bars shown are 100σ error bars to ensure visibility. 60

University of Cape Town

6.13 The difference in the mean bias level measured in the prescan and image regions (ADU counts) plotted against time (UT) for the first and the second channels of the **second CCD** (channel 3 and 4), respectively, for **fast readout mode**. The numbers 1, 2, 3 and 4 indicate the windows created in each individual image and the prescan region of the CCD (see Table 6.5). The error bars shown are 100σ error bars to ensure visibility. 61
6.14 The difference in the mean bias level measured in the prescan and image regions (ADU counts) plotted against time (UT) for the first and the second channels of the **first CCD** (channel 1 and 2), respectively, for **slow readout mode**. The numbers 1, 2, 3 and 4 indicate the windows created in each individual image and the prescan region of the CCD (see Table 6.5). The error bars shown are 100σ error bars to ensure visibility. 62
6.15 The difference in the mean bias level measured in the prescan and image regions (ADU counts) plotted against time (UT) for the first and the second channels of the **second CCD** (channel 3 and 4), respectively, for the **slow readout mode**. The numbers 1, 2, 3 and 4 indicate the windows created in each individual image and the prescan region of the CCD (see Table 6.5). The error bars shown are 100σ error bars to ensure visibility. 63
6.16 Plots of the mean bias level difference (in Figures 6.12 to 6.15) averaged over the four windows created in every channel of the four frames (y-axis) plotted against the window number (x-axis). These plots show that there is a spatial variation of bias level difference (image − prescan) from top to bottom in each channels (i.e. from windows 1 to 4, corresponding to measured y-position on the CCD). 65
6.17 Plots of the mean bias level differences averaged over the four windows created in every channel of the four frames (y-axis) plotted against the window number (x-axis). These plots show that there is a spatial variation of bias level difference (image − prescan) from top to bottom in each channel (i.e. from windows 1 to 4, corresponding to y-position on the CCD). 68
6.18 Plots of the mean bias level difference averaged over the four windows created in every channel of the four frames (y-axis) plotted against the window number (x-axis). These plots show that there is a spatial variation of the bias level difference (image − prescan) from top to bottom in each channel (i.e. from windows 1 to 4, corresponding to y-position on the CCD). 70

University of Cape Town

6.19 The spatial variation along the first readout section (A, i.e. channel 1) of the first CCD for different binning factors (top: 1 × 1, middle: 4 × 4, bottom: 9 × 9). For each binning the difference (shown by filled squares) and the individual values (image region: filled circles, overscan image: crosses) were plotted against position on the CCD. These plots are for the **fast readout mode**. 73
6.20 The spatial variation along the first readout section (A, i.e channel 1) of the first CCD for different binning factors (top: 1 × 1, middle: 4 × 4, bottom: 9 × 9). For each binning the difference (shown by filled squares) and the individual values (image region: filled circles, overscan image: crosses) were plotted against position on the CCD. These plots are for the **slow readout mode**. 74

7.1 This is an artificial SALTICAM image generated using a program developed by Dr. L.A. Balona. This frame shows all the stars that were used in the experiments performed in this chapter 76
7.2 These plots show the curves of growth(aperture-correction) for channels 2 (bottom panel) and channel 3 (top panel). 78
7.3 These plots show the deviation of the measured magnitude from the true magnitude in channels two (left panel) and three (right panel). . 79
7.4 The difference of the averaged-aperture magnitudes and the 'true' magnitude as a function of brightness of the star. Significant deviations occur for faint stars. 81
7.5 These plots show the deviation of the aperture magnitude from the profile fitting magnitude in channels two and three respectively. . . . 83
7.6 The difference of the averaged-aperture magnitude and the 'psf-fitted' magnitude as a function of brightness of the star. A much better agreement is found over all brightnesses compared to Figure 7.4. . . . 85

A.1 The mean bias level is plotted against the variance. A first order polynomial is fitted to the data to obtain the slope of the curve. . . . 92

C.1 Mosiac of 4k×4k with two 2k×4k CCDs, with each CCD having two amplifiers. 98
C.2 A region of interest (ROI) is specified in the CCD. 99

University of Cape Town

List of Tables

3.1 The gain setting and the resultant readout noise of different SALTICAM readout speeds. 19

6.1 The coordinates (X_1, Y_1) and (X_2, Y_2) of diagonally opposite corners of windows created on the prescan region of the bias frame in 1×1 binning mode. 45
6.2 The coordinates (X_1, Y_1) and (X_2, Y_2) of diagonally opposite corners of windows created on the image region of the bias frame in 1×1 binning mode. 46
6.3 The values of the coefficients and the Norm of residuals of the best fit to the data (**Fast readout mode**). 56
6.4 The values of the the coefficients and the Norm of residuals of the best fit to the plots A,B and C (**Slow readout mode**). 57
6.5 Coordinates (X_1, Y_1) and (X_2, Y_2) of diagonally opposite corners of the windows created on both the image and prescan regions of the CCD. 59
6.6 Coordinates $(X_1, Y1)$ and (X_2, Y_2) of diagonally opposite corners of the windows created on both the image and prescan regions of the CCD. 66
6.7 Coordinates of diagonally opposite corners of the windows created on both the image and prescan regions of the CCD using 9×9 binning. . 69
6.8 The offset of the averaged bias difference (averaged per channel) between the slow and fast readout modes (slow - fast) for different binning factors. 72

7.1 The parameters used to generate the image that was used for this work. 77
7.2 The measured magnitudes of stars in channel two and a row containing the true magnitudes of these stars. All magnitudes are calculated relative to the brightest star in channel 2, Star 2. 80
7.3 The measured magnitudes of stars in channel three and a row containing the true magnitudes of these stars. All magnitudes are calculated relative to the brightest star in channel 2, Star 2. 80
7.4 The magnitude difference between the aperture-corrected magnitude and the true magnitude of the star in channel two (i.e. the true magnitude is subtracted from the measured magnitude). 82

University of Cape Town

7.5 The magnitude difference between the aperture-corrected magnitude and the true magnitude of the star in channel three (i.e. the true magnitude is subtracted from the measured magnitude). 82
7.6 This table shows the values of the difference between the aperture magnitudes and the profile fitting magnitudes of the stars in channel two (i.e. the profile magnitude is subtracted from the measured magnitude). 84
7.7 This table shows the values of the difference between the aperture magnitudes and the profile fitting magnitudes of the stars in channel three (i.e. the profile magnitude is subtracted from the measured magnitude). 84
7.8 The difference between the profile and the true magnitudes of the stars in channel two. 86
7.9 The difference between the profile and the true magnitudes of the stars in channel three. 86
7.10 This table shows the values of the magnitude errors of the stars in channel two. All the errors are calculated relative to the bright star. . 87
7.11 This table shows the values of the magnitude errors of the stars in channel three. All the errors are calculated relative to the bright star. 87

A.1 The values of the coordinates of the points where we measured the mean and the standard deviation on the difference image. 91
A.2 The values of the measured mean counts and the variance at those points on the difference image. 92
A.3 The values of the coefficient of the polynomial fitted to the data plotted above in Figure A.1. 93

University of Cape Town

Chapter 1

Introduction

University of Cape Town

This thesis is divided into two parts. The first part, Part I, presents the background needed for this work while the second part, Part II, presents the tests and applications to both the real SALT data and simulated data.

- **Part I**
  This part consists of four chapters:
  - Chapter 2
    Provides an introduction to Charge Coupled Devices (CCDs) and their characteristics. This introduction to CCDs explains how CCDs are read out, the calibration of the bias level, dark current and the use of the flat fields. The readout noise and the gain of the CCD are also explained.
  - Chapter 3
    Gives a detailed description of the SALTICAM camera and an overview of the software that is employed to operate the SALTICAM camera.
  - Chapter 4
    Provides a general description of the Flexible Image Transport System (FITS) and a discussion of the image extension. CCD coordinate transformations are also presented in this chapter.
  - Chapter 5
    Discusses photometry in general and some photometric packages that have been developed over the years, including the IRAF[1]/SALT software package for reduction of the SALT photometric data.

[1]IRAF is the Image Reduction and Analysis Facility, a general purpose software system for the reduction and analysis of astronomical data. For more information visit the IRAF website http://iraf.noao.edu/

- **Part II**

  The second part of the thesis presents original work undertaken for this thesis. Conclusions and recommendations are also presented at the end of this part.

  - Chapter 6
    Deals with tests that were performed on the SALTICAM CCDs, the method that was used to obtain the data and the results that were obtained.
  - Chapter 7
    Presents results of stellar photometric analysis (aperture versus psf-fitted) using an artificially generated sparse stellar field.

University of Cape Town

Part I

Background

University of Cape Town

Chapter 2

Charge Coupled Device (CCD)

2.1 Introduction

In this chapter, a discussion of the Charge Coupled Device (CCD) in general and of the practical issues that must be dealt with when observing with CCDs (see McLean 1989 and Howell 2000) are presented. In the late 1960s, the CCD was developed as a memory device for storing data. It was only later that the CCD's capabilities as a light detector were discovered. The CCD is an array of coupled capacitors, which is used to store charge. The charge is generated by the photoelectric effect and can be transferred to neighbouring capacitors.

The CCD is constructed on a silicon wafer. Silicon is a semi-conductor with a valence band and a conduction band. An electron can move from the valence band to the conduction band leaving a hole (an unoccupied site) in the valence band. This silicon wafer has a large numbers of tiny light sensitive squares each surrounded by a non-conducting boundary, thus forming a large number of tiny potential wells (photosites), each corresponding to a pixel in the final image. The sensitivity of a CCD is wavelength-dependent, e.g. longer wavelength photons, ~700 nanometers (nm), penetrate deeper into the silicon wafer compared to shorter wavelength photons, (~400 nm). This led to the development of different types of CCDs such as the back-illuminated and the front-illuminated CCD. The back-illuminated CCD has better sensitivity at shorter wavelengths than the front-illuminated CCD and vice versa. In the front-illuminated CCD, photons are absorbed in the top layer of the wafer, while in the back-illuminated CCD photons are absorbed primarily in the bottom layer, as the name suggests.

The popularity of the CCD is due in part to its superior quantum efficiency (the effectiveness of the detector in converting the incident photons into charge) and better linearity of the response of the detector to light when compared with traditional photographic plates. CCDs also have better quantum efficiency when compared with

University of Cape Town

photomultiplier tubes. Further advantages over traditional detectors are the ability to record two-dimensional images, to integrate for long exposure times and a larger dynamical range (the ratio of the maximum to minimum detectable light intensity). All of these factors make the CCD a better detector than the photographic plate and the photomultiplier tube. However, for scientific purposes CCDs have to be cooled to very low temperatures, ~140 K. This reduces the thermal motion of electrons in the CCD and hence the electronic noise, allowing for high precision measurements.

2.1.1 Operation of CCDs

When taking an exposure of a star for example, photons from the star strike the silicon wafer on the CCD detector as previously described. These photons eject electrons from the valence band into the conduction band and are stored in the photosites. After an exposure, these electrons have to be transferred to the readout devices. This is achieved by a process called clocking in which the voltage on the photosite is reduced and the voltage on the adjacent photosite is increased so that the electrons can be transferred to the neighbouring photosite.

As these electrons are shifted down the columns, they reach the bottom of the array. At the bottom of the array there is another row of photosites called the serial register which is connected to the readout devices (i.e. the amplifier and the analogue-to-digital (A/D) converter). As electrons enter the serial register, the same clocking process is used again to shift the electrons along the serial register onto the on-chip amplifier. The on-chip amplifier amplifies the signal which is then digitized in the A/D converter and stored in the computer. The next row now enters the serial register and is transferred to the readout devices in the same way. This process of shifting the electrons down the columns and along the serial register is repeated until all the photosites are read out and data transfer is complete.

2.2 Bias Level

When a photon strikes the silicon wafer, it knocks an electron from the valence band into the conduction band as explained previously. When this electron leaves the valence band it creates an electron-hole pair. To prevent this pair from recombining in a short space of time, a voltage is applied to the electrode structure attached to the silicon, creating a potential well for the electron to fall into. Applying this voltage to the chip will fill the photosite with electrons, even if no light is present (McLean 1989). The number of these electrons does not increase with time.

Since the A/D converter can only deal with positive values, applying an offset value helps to avoid negative numbers in the output signal. This additive value represents the zero level in the counts. CCD electronics are set to provide a positive offset value for each image that is obtained, by using an overscan region located on one

University of Cape Town

side of the CCD imaging region (Howell 2000). This offset value is called the bias level or overscan level. The bias level should not change with time provided the electronics remains unchanged. However, variations in the CCD temperature can cause variations in the bias level.

2.2.1 Overscan and Prescan

The bias region mentioned above can either be an overscan region or a prescan region. An overscan region is generated at the end of readout of a row of pixels. On the other hand, a prescan region is generated before the readout of a row. The overscan/prescan region is not a physical region on the CCD chip. No pixels are present in these regions; instead the overscan/prescan levels are generated by the electronics. Sending additional clock cycles to the electronics (e.g. 522×522 instead of 512×512) will create these pseudo pixels (see Howell 2000). The resulting image will consist of a row of pseudo pixels adjacent to the real image, forming a region called the overscan (or prescan) region which shows how the bias level varies from row to row.

2.2.2 Bias frame

A bias frame is a zero-second exposure frame that is taken with the shutter of the camera closed, in which the resulting frame simply contains the bias level. The distribution of counts in the frame will centre on the mean bias level and will have a spread depending on the readout noise. The readout noise is produced specifically by the on-chip amplifier in a properly operating system. Averaging several consecutive bias frames one can obtain a good bias frame.

2.2.3 Bias-corrected frame

When taking an exposure of a star for a certain exposure time, the resulting frame (let us call this frame the astronomical frame) will contain the star light, bias level and some other noise (e.g. the readout noise, the photon noise, the thermal noise and the shot noise) at readout time. In order to isolate the star light one has to remove all the other effects of the CCD, the bias level being one of those effects. This bias level can be obtained by computing the average of the pixels for a row in the overscan region. However, this bias level will be for that particular row. The bias level may vary with row number in the CCD array. This can be seen by plotting the mean bias level for the row as a function of row number. To obtain the best estimate of the bias at a given row, one fits a low-order polynomial to the mean bias level plotted against row number. The bias at a given row, as obtained from the fit is then subtracted from the astronomical frame to remove the bias level at that row.

In a perfect CCD, removing the bias level using the overscan (or prescan) region in the way described above should remove the bias from the entire frame. However,

University of Cape Town

because of imperfect electronics, there may be some residual pattern in the bias-subtracted frame. We can test this by using the overscan (or prescan) region to remove the bias in the bias exposure. The resulting frame should be flat and have zero mean. If not, the overscan-corrected bias frame needs to be subtracted from astronomical frames. To obtain a good estimate of the pattern it is important to average a large number of bias frames to obtain a master bias frame which can be used to correct for this effect.

2.3 Dark Current

Thermal excitation within the silicon wafer on the CCD causes electrons to be ejected from the valence band to the conduction band. These electrons are collected in the photosites, and they are counted as part of the signal. The offset caused by these electrons on the signal is called the dark current. A frame taken with the shutter closed for a certain exposure time at a specific temperature called the dark frame, is used to remove these dark current electrons from the astronomical frame. Ideally, a dark frame has to be taken at the same temperature and the same exposure time as the astronomical frame. The statistical fluctuations in the dark frame are known as dark current noise. Dark current in a CCD can be represented with this expression (McLean 1989) :

$$D = C\,T^{1.5}\,e^{-E_g/(2kT)}, \tag{2.1}$$

where k is the Boltzmann constant, T is the operating temperature of the CCD, E_g is the silicon gap energy, C is a constant and it can be evaluated at room temperature $T_0 = 300$ K. The constant, C, is given by

$$C = \frac{I_0\,P_s}{q\,T_0^{1.5}\,e^{-E_g/(2kT_0)}},$$

and E_g varies with the operating temperature of the CCD, is given by

$$E_g = 1.1557 - \frac{7.021 \times 10^{-4} T^2}{1108 + T}.$$

Substituting C and the value of the gap energy E_g we get

$$D = \frac{1}{q} I_0 P_s e^{-(T_0 - T)/9.96}, \tag{2.2}$$

where D is the dark current given in electrons per pixel per second, I_0 is the dark current at room temperature T_0, T is the operating temperature of the CCD, P_s is the pixel size and q is the charge on the electron. Dark current falls to about one-third of its previous value each time the temperature is reduced by 10 degrees Celsius, since dark current strongly depends on the temperature. Thus, it is important to cool the

University of Cape Town

CCD down to a very low temperature to reduce dark current. This was particularly true in the earlier generations of CCDs (in the 1980s). For more recent CCDs, the dark current is negligible thanks to better quality control of the silicon substrate, and improvements in the manufacturing process, so it is not even important to subtract the dark frame from the astronomical frame. The dark frame consists of bias noise and the thermal noise, this means that we have to subtract the bias level from the dark frame.

2.3.1 Master Dark Frame

Since fluctuations in a single dark frame are large, it is important to use several dark frames to subtract the dark current in an astronomical frame. A dark frame with high signal-to-noise ratio is created by averaging several consecutive dark frames with the same exposure time. The resulting frame with high signal-to-noise ratio is called the master dark frame. The expression representing a typical dark frame exposure is (see Corlan 2004) :

$$d(x,y) = B(x,y) + t_{dark}D(x,y) + noise, \tag{2.3}$$

where $d(x,y)$ is the dark frame, $B(x,y)$ is the bias offset and $D(x,y)$ is the dark current over time t_{dark}. If the dark current contribution is not very large, the *noise* term in Equation 2.3 will be equal to the readout noise of the CCD. Subtracting the bias level from the dark frame and dividing by the exposure time to get the estimate of dark current in the detector

$$D(x,y) = \frac{d(x,y) - B(x,y)}{t_{dark}}.$$

Averaging several (M) dark frames to create the master dark frame with high signal-to-noise ratio will reduce the noise.

$$\widetilde{D}(x,y) = \frac{1}{t_{dark}}\frac{1}{M}\sum_i d_i(x,y) - \tilde{B}(x,y),$$

where M is the number of bias-subtracted dark frames and

$$\tilde{B}(x,y) = \frac{1}{N}\sum_i b_i(x,y),$$

where N is the number of bias frames, therefore

$$\widetilde{D'}(x,y) = t_{dark}\widetilde{D}(x,y) = \frac{1}{M}\sum_i d_i(x,y) - \tilde{B}(x,y). \tag{2.4}$$

This is the expression representing the bias-subtracted master dark frame. If the bias offset is not removed from the dark frame the equation of master dark frame will become

$$\widetilde{D'}(x,y) = t_{dark}\widetilde{D}(x,y) = \frac{1}{M}\sum_i d_i(x,y). \tag{2.5}$$

University of Cape Town

2.3.2 Dark Current Noise Contributions

The amount of noise in a dark frame is random, but, not quite repeatable. If the noise is repeatable it is expected that the same amount of noise is obtained if the exposure is repeated under the same circumstances (i.e. temperature and time). The dark current noise follows Poisson statistics, so the root-mean-square (σ_d) of the dark current is the square root of the dark current (D),

$$\sigma_d = \sqrt{D} \tag{2.6}$$

The noise sources in CCDs add in quadrature (i.e. the square root of the sum of the squares). The subscript $_e$ in the following expression is just to show that the noise is measured in electrons. The resulting noise is given by the following expression (see Gudehus and Hegyi 1985)

$$\sigma_{D_e}^2 = \sigma_{R_e}^2 + \sigma_{d_e}^2 + \sigma_{S_e}^2,$$

where σ_{D_e} is the total noise in electrons, σ_R is the readout noise, σ_S is the shot noise in electrons and σ_d is the dark current signal-dependent noise given by Equation 2.6, all measured in electrons. Substituting the value of σ_d in the above equation we get

$$\sigma_{D_e}^2 = \sigma_{R_e}^2 + D_e + \sigma_{S_e}^2.$$

If the gain, λ, is in electrons/ADU (refer to Section 2.5.2), $\sigma_{D_{ADU}}^2$ is multiplied by λ^2 to convert $\sigma_{D_e}^2$ into ADU, and to get

$$\lambda^2\sigma_{D_{ADU}}^2 = \sigma_{R_e}^2 + D_e + \sigma_{S_e}^2.$$

But, $D_e = \lambda S_{d_{ADU}}$ so that

$$\sigma_{D_{ADU}}^2 = \frac{\sigma_{R_e}^2}{\lambda^2} + \frac{\lambda S_{d_{ADU}}}{\lambda^2} + \frac{\sigma_{S_e}^2}{\lambda^2},$$

where $S_{d_{ADU}}$ is the signal of the dark noise in ADUs. Therefore,

$$\sigma_{D_{ADU}}^2 = \frac{\sigma_{R_e}^2}{\lambda^2} + \frac{S_{d_{ADU}}}{\lambda} + \frac{\sigma_{S_e}^2}{\lambda^2}. \tag{2.7}$$

Keeping the gain constant, the readout noise is going to be the same for all the exposures. When observing faint stars, the dominant sources of noise in a CCD are the readout noise and the dark current noise. The dark frame is linear in time but the amount varies from pixel to pixel. If an individual pixel generates more dark current than the other pixels it is called a hot/bad pixel. Cosmic rays also contribute to the noise in the CCD. For observatories that are situated on mountain-tops, cosmic rays are seen more often than for those observatories situated at an altitude that is closer to sea level, since cosmic rays are scattered by the atmosphere.

University of Cape Town

2.3.3 Dark current subtraction

In order to perform dark current subtraction, one starts by obtaining dark frames at a certain temperature for a particular exposure time. It is important that these dark frames be obtained at the highest signal-to-noise. If a single dark frame of low binning factor (and short exposure time) is used to subtract the dark current, noise will be increased instead (by error propagation rules, see Taylor 1997). Assuming that hot/bad pixels (see discussion Section 2.2.3) do not dominate the dark current statistics, it can sometimes be useful to obtain dark frames at the highest binning (for time efficiency), because pixel binning reduces the noise level in each superpixel[1]. Under the assumption of relatively few hot/bad pixels, the average dark current should be the same for every pixel binning, since the hardware does not change, e.g. a dark frame of 9×9 binning should result in the same average dark current per pixel per unit time as a dark frame of 1×1 binning. It is important to expose the CCD chip for a substantial time, because it takes a long time for a pixel to be filled by the dark current electrons. These dark frames are averaged to create a master dark frame.

As previously explained in Section 2.2.3, one can remove the bias level in each dark frame to create bias-subtracted dark frames. These bias-subtracted dark frames will contain the dark current and noise; the latter will average out during the averaging of these frames. The dark current is determined from the average of the pixels. It is generally advisable to obtain a large number of dark frame, and then combine them to create a master dark frame that can be used to subtract the dark current.

2.4 Flat Fields

CCD pixels have non-uniform response to light because of the imperfect manufacturing of the CCD. Illuminating the CCD with uniform light will not generate an equal signal in all pixels, but it can help in calibrating the relative sensitivities of the pixels. The non-uniform image thus obtained is called the flat field and resembles the non-uniformity of the CCD. When taking flat field frames the same filter as the one that will be used during the observation of the target object should be used, since flat field effects depend on wavelength. The flat field frames can also be used to correct other effects such as vignetting (the dimming of observed objects towards the edge of the telescope field of view), small sharp in-focus features caused by dust on the CCD chip and vague ring-like shaped features that are caused by dust particles on the cryostat window. It is very difficult to obtain a good flat field. A flat field frame can be obtained using either the screen on the inside of the dome (called a dome flat) or the twilight sky (called a sky flat).

[1]Charge in adjacent pixels is combined to form a superpixel, e.g. in an $N \times M$ binning, N columns and M rows are combined to form a superpixel.

University of Cape Town

2.4.1 Types of Flat Fields

1. Dome flat

   A dome flat is obtained by using a screen on the inside of the dome. This screen is illuminated by a bright continuum source that has no emission lines. In this way, a flat field frame can be taken at any time of the day. However, a dome flat has the following disadvantages (Davenhall et al. 1999) :

   (a) the colour of the sky is not the same as the colour of the lamp used to illuminate the screen or the interior of the dome.

   (b) light reflected from the dome is incident to the telescope at an angle different to light from the sky. This can affect the vignetting and the images caused by dust particles, but it does not affect the sensitivity variation of the pixels.

2. Sky flat

   A sky flat is obtained using the twilight sky; observation of the sky flat is dependent on the weather. Using the dark sky is an alternative way, creating a superflat.

   (a) Twilight flat

   A twilight flat is obtained by taking a frame of the bright area of the evening or morning twilight sky. The sky should be brighter than any star that could be in the field of view. However, if the sky is too bright the CCD will be saturated. The telescope drive should be switched off so that the sky can move across the field of view. Any star that would fall on the CCD drifts out of the field of view and can be rejected by averaging several consecutive flat field frames; since the position of these stars in each frame will be different. Obtaining this type of flat is difficult when trying to get flats for different kinds of filters because twilight is short and it takes a fair amount of time to read out a CCD (~30 seconds for a 1024×1024 CCD).

   (b) Superflat

   In the case of bad weather at twilight, a dark sky exposure can be used to make a flat field image. Such superflats are widely used in the infrared; since at these wavelengths the sky is relatively bright. A superflat frame is obtained from an image frame that is already flat-corrected using a dome flat. From the flat-corrected image frame we choose an empty field to create a superflat. To get a good superflat at least ten astronomical frames are needed. These frames must not contain large objects, and the offset of these frames must be larger than the size of the largest object in the frames. A superflat can correct for the fringing in the image frame.

University of Cape Town

2.4.2 Flat fielding

Flat fielding is the process of correcting for the pixel-to-pixel variations and large scale effects (such as vignetting) on the astronomical frame. Flat fielding becomes more important when observing stars fainter than the sky level. It is important to choose correctly exposed flat field frames, and correct each frame for the bias offset level and trim the overscan. Flat fields have random noise fluctuations associated with them. It is important to use as many flat field frames as possible to create a master flat field frame with reduced noise level. A master flat field frame has to be created for every filter that will be used in obtaining astronomical frames.

In order to achieve the best result, the mean pixel level from the master flat field is plotted against the pixel position. This will enable us to determine if there are pixel-to-pixel variations on the master flat. If there are no pixel-to-pixel variations on the master flat frame, one can just apply it to the astronomical image (Chromey and Hasselbracher 1996). If there are pixel-to-pixel variations, however, we can fit a surface to the plot of the mean pixel level against the pixel position to get the best (normalized to 1) flat field frame that is used to correct the astronomical frame. One divides the image frame by the normalized flat field, since the flat field correction is multiplicative.

2.5 Readout noise and the Gain

2.5.1 Readout Noise

The readout noise is the number of electrons introduced per pixel into a final signal during the CCD readout. It is produced in the on-chip amplifier where the charge collected by each pixel is converted to a voltage which is subsequently presented to the A/D converter for digitisation.

Introduction of these additional electrons into the signal by the electronics causes unwanted random fluctuations, producing uncertainty in the output signal of each pixel. A CCD with a readout-noise of 30 electrons, will have a fluctuation with a standard deviation of 30 electrons about the mean value in the readout signal. As a consequence, high readout noise CCDs (more than 80–100 electrons) are not very good to use for faint sources. Modern CCDs have readout noise values that are very low, in the range of 10 electrons per pixel per frame or even less.

Calculating the Readout Noise

The readout noise of the CCD can be calculated using calibration frames. Two consecutive bias frames are needed to calculate the readout noise of the CCD. These two consecutive bias frames are subtracted from each other to remove the large-scale variations in the mean bias level caused by the faulty electronics; the expectation

University of Cape Town

is that these variations should be the same on the two frames, leaving only the fluctuations in output signal due to readout noise when they are differenced.

The standard deviation of the difference frame will be a factor of $\sqrt{2}$ higher, because the fluctuation will be a contribution of the two frames. We take the standard deviation from different spots on the difference frame and then we average. Since there was no light falling on the CCD, the averaged standard deviation of the difference frame (divided by $\sqrt{2}$) will be the readout noise. Let z be the difference frame and x and y be the two bias frames

$$z = x - y$$

The deviation in intensity found for each frame will be given by

$$dz = dx - dy.$$

Then squaring both side to get

$$(dz)^2 = (dx)^2 - 2(dx)(dy) + (dy)^2,$$

the mixed term will vanish on average because the two terms are not correlated, therefore

$$\frac{1}{N}\sum(dz)^2 = \frac{1}{N}\sum(dx)^2 + \frac{1}{N}\sum(dy)^2;$$

where N is the number of the bias frames and the variance will be given by

$$\sigma_z^2 = \sigma_x^2 + \sigma_y^2.$$

The standard deviation will be given by

$$\sigma_z = \sqrt{\sigma_x^2 + \sigma_y^2},$$

but σ_x and σ_y have to be the same (since there is no light on the CCD), so that the above equation becomes

$$\sigma_z = \sqrt{2\sigma^2},$$

or

$$\sigma = \frac{\sigma_z}{\sqrt{2}}. \tag{2.8}$$

σ is the readout noise of the CCD and the units are in ADUs.

2.5.2 CCD Gain

In the previous sections it has been described how electrons can be ejected from the valence band to the conductive band in the silicon wafer. The steps involved in reading the value of a pixel are as follows. The electrons are transferred to the amplifier (coulombs), then the voltage induced by this charge is measured. An A/D converter converts the voltage into a number that will be passed from the CCD

University of Cape Town

hardware to the computer software as a pixel value in the range $0 - 2^n$, where n is the number of bits. The unit of this pixel value is counts, also called Data Numbers (DN) or (ADUs).

The end result is that there is some value which relates the initial number of electrons in a pixel to the final number of counts that is transferred to the computer. The ratio of these two numbers is the gain of the camera. There are two ways in which the gain can be chosen :

- CCD pixels are designed to hold a certain number of electrons before they become saturated and start leaking to the neighbouring pixels. This maximum of a pixel is called the full well depth. The gain can be chosen such that the number of electrons in the full-well depth corresponds to the maximum pixel value.

- The gain can be chosen so that the smallest pixel value corresponds to roughly the readout noise of the CCD. Any finer measurement of the pixel values would yield differences, which would be essentially random.

Calculating the Gain

To calculate the gain, a number of flat field frames at different exposure times are needed. Two exposures for each specific exposure time are needed so that they can be subtracted from each other, to get rid of variations in pixel sensitivity.

The averaged standard deviation can be obtained as specified by Equation 2.8 for each difference frame. However, to get the variance, the standard deviation is squared and divided by 2.

$$\text{Variance} = \left(\frac{\sigma^2}{2}\right).$$

Using Equation 2.7 (on page 9), it can be seen that a plot of the variance, σ^2_{ADU}, versus the mean counts, $S_{d_{ADU}}$, has a slope of λ and an intercept of σ^2_{ADU}. Thus the gain, λ, may be found from the slope of this straight line of Equation 2.7 (see Appendix A on page 91 for an example of gain calculation). The intercept gives the readout noise. However, because the intercept is very sensitive to the gain that is used, it is preferable to use the method described in Section 2.5.1 rather than the value obtained by the intercept.

University of Cape Town

Chapter 3

SALTICAM

3.1 Introduction

SALTICAM (SALT imaging camera) is one of the two first-light instruments available on SALT; the other is the Prime Focus Imaging Spectrograph (PFIS), also called the Robert Stobie Spectrograph (RSS). SALTICAM can be used in the following modes :

- to display the field of view during acquisition;
- for autoguiding;
- for science exposures.

The SALTICAM camera uses a mosaic of two CCDs, each CCD has 2048 × 4102 pixels. Both these CCDs are back-illuminated for high quantum efficiency and to take advantage of the good UV (ultraviolet) sensitivity (O'Donoghue et al. 2003) down to 320 nm. Each of the two CCDs is read by two low noise output amplifiers to increase the readout speed. Each amplifier reads out 1024 × 4102 pixels and also 50 prescan pixels (i.e. prescan/overscan region). These additional 50 pixels are physically present on the detector. They are situated in the readout register following the readout amplifier and preceding the pixel corresponding to the first column of the imaging area of the CCD. Every row that is read out is preceded by the 50 pixels of the prescan. These prescan pixels are used to calibrate the bias offset (see section 2.2). The amplifiers are also capable of binning in either rows or columns or both. The purpose of prebinning is to reduce the readout noise. Prebin factors of up to 9 × 9 are possible.

SALTICAM was commissioned on SALT in 2003 September and used for the first light pictures from SALT on July 2003. It was used to obtain the first guided image of a star in autoguiding mode on December 2003. It was placed at the VI (Verification Instrument) position, where the optical axis of the instrument coincides with the

University of Cape Town

optical axis of the telescope. In its final position, SALTICAM will be placed in the so-called ACSI ("acquisition camera and science imager") position, at a Newtonian focus. Light will be directed towards SALTICAM by means of a mirror positioned at a 45° angle (O' Donoghue et al. 2003), see Figure 3.1. When the mirror is removed, light is directed to PFIS.

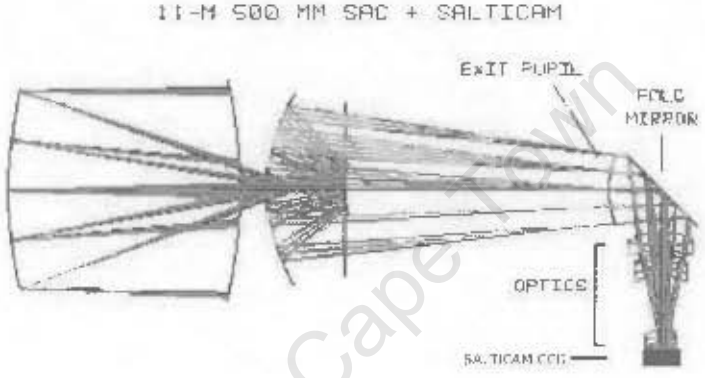

Figure 3.1: The SALTICAM optics layout (O' Donoghue 2000). The CCDs are at the lower right. Light emerges from the exit pupil via the fold mirror to SALTICAM. If the fold mirror is out of the beam, light will go straight to PFIS.

It is important that the operation of SALTICAM be monitored very carefully, with rapid reporting of faults to ensure data quality, otherwise the data obtained by SALTICAM may not be useful. For this purpose it is essential that the readout noise of the CCDs be kept within specified levels.

University of Cape Town

3.2 SALTICAM Software Overview

SALTICAM is designed to be operated remotely by the telescope control system (TCS). In this mode, the SCAM LabView (the computer program used for data acquisition and for operating SALTICAM) interface (Figure 3.2) communicates with the TCS and downloads the required settings to start an exposure. This will include the RA (right-ascension) and DEC (declination) of the target, the exposure time, the filter position, the binning factor, readout mode, etc. After an exposure, the image will be displayed on the C-code image viewer (Figure 3.3). The image can be manipulated in various ways (pan, zoom, contrast, colour, etc) and there are facilities for measuring the size of the stellar images.

The SCAM LabView interface may also be switched to "maintenance mode". In this configuration, there is no communication with the TCS. Instead, the operator

may control SALTICAM by entering information directly on the LabView interface. Each sequence of exposures comprises a "program". A program contains the exposure time and filter to be used. SALTICAM will execute each line of a program automatically and stop when the end of a program is reached. The "STOP" and "TERMINATE" buttons are used to abort the program sequence immediately or at the end of the current exposure. SALTICAM is used for two purposes:

1. As an acquisition camera
2. For science exposures

In its role as an acquisition camera, SALTICAM can take continuous exposures of the field using exposure times of one second or less. An object in the field may be dragged to a desired position on the CCD by means of the mouse. This information is converted to the telescope offsets and rotation and passed to the TCS. SCAM can also be used in autoguiding mode by selecting one or more field stars as guide stars. This may be used in conjunction with PFIS/RSS.

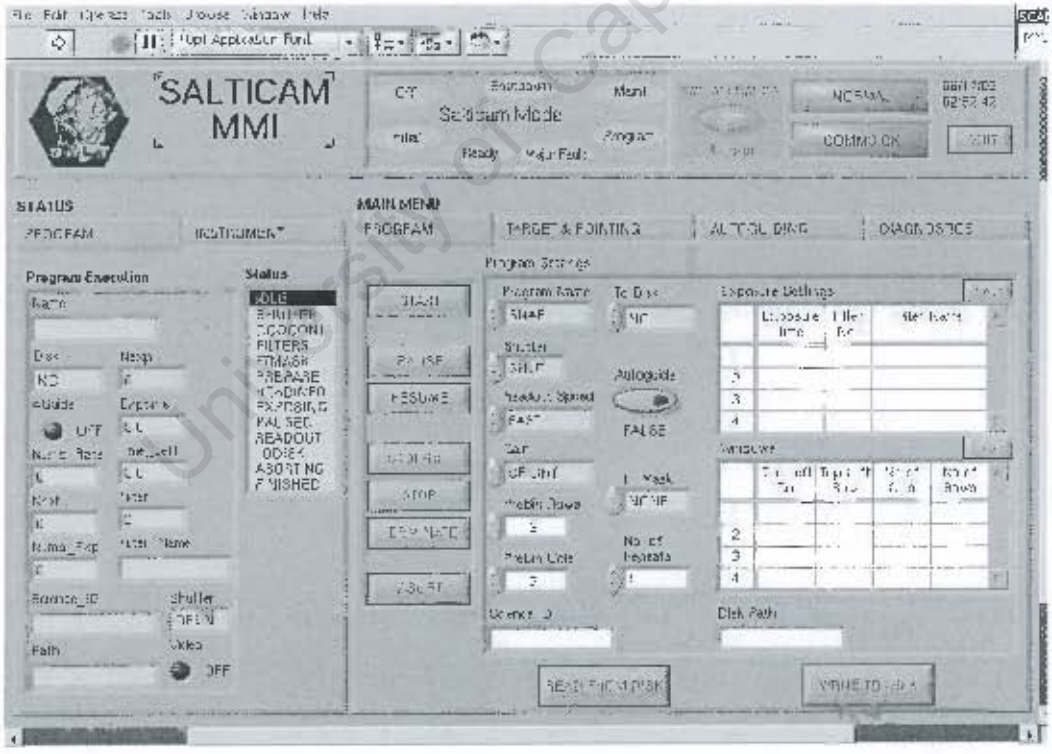

Figure 3.2: A screenshot of the 'Man-Machine Interface'. This diagram shows the interface software used for operating SALTICAM.

University of Cape Town

Figure 3.3: A screenshot of the SALTICAM interface that is displayed on a large monitor. It displays an image of the part of the sky at which the telescope is pointing. The buttons at the bottom of the window are clickable to change the scale of the image, to allow zooming, for creating windows on the image, etc.

3.3 SALTICAM Modes

In conventional operation, the SALTICAM CCDs will be read out in full-frame mode. However, "frame transfer" (FT) mode can be used to reduce the dead-time between exposures. In FT mode, one half of the CCD is used as a memory store and the other half as image store. To accomplish this, an opaque screen is used to prevent light from falling on the half of the CCD used as a memory store. After the exposure, the image data are moved very rapidly to the memory storage area where it can be read out. In this way, continuous exposures may be obtained with no dead-time between them. However, only half the field of view is accessible.

For more rapid exposures, one can use "VIDEO" mode. VIDEO mode is the same as FT mode, but the exposure time is set to the shortest possible duration. This is normally just a little larger than the time taken for readout.

For the shortest exposure times, one may use "SLOT" mode. SLOT mode is similar to FT mode except that the CCD is entirely obscured except for a narrow slot. One may position a program star and comparison star in the slot. After each exposure, the narrow strip is moved to a storage area. After many such data transfers,

University of Cape Town

the image reaches the end row and is read out. Because only a small fraction of the CCD is used for imaging, data transfer is higher and readout times are much shorter and the minimum exposure time (including disk storage time) may be as short as 0.05 seconds using 9×9 binning. More typically, one can perform continuous 0.1 second exposures with disk saves using a prebin factor of 6×6. It is expected that this unique capability of SALTICAM will enable high-speed photometry as a prime area of research using SALT.

Finally, the "DRIFT SCANNING" mode can be used to record very long strips of the sky. This is accomplished by turning off the telescope drive and matching the speed of the readout to be exactly the same as the speed at which the sky drifts across the CCD with the rotation of the earth.

3.4 SALTICAM Readout Speeds and Gain Settings

SALTICAM can perform fast or slow readouts. Fast readouts are required for high-speed photometry, field acquisition and guiding. Slow readout should be used when the readout noise is to be kept to a minimum.

For each readout speed setting (fast or slow), two possible gain settings are allowed: bright and faint. Bright gain settings are used for a high dynamical range and in a field of bright stars. On the other hand, the faint gain setting allows a more precise measure of the intensity but the brightest stars will be saturated. Typical gain settings and the resultant readout noise are as follows (see Appendix A) :

Gain Setting	Gain (electrons/ADU)	Readout noise (electrons)
BRIGHT FAST	4.1	5.0
BRIGHT SLOW	2.5	3.0
FAINT FAST	1.5	5.0
FAINT SLOW	1.0	3.0

Table 3.1: The gain setting and the resultant readout noise of different SALTICAM readout speeds.

To reduce the effects of readout noise one can use prebinning. Prebinning is important when dealing with faint objects and short exposures. SALTICAM has the ability to perform prebinning into any arbitrary $M \times N$ (where both M and N can take values from $1 - 9$) binned pixels (super-pixels) through simple software control. Because the readout noise per pixel is constant, using 4×4 prebinning will reduce the readout variance by 16 and the readout noise by 4. Hence we can detect signals in 4×4 prebinning which may be obscured by noise in 1×1 prebinning.

University of Cape Town

Chapter 4

The Flexible Image Transport System

University of Cape Town

4.1 Introduction

In this chapter the data image structure definition of the Flexible Image Transport System (FITS) is discussed. Data from different observatories may not be easily interchangeable, since every observatory may use different software for data processing. To solve this problem, FITS was developed in the late 1970s to transport astronomical data between observatories (Hanisch et al. 2001). Nowadays, astronomical software has adopted FITS for data exchange and as data format. In developing FITS some important factors were taken into consideration (Wells et al. 1981) :

- It is required to be very flexible.
- It must make it easy for images to be transported.
- It must provide a way of transporting any extra parameters that are associated with the image(s).
- There should be no limit on the amount of text that can be transported.
- The format has to be general so that information associated with the image(s) can be altered.

A basic FITS file consists of two main parts: the header section and the data section, with the logical records having a length of 23040 bits corresponding to 2880 8-bit bytes. The header forms the first part of a FITS file and it is followed by the image data. The FITS header provides a means of recording information about the object, e.g. its position in the sky, the telescope that was used for the observation, the time of observation, the filter that was used and various other essential information. A data structure in a FITS file is a combination of the Header and Data Unit (Appendix D

gives an example of a FITS Data Header). Sometimes the header and data unit (HDU) may consist of a header with no data unit. As detectors evolved, the image extension was developed to store different but related data sets when using multiple amplifiers and/or multiple CCDs. The FITS extension is just a replica of the primary HDU and has a format which must provide the following (Ponz et al. 1994):

- allow storage of unlimited data,
- allow each data section to have its own header using FITS extensions,
- FITS readers have to able to skip through extensions easily,
- require only small software changes to the FITS readers to handle image extension,
- there should be no need to adopt additional keywords (discussed below),
- it should be easy to single out an image extension as a separate file to produce a simple FITS file without extensions.

4.2 Primary Header Records

The header unit carries information about the structure of the data array, the observational parameters, etc. For easy interpretation of the header records by both man and computer, ASCII codes are used in FITS. The use of a comment is encouraged on both the standard parameter card[1] images and a comment card. No limits are placed on the number of card images that can be supplied. The end of the header records is specified by the keyword END. The basic representation of a FITS header card image (Wells et al. 1981) is given by

$$keyword = value\,/\,comment.$$

Unless specified otherwise, keywords may appear in any order. The keyword is an 8-character string using only digits and upper case alphabetic characters. The equals sign indicates the presence of the value field associated with the keyword. If the value field is undefined it will be null. The value field has two formats: fixed and free. The fixed format is needed for mandatory keywords and is recommended for any other keywords. If a comment is present, a slash is needed to separate the value field from the comment which consists of ASCII text. Fixed formats that are required are (Hanisch et al. 2001) :

- Logical variable

  It will have the value T or F appearing in column 30. These characters can be followed by spaces and a slash (which can be followed by a comment).

[1] A sequence of 80 bytes containing ASCII text, treated as a logical entity

University of Cape Town

- Integer variable

  This is for a fixed format integer value, and must appear right justified in columns $11-30$. A free format integer value, in contrast, must appear right justified in columns $11-80$.

- Real variable

  A fixed format real variable must be right justified and start in columns $11-30$. A free format real variable must start in column $11-80$ and be right justified as well.

- Character

  It is recommended to be 8 characters long even though longer strings are allowed; it is represented starting with a " ' " in column 11, and ending with a " ' " which cannot occur before column 20 and should end before or on column 80.

Mandatory keywords are required in every HDU and their value must be written in fixed format. These keywords occupy a certain fixed order in the header records, namely :

- SIMPLE Keyword

  This has a logical constant value, T, if the file conforms to the FITS basic standard or F, if it does not conform. This keyword is not permitted in the extension header.

- BITPIX keyword

  This is the number of bits used to represent each pixel value. It has an integer value, B, used for computing the size of the data in the FITS file.

- NAXIS keyword

  This is a non-negative integer value representing the number of image coordinate axes. If this value is zero there is no data following the header.

- NAXISn keyword

  This is a non-negative integer value that represents the number of pixels in the image along the n-th coordinate axis.

- END keyword

  This keyword has no value and marks the end of the FITS header.

The size of the data is then given by :

$$S = |B| \times (N_1 \times N_2 \times \ldots \times N_{NAXIS}),$$

University of Cape Town

where S is the size of the primary data array and is non-negative, B represent the value of the keyword BITPIX, and the N_n are the values of the keywords NAXISn for n=1, 2,..., NAXIS.

There are some optional parameters in FITS that are often important. For example, if one did not specify the coordinate system, the recipient will have a hard time trying to figure out if the image is flipped. Amongst others, there are the following optional parameters: OBJECT, DATE, TELESCOPE, OBSERVER, etc.

4.3 Extension Header Records

As mentioned before, the image extensions allow the storage of multiple images. The image extension begins just after the last record of the primary data array or the previous image extension. The extension header format is basically the same as the primary header format. If there are extensions, the primary header of the FITS file must have the keyword EXTENT set to T. The following keywords are mandatory in the extension header format (Ponz et al. 1994) :

- XTENSION keyword

  This keyword describes the type of the extension and must not appear in the primary header. The value field contains the character 'IMAGE'.

- BITPIX keyword

  This is the integer value used to specify how many bits are used to represent each pixel value. BITPIX can appear in both the primary header and the extension header.

- PCOUNT keyword

  This is a non-negative integer value, P, used to define the number of parameters per group in the data structure. A simple image extension shall have PCOUNT = 0.

- GCOUNT keyword

  This is a non-negative integer value, G, defining the number of groups in the data structure. A simple image extension has GCOUNT = 1.

- END keyword

  This keyword has no value associated with it.

- EXTEND keyword

  This keyword appears in the primary header after the NAXISn keyword if the FITS file contains an extension image in which case it should has the logical value, T.

University of Cape Town

To compute the data size we use the absolute value of the BITPIX, using this equation :

$$S = |B| \times G \times (P + N_1 \times N_2 \times \ldots \times N_{NAXIS})$$

where S is the extension size in bits, B is the value of the BITPIX, G is the value of the GCOUNT, then P is the value of the PCOUNT and N_n are the value of NAXISn for n=1, 2, ..., NAXIS, as defined before

4.4 The Image Data Model

In this section a brief description of the basic data structure for image data produced by a CCD is presented. For a camera consisting of a single CCD with a single amplifier, data will be recorded as a single FITS file consisting of a single ASCII header and a data array "HDU". For observations made with a CCD with multiple amplifiers, the data will be recorded in a single FITS file with multiple HDUs by using image extensions as explained previously. The primary header will be used to store the common information of all the amplifiers. The connection between the image extensions units corresponding to each amplifier is provided in two ways (Valdes 2000):

1. The primary connection occurs by giving all image units a common observation identification and appears in the keyword `OBSID` (e.g. image units obtained using the SALT telescope can have OBSID = SALT-012345).

2. The second connection is through the grouping of image units within a single FITS image extension.

For a single CCD with multiple amplifiers an image unit in a set of data from the same observation has a unique identification number, which identifies each amplifier in a detector uniquely. In the FITS extensions, images have geometrical relationships which are defined by linear coordinate transformations between the various pixel coordinate systems. The logical pixel raster is used to describe the full mosaic in the detector coordinates system (e.g. 2048×2048 for a 2×2 mosaic of 1024×1024 CCDs). This size includes the gaps between the CCDs as a number of missing pixels, but it must be rectangular.

Each amplifier reads the CCD data in a different order. The pixel order may be flipped when they are written to the image raster. Specification of the flips must be described so that the array is correctly mapped to the pixel raster. For a single CCD with multiple amplifiers the single image will be geometrically correct with respect to the CCD array. For a mosaic this is not true due to the alignment of the CCD chips. We now discuss four coordinates systems (also see an example of their calculations in Appendix C): the CCD, amplifier, image and the detector coordinate system (Valdes 2000). The pixel coordinate systems have integer coordinate values for the centres of the pixels which relate to the raster array indices of the CCD or image.

University of Cape Town

The CCD Coordinate System

This coordinate system gives the true size of the CCD, defined by the unbinned pixels. Drift scanning causes the final output image to consists of more pixels than the physical size of the CCD. The prescan will have negative CCD coordinates. Any corner of the image can be used as the origin of the coordinates. This coordinate system can be used to specify the region of interest (ROI). To map the CCD coordinate system to other (amplifier, image or detector) coordinate systems one must define, an amplifier transformation matrix (ATM) that expresses the differences in orientation and scale between the coordinate systems and amplifier transformation vector (ATV) that expresses the displacement between the two coordinate systems. The CCD coordinate is defined by (C_x, C_y), and appears as `CCDSEC = '[Cx1:Cx2,Cy1:Cy2]'` in the image header.

The Amplifier Coordinate System

This coordinate system is defined by (A_s, A_p), where A_s is the serial coordinate and A_p is the parallel coordinate. It appears as follows in the image header:
`AMPSEC = '[As1:As2,Ap1:Ap2]'`. This coordinate system defines the order in which pixels were read out by the controller. Unused columns or lines in the CCD are not counted. Only the prescan pixels can have negative amplifier coordinates. The linear transformation between the amplifier and the CCD coordinates is given by:

$$A_s = ATM_{11} \times C_x + ATM_{12} \times C_y + ATV_1, \tag{4.1}$$

$$A_p = ATM_{21} \times C_x + ATM_{22} \times C_y + ATV_2. \tag{4.2}$$

Isolating C_y in Equation 4.2 one obtains

$$A_p - ATV_2 - ATM_{21} \times C_x = ATM_{22} \times C_y,$$

then

$$C_y = \frac{A_p - ATV_2 - ATM_{21} \times C_x}{ATM_{22}}.$$

Substituting C_y in Equation 4.1 and performing some algebra one obtains

$$C_x = \frac{ATM_{22} \times (A_s - ATV_1) - ATM_{12} \times (A_p - ATV_2)}{ATM_{11} \times ATM_{22} - ATM_{12} \times ATM_{21}}.$$

The same can be done for C_y, but one has to use equation 4.1 to isolate C_x. From Equation 4.1

$$C_x = \frac{A_s - ATV_1 - ATM_{12} \times C_y}{ATM_{11}}.$$

Substituting C_x in Equation 4.2 to eliminate C_x, one finds

$$C_y = \frac{-ATM_{21} \times (A_s - ATV_1) + ATM_{11} \times (A_p - ATV_2)}{ATM_{11} \times ATM_{22} - ATM_{12} \times ATM_{21}},$$

University of Cape Town

where ATM is the amplifier transformation matrix, and ATV is the amplifier transformation vector. The transformation coefficients are recorded in the FITS image header. When multiple amplifiers are used, these coefficients become more important in determining the readout order of the pixels. These values appear in the FITS file header in the order:

`ATM1_1`, `ATM1_2`, `ATV1`, `ATM2_1`, `ATM2_2` and `ATV2`.

The Image Coordinate System

The image coordinate system (I_c, I_l) defines the pixels in the recorded image, including both the overscan and the prescan regions. The acquired data only occupies the image region. The coordinates of the first pixel in the image section start with $(1, 1)$ in the image coordinate system. The data section in the FITS file appears as DATASEC, with the format `DATASEC = '[Ic1:Ic2,Il1:Il2]'`. The linear transformation between the CCD and the image coordinates is given by

$$I_c = LTM_{11} \times C_x + LTM_{12} \times C_y + LTV_1, \tag{4.3}$$

$$I_l = LTM_{21} \times C_x + LTM_{22} \times C_y + LTV_2. \tag{4.4}$$

Using the same method as before one finds:

$$C_y = \frac{I_l - LTM_{21} \times C_x - LTV_2}{LTM_{22}}.$$

Substituting the value of C_y in Equation 4.3 and performing some algebra to get

$$C_x = \frac{LTM_{22} \times (I_c - LTV_1) - LTM_{12} \times (I_l - LTV_2)}{LTM_{11} \times LTM_{22} - LTM_{21} \times LTM_{12}},$$

and

$$C_y = \frac{LTM_{11} \times (I_l - LTV_2) - LTM_{21} \times (I_c - LTV_1)}{LTM_{22} \times LTM_{11} - LTM_{12} \times LTM_{21}}.$$

It is recommended that I_{c1} be less than I_{c2} and I_{l1} be less than I_{l2}. If the order is reversed, then the image sections will be flipped. The data section is related to the amplifier section (AMPSEC), the CCD section (CCDSEC) and the detector section (DETSEC) by transforming I_{c1}, I_{c2}, I_{l1} and I_{l2} to I_{c1} - 0.5, I_{c2} + 0.5, I_{l1} - 0.5 and I_{l2} + 0.5 respectively.

The Detector Coordinate System

The detector coordinate system (D_x, D_y) is important when multiple amplifiers and/or multiple CCDs are used. The detector coordinate system describes a mapping of multiple amplifiers/CCDs pixels into a single pixel raster of unbinned CCD pixels

University of Cape Town

to form a single simple image. It has to be consistent with the flips, offsets, transposes between the image pixel since it is used to display multiple CCD/amplifier data set. This coordinate system is represented as `DETSEC = '[Dx1:Dx2,Dy1:Dy2]'` in the image header. For CCDs with multiple amplifiers the coordinate system of the detector and the CCD are the same. For a mosaic of CCDs the detector and the CCD coordinate systems will have the same orientation but with different origins for each CCD. The linear transformation between the CCD coordinate system and the detector coordinate system are given by

$$D_x = DTM_{11} \times C_x - DTM_{12} \times C_y + DTV_1, \tag{4.5}$$

and

$$D_y = DTM_{21} \times C_x + DTM_{22} \times C_y + DTV_2. \tag{4.6}$$

Using the same methods as before gives:

$$C_x = \frac{DTM_{22} \times (D_x - DTV_1) - DTM_{12} \times (D_y - DTV_2)}{DTM_{11} \times DTM_{22} - DTM_{12} \times DTM_{21}}.$$

and

$$C_y = \frac{DTM_{11} \times (D_y - DTV_2) - DTM_{21} \times (D_x - DTV_1)}{DTM_{22} \times DTM_{11} - DTM_{21} \times DTM_{12}}.$$

4.4.1 Binning

There is a non-integer relationship between the image coordinate system and the other coordinate systems when pixels are binned. However, the image coordinates of binned pixels will have integer values at the center of the binned pixels. The centre of binned pixels transfoms to the middle of the unbinned pixels. If the first two CCD pixels are binned to form the first image pixel, the centre of the binned pixel in the CCD coordinate system would be 1.5. In the FITS file header the CCDSUM keyword stores the value of the binning factor.

The value field of the keyword CCDSUM will contain N_s, N_p, N_{s1} and N_{p1}, where N_s is the number of the serial pixel summed for each output pixel in the amplifier coordinate system, and N_p is the parallel summed pixels. It is possible that the first and last output pixels could be partial sums of fewer pixels, that is where the parameters N_{s1} and N_{p1} come into use which indicate how many amplifier pixels are in the first sum. If N_{s1} and N_{p1} are the same as N_s and N_p they can be omitted. The CCDSUM will appear in the FITS file header as: `CCDSUM = 'Ns Np Ns1 Np1'`.

University of Cape Town

4.4.2 Deriving the Transformation Coefficients

The transformation coefficients are derived when mapping sections in other coordinate system to the section of CCDSEC. We consider the case of no partial pixel sum $N_{sI} = N_s$, $N_{pI} = N_p$. When there is no transpose, the mixed terms from the coordinate systems disappear from Equations 4.3 and 4.4:

$$LTM_{12} = 0,\ LTM_{21} = 0;$$

Equation 4.3 and 4.4 become

$$I_c = LTM_{11} \times C_x + LTV_1 \tag{4.7}$$

$$I_l = LTM_{22} \times C_y + LTV_2 \tag{4.8}$$

for the range of image pixel columns Equation 4.7 one has

$$I_{c1} = LTM_{11} \times C_{x1} + 0.5 \times (1 - LTM_{11}) + LTV_1,$$
$$I_{c2} = LTM_{11} \times C_{x2} - 0.5 \times (1 - LTM_{11}) + LTV_1,$$

for the range of image pixel lines Equation 4.8

$$I_{l1} = LTM_{22} \times C_{y1} + 0.5 \times (1 - LTM_{22}) + LTV_2,$$
$$I_{l2} = LTM_{22} \times C_{y2} - 0.5 \times (1 - LTM_{22}) + LTV_2.$$

One can solve for the C_x's and the C_y's, to obtain

$$C_{x1} = \frac{(I_{c1} - 0.5 \times (1 - LTM_{11}) - LTV_1)}{LTM_{11}},$$
$$C_{x2} = \frac{(I_{c2} + 0.5 \times (1 - LTM_{11}) - LTV_1)}{LTM_{11}},$$
$$C_{y1} = \frac{(I_{l1} - 0.5 \times (1 - LTM_{22}) - LTV_2)}{LTM_{22}},$$

and

$$C_{y2} = \frac{(I_{l2} + 0.5 \times (1 - LTM_{22}) - LTV_2)}{LTM_{22}}.$$

The transformation coefficients are then given by:

$$LTM_{11} = \frac{(I_{c2} - I_{c1} + 1)}{(C_{x2} - C_{x1} + 1)},$$

and

$$LTM_{22} = \frac{I_{l2} - I_{l1} + 1}{C_{y2} - C_{y1} + 1}.$$

If the image pixel order is the same as the CCD pixel order, the image is not flipped. If these orders (image pixel and the CCD pixel) are not the same then the image is flipped. Replacing LTM_{11} with LTM_{12}, LTM_{22} with LTM_{21} and C_x with C_y transposes the coordinate systems.

University of Cape Town

Chapter 5

Photometry

5.1 Introduction

In this chapter photometry and various photometric packages are discussed. Photometry is the study of the colour and brightness of point-like objects like stars, but it also includes the investigation of the surface brightness of extended objects such as galaxies. Two stars that might seem to have the same brightness to the human eye, actually have different brightness when recorded on a photographic plate. This led to the development of filters that allow light of certain wavelengths to pass through to the detector, while blocking light of other wavelengths.

There are different types of filter systems that are used in astronomy, such as, the Johnson, Kron-Cousins and Strömgren filter systems. The Earth's atmosphere also acts as a filter, since it affects (i.e. absorbs and scatters) the transmission of light differently in different wavelengths. The Johnson UBV system is transparent to the ultraviolet, (U), blue, (B), and visual, (V). The Johnson red, (R), and infrared, (I), are broader and further redward than the Cousins R and I bands. The Strömgren filter system in contrast uses intermediate-width bands (a few hundred Angstroms wide). The Strömgren filter system is very important for determining the metalicities, temperatures and absolute magnitudes of hot stars. These filters are denoted by u, v, b and y and were chosen to correspond to certain astronomical effects (Strömgren 1963 and Napiwotzki et al. 1993). The u filter relates to the Balmer discontinuity, while the v filter was chosen to coincide with that section of the spectrum that shows metal excess in the stars. The wavelengths of the b and y filters were chosen to correspond to those sections of the spectrum almost purely determined by stellar temperature.

University of Cape Town

5.2 Aperture Photometry

Aperture photometry is the measure of light that falls within a particular circular aperture centred on the target star. To measure the flux of a star, one adds together the intensity values from the central aperture and subtracts the background sky contribution estimated from the annular region (made of two apertures: the inner and the outer apertures) surrounding the target star. The central aperture size must be large enough to include as much of the target star image as possible but with as little extra light from the background sky as possible. Assuming there are N pixels inside the central aperture, the total flux S, (star + background) is given by

$$S = \sum_{ij}(E_{ij} + b_{ij}). \tag{5.1}$$

Where i and j are pixel positions inside the aperture, b_{ij} is the background sky contribution and E_{ij} is the star intensity above the sky. The summation is over the pixels that are inside the aperture. Let the mean sky background B measured within an annulus with N_A pixels be given by

$$B = \frac{1}{N_A}\sum_{ij} b_{ij}. \tag{5.2}$$

To get only the measure of intensity of the star we subtract the mean sky background B from the total flux S, then we get

$$S = \sum_{ij}(E_{ij} + b_{ij}) - NB. \tag{5.3}$$

The first problem of this method is that it is not easy to choose a good aperture size. If the aperture is too large, it will include light from neighbouring stars and too much of the sky surrounding the star. The smallest stellar photometric errors (i.e. the largest signal-to-noise ratios) are generally obtained with relatively small apertures. Large apertures have large photometric errors; because the total number of stellar photons in the aperture becomes comparable with the total number of background photons in the aperture. A good compromise is an aperture which is a little bigger than the visible extent of faint stars. In practice, a good choice for a central aperture size is about 1.5 or 2.0 times the full width at half maximum (FWHM) of the stellar profile. In these aperture sizes, reasonable variations in the seeing will not result in measurable variations in measured counts. The reasonable values for the sky annuli are around 4 to 5 times aperture radius for the inner boundary and around 6 to 7 times the aperture radius for the outer boundary.

The second problem of this method is that all pixels are treated equally. Pixels at the centre of the aperture are given the same weight as the pixels at the circumference of the aperture, even though pixels at the centre of the aperture are brighter than pixels at the circumference.

University of Cape Town

5.3 Photometric errors

The intensity contribution of a star within an aperture with N pixels is given by Equation 5.3. In determining the error in the measurement of S, there are components due to the Poisson statistics of the star and the sky background. Adding the variance from Gaussian readout noise, we get the following equation

$$\sigma_S^2 = \sum_{ij}(E_{ij} + b_{ij} + \sigma_{RO}^2) + N^2\sigma_B^2, \tag{5.4}$$

where σ_{RO}^2 is the variance in the readout noise and σ_B^2 is the error that is associated with the measurement of B in Equation 5.2,

$$\sigma_B^2 = \frac{1}{N_A^2}\sum_{ij}(b_{ij} + \sigma_{RO}^2). \tag{5.5}$$

From σ_B^2 we can see that errors in determining the background are small contributors to the total error in the star if $N_A \gg N$, which is generally the case. We then have

$$\sigma_S^2 = \sum_{ij}(E_{ij} + b_{ij}) + N\sigma_{RO}^2 + N^2\sigma_B^2,$$

with the constraint

$$\sum_{ij}(E_{ij} + b_{ij}) = S + NB.$$

Therefore

$$\sigma_S^2 = (S + NB) + N\sigma_{RO}^2 + N^2\sigma_B^2.$$

Re-arranging the equation gives the following

$$\sigma_S^2 = S + N(B + \sigma_{RO}^2) + N^2\sigma_B^2.$$

The signal-to-noise ratio (Howell 1989) is then S/σ_S, and is given by

$$\text{Signal/Noise} = \frac{S}{\sqrt{S + N(B + \sigma_{RO}^2) + N^2\sigma_B^2}}. \tag{5.6}$$

This equation is given in photons and it is sometimes referred to as the "CCD equation". Clearly, as the aperture size increases, the signal-to-noise decreases as the number of pixels, N, increases. This is especially true for fainter stars. The optimal choice of aperture size will depend on the brightness of the star (Howell 2000). A larger aperture is better for brighter stars and a smaller aperture for fainter stars. Using a small aperture, one is unable to compare results from different frames because of changes in the point spread function (PSF). One must use the same aperture size for all stars as long as one is sure that there is no variation of the star image with position on the CCD.

University of Cape Town

This leads to the technique of using small apertures for all the stars on the frame and larger apertures for few remaining bright stars. All of the small aperture measurements can be aperture-corrected to large aperture measurements without increasing the noise which is smaller compared to the noise you would get for a large aperture.

5.4 The Point Spread Function

The point spread function (PSF) is the apparent surface brightness profile of a point source just above the detector. Light from the star is scattered by the Earth's atmosphere and the detector transforming the stellar image from being a point source into a two-dimensional distribution. The PSF samples the distribution in CCD pixels and includes the diffusion of electrons within the detector, and reflection and absorption of photons in the detector substrate. The resulting PSF is the Point Response Function (PRF).

Consider a CCD image containing several stars and assume that the PSF is the same for all stars in the frame. The PSF is approximated by sampling a few brightest, non-saturated stars in the frame with greater signal-to-noise ratio. Adding such PSF samples one finds a reasonably accurate PSF which is approximately represented by a Gaussian function near the centre $z = z(0)$, while the wings of the PSF can be represented by the Moffat function (Moffat 1969), given by

$$z = z_0 \left[1 + \left(\frac{r}{\alpha}\right)^2\right]^{-\beta}, \tag{5.7}$$

where z is the intensity, $z_0 = z(0)$ is the initial intensity, r is the distance from the centre of the profile at the focus, α is the width parameter and β is a constant. Both α and β depend on the seeing; for poor seeing they both become large.

5.4.1 Photometry using the PSF

The general formula for summing the intensity S within an aperture is

$$S = \sum_{ij} W_{ij}((E_{ij} + b_{ij}) - b_{ij}), \tag{5.8}$$

where the sum is over all the pixels (i,j) within the aperture. The total counts in a pixel are $E_{ij} + b_{ij}$, where b_{ij}, is the estimated sky level and E_{ij} is the intensity of a star above the sky. W_{ij} is the weight for each pixel; for aperture photometry the weight is 1 within the aperture and zero outside the aperture. The weight is given by

$$W_{ij} = \frac{\mathrm{I}}{V_{ij}}$$

where V_{ij}, is the variance of pixel ij. To determine the weight so that the signal-to-noise is optimum, one fits a model profile, P_{ij} normalized to 1, to a nearby star in

University of Cape Town

the frame. As derived by Naylor (1998), the optimal signal-to-noise is obtained if the weights are given by

$$W_{ij} = \frac{P_{ij}/V_{ij}}{\sum P_{ij}^2/V_{ij}}. \tag{5.9}$$

The value of the weights, W_{ij}, is used to get a better estimate of E_{ij}. Let the total counts within each pixel be $I_{ij} = E_{ij} + b_{ij}$, then substitute the weight W_{ij} given by Equation 5.8 and assume that the variance for each pixel is the same (Naylor 1998). The equation of the total flux S will then take the form

$$S = \frac{\sum (I_{ij} - b_{ij}) P_{ij}/V_{ij}}{\sum P_{ij}^2/V_{ij}}. \tag{5.10}$$

The assumption of constant variance is not good for bright stars since the counts in each pixel are not due to the sky; it means that the extraction will be optimal for faint stars. In extracting optimal photometry, one fits a profile directly to the data, using the weighted least square statistics. We define χ^2 to be

$$\chi^2 = \sum (hP_{ij} - (I_{ij} - b_{ij}))^2/V_{ij},$$

where h is the scaling constant which represents the relative brightness of the star, hP_{ij} is the fitted profile, and $(I_{ij} - b_{ij})$ is the observed profile. The weight appears as inverse of the variance of each point. We use the following condition to find the minimum of χ^2:

$$\frac{\partial \chi^2}{\partial h} = 0,$$

one finds

$$2 \sum_{ij} (hP_{ij} - (I_{ij} - b_{ij}))P_{ij}/V_{ij} = 0.$$

Evaluating the summation one finds

$$h \sum P_{ij}^2/V_{ij} - \sum (I_{ij} - b_{ij}))P_{ij}/V_{ij} = 0,$$

and

$$h = \frac{\sum (I_{ij} - b_{ij}) P_{ij}/V_{ij}}{\sum P_{ij}^2/V_{ij}}. \tag{5.11}$$

This equation is similar to Equation 5.10, that was obtained after assuming that the variance for each pixel is the same. If the observed profile is not accurately measured, the terms due to the variance add magnitude dependence to the estimated profile. There will be systematic errors in the estimated flux that depend on magnitude, if the fitted profile is not a good match to the data. This method therefore relies on the model being a good fit to the data.

University of Cape Town

5.5 Profile Fitting programs

In this section various photometric packages are discussed. There are several different profile fitting programs that are generally used. Around 1983 the ROMAFOT program, discussed in Buonanna and Iannicola (1989), was developed to do profile fitting of photographic plate data. This program uses the Gaussian or the Moffat PSF functions to model the PSF. In 1987, DAOPHOT was developed (Stetson 1987), and has probably become the most widely used photometric package, included in the Image Reduction and Analysis Facility (IRAF). The program uses a hybrid approach to PSF building using Gaussian, Moffat and Lorentz profiles. Since then, DAOPHOT has been modified to use both the hybrid and the non-hybrid approachs to PSF building.

In 1993, the DoPhot was developed (Schechter et al. 1993) which uses an analytical PSF function to model the PSF. DoPhot is capable of detecting cosmic rays and saturated pixels on an image. A stand-alone program using the hybrid approach to PSF building using Gaussian, Empirical and Lorentz profiles (Penny and Leese 1986) was developed around 1995 and called Starman. The program can deal with crowded and undersampled images as well as field-variable PSF. In 2000, The HSTphot (Dolphin 2000) was developed to use the Tiny Tim PSF library with pre-image adjustments, bad pixel mask and charge transfer efficiency (CTE) corrections. HSTphot is optimized for running in undersampled conditions.

In the following subsections a detailed description of the two most common used packages, DoPhot (in subsection 5.5.1) and DAOPHOT (in subsection 5.5.4) is provided. Also a description of the IRAF environment in which DAOPHOT and SALT tools are embedded is provided.

University of Cape Town

5.5.1 DoPhot

DoPhot (Schechter et al. 1993) is a computer program that automatically detects stellar objects in a FITS frame and outputs the positions and the magnitudes of objects and crudely classifies them. DoPhot is able to adopt models of any kind for objects that need to be identified. The PSF model can be an elliptical Gaussian for a star or a galaxy, but with a star having a smaller Gaussian than a galaxy. The model of a double star is treated differently.

The model that best fits the object will be chosen as the model of that object. This model is then used as a filter in searching for new objects and will be used for detection and photometry. A cosmic ray, in contrast is modelled as a single high intensity pixel.

DoPhot Models

DoPhot models are specified in terms of analytic functions with free parameters. The PSF function is given by

$$z = z_b + z_0 \left(1 + t^2 + \frac{1}{2}\beta_4 (t^2)^2 + \frac{1}{12}\beta_6 (t^2)^3\right)^{-1},$$

where

$$t^2 = \left[\frac{1}{2}\left(\frac{x^2}{\sigma_x^2} + 2\sigma_{xy}xy + \frac{y^2}{\sigma_y^2}\right)\right],$$

and

$$x = x' - x_0 \quad ; \quad y = y' - y_0$$

with the centre of the image at (x_0, y_0). β_4 and β_6 are dimensionless parameters that can be adjusted by the user, but they are normally taken to be unity. The shape parameters are given by σ_x, σ_y and σ_{xy}. z_0 is the central intensity and z_b is the background intensity. If the number of parameters is increased the models will generally improve, but the function will be more complex. The gain and the readout noise have to be specified for every set of images. DoPhot uses the estimate of the seeing supplied by the user to identify bright stars that are brighter than a given threshold.

The analytical function used to represent a star is fitted to the subraster that is centred on different objects, to determine the shape of a typical star. If an object fits better to a nonstellar object (cosmic ray or galaxy) it is then classified as such. The fitted model is subtracted from the image, the resulting image is called the "working image". This process is repeated, but to detect faint objects in the object-subtracted working image we have to lower the detection threshold. To improve the estimate of the model parameters one has to add the previous best-fitting model to the working image.

Systematic Error

After each pass an image is created, called the noise image, which is updated throughout the process. This noise image provides weights for each pixel used in least squares fitting and is used to test whether an object is above the background sky. Large positive residuals are believed to cause phantom stars (these are PSF residual structures near to the bright objects) which are removed by adding extra noise to the noise image each time objects are subtracted from the working image. The disadvantage of adding extra noise is that the likelihood of detecting faint stars that are near to the brighter object is decreased.

It is expected that the total fluxes derived from fitting the model PSF suffer systematic errors, since the star-subtracted images have a systematic pattern of residuals. In order to correct for these errors, DoPhot calculates the total fluxes in an aperture.

University of Cape Town

The fitted magnitudes have larger uncertainties than the aperture magnitudes, because of the Poisson noise from the background sky inside the aperture. In a model of an object, the sky level appears in the equation as a free parameter, which can be used to determine the background sky. This background sky can then be used as a threshold in subsequent passes.

Running DoPhot

The input to DoPhot is simply the name of the input FITS file to be analysed and a tuneable parameter file, with the extension `.inp`. The process is entirely automatic and results in an output file which contains the following information :

1. N - a running number which identifies object
2. T - the type of object identified on the frame
3. Sky - the fitted sky background, z_b
4. X - the x-coordinate of the centre of the object
5. Y - the y-coordinate of the centre of the object
6. Int - the relative intensity (the scaling factor of the PSF, h), z_0
7. $Sig2x$ - the squared width of the PSF in the x direction, σ_x^2
8. $Sigxy$ - the ellipticity of the image cross section, σ_{xy}
9. $Sig2y$ - the squared width of the PSF in the y direction, σ_y^2
10. $StrAp$ - the total star count inside the aperture
11. $SkyAp$ - the mean sky count within the sky annulus

The main parameter is Int, which when converted to magnitudes, yields the relative magnitude differences. DoPhot recognizes different types of objects by comparing the image with the adopted PSF. Objects will be classified by the following values of T :

1. A star used to determine the PSF
2. A galaxy
3. A close pair (double star)
4. Unconverged
5. Too few pixels

University of Cape Town

6. Deactivated

7. Star not used to determine the PSF

8. Saturated object

Dophot begins by looking at the brightest object and obtaining approximate value for the PSF. The program identifies objects by looking at pixels above a certain threshold intensity, identifying them and removing them from the image. The process is repeated until the level reaches a minimum value near the background sky value. Uncontaminated stars above a certain threshold are used to determine the best value for σ_x^2, σ_{xy} and σ_y^2. The stars are placed back on the image and fitted using the values of σ_x^2, σ_{xy} and σ_y^2, with the remaining coefficients as free parameters.

5.5.2 The Image Reduction and Analysis Facility (IRAF)

This section deals with the Image Reduction and Analysis Facility (IRAF)[1] software and some of its packages which perform related tasks. The IRAF software was developed to allow the reduction and analysis of astronomical data and has a wide range of options which include the display of images and graphs, piping and redirection as well as online help facilities. As we will be intersted only in CCD reductions, we restrict our discussion to a brief description of packages which relate to photometric CCD analysis.

IRAF uses two types of image data formats: FITS (discussed in chapter 4) and its own format called IMH. In the IMH format, the header and the image data are stored in separate files. Whenever possible, one should avoid using the IMH format since IRAF was developed before the FITS image extension format. As a result it is not well suited for the analysis of FITS file with multi-extensions. This led to the development of a special package called '**SALT**' which is used to reduce multi-extension FITS data files acquired using SALTICAM.

A task is a command or a program. Before being used, its package must be loaded. Each of the tasks included in IRAF packages have parameter files which can be edited to meet the needs of the user. The following are some of the tasks used in IRAF taken from Davis (1994):

- **imstat**

  This is a task used to compute the image statistics (i.e. standard deviation, mean, min, max, number of pixels).

- **imcombine**

  This task is used to combine images pixel-by-pixel.

[1]IRAF is the Image Reduction and Analysis Facility, a general purpose software system for the reduction and analysis of astronomical data. For more information visit the IRAF website http://iraf.noao.edu/

University of Cape Town

- **imcopy**

  This is used to copy an image.

- **hedit**

  This is used edit the image header.

- **imdelete**

  This is used to delete a list of images.

- **imheader**

  This task is used to print an image header.

- **imexamine**

  This task is used to examine images using image display.

Using the SALT Package

The **SALT** package allows the user to remove the bias from a CCD image and to apply flat field corrections. The package is called up in the usual way of calling IRAF packages:

- start IRAF by running "xgterm".
- type "cl" to call up the IRAF command language.
- load the "**SALT**" package. The "**SALT**" package contains the following packages:
  - "**pfis**"
  - "**salticam**"
  - "**saltools**"

Suppose we have four bias files:

1. s200501110001.fits,
2. s200501110002.fits,
3. s200501110003.fits,
4. s200501110004.fits.

Four flat field files:

1. s200501110005.fits,

University of Cape Town

2. s200501110006.fits,

3. s200501110007.fits,

4. s200501110008.fits,

and four target FITS files containing the target star(s):

1. s200501110009.fits,

2. s200501110010.fits,

3. s200501110011.fits,

4. s200501110012.fits.

Our objective is to correct the bias and the flat fields on the target files.

The first step is to load the "**salticam**" package and then edit the parameter file of the "sbias" package in order to create a master bias frame. A list of bias files in the file "bias" is created and the "inimages" parameter has to be edited to "@bias". For the output file the "outbias" parameter is changed to "zero.fits" meaning that the master bias frame will be created with the name "zero.fits". Other parameters that may need editing include the order of its fit to the overscan strip, etc.

Next, the "siflat" parameter file is edited in the same way and place a list of flat field frames in the file called "flat" and change the "inflats" parameter to "@flat". For the "outflat" parameter we will use "flat.fits". The "bias" parameter must be changed to "zero.fits" since we are using the master bias frame to remove the bias on the flat field frames. This creates a master flat field file "flat.fits" for the particular prebin factor and filter.

Finally, the "sireduce" parameter file has to be edited, putting in the respective names of the master bias and master flat field files created as explained above. The resulting bias-corrected and flat fielded FITS files will have a prefix "ca" e.g. caS200501110005.fits. This completes the basic calibration process for FITS file obtained using SALTICAM camera. It may also be necessary to correct for dark and bad pixels at some stage.

University of Cape Town

5.5.3 Other IRAF packages

The following packages are included in IRAF:

- **dataio**

  This package allows the user to convert the format of the data.

- **noao**

  This package gives the user a wide range of options, to generate artificial data, to do aperture photometry and photometry of crowded fields, etc. **Digiphot** is a photometric package that is included in the **noao** package. Within the **digiphot** package there are following packages that are used for photometry :

  1. **apphot**
     This package is used for aperture photometry.
  2. **daophot**
     This package is used for photometry on crowded fields.
  3. **photcal**
     This package is used for photometric calibrations.
  4. **ptools**
     This package contains photometry tools.

- **plot**

  This is a plotting package that generates greyscale plots of an image, makes contour plots, etc.

- **image**

  This is used for image processing e.g. to compute the coordinate transformations, to do image arithmetic, etc.

5.5.4 DAOPHOT

DAOPHOT is a computer program for obtaining photometric magnitudes and positions for stellar objects in a CCD image. Displaying of images and a few other procedures may be done outside of DAOPHOT (e.g. the DS9 image displaying program). The user must have knowledge of, amongst other things, the gain, readout noise and FWHM of objects in the frame.

DAOPHOT will find star-like objects above a certain threshold and derives aperture photometry for these objects. DAOPHOT will also obtain the PSF of the entire frame using one star or several stars. When fitting the PSF to each star, DAOPHOT will obtain their positions and magnitudes.

DAOPHOT Models

DAOPHOT offers a wide range of choices in modelling the PSF. The PSF model consists of an analytical function (e.g. a Gaussian) together with a semi-emperical lookup table representing the deviations of the PSF from a Gaussian. Apart from a Gaussian, Lorentz and Moffat function may also be used.

University of Cape Town

- The Gaussian function has two free parameters: the half width at half maximum (HWHM) in x and y. The Gaussian function may be elliptical, but the axes are aligned with the x and y directions in the image.
- The Lorentz function has three free parameters: the HWHM in the x and y directions, and a position angle for the major axis of the ellipse.
- The Moffat function is proportional to

$$\frac{1}{(1+z^2)^\beta}$$

where $z^2 = x^2/\sigma_x^2 + \sigma_{xy}xy + y^2/\sigma_y^2$. β has two cases. The first case, $\beta = 1.5$ and the second case is when $\beta = 2.5$. There are also three free parameters called the shape parameters.

- A "Penny" function (Penny and Dickens 1986) is the sum of the Gaussian and the Lorentz functions, having four free parameters: the HWHM in the x and y directions, the fractional amplitude of the Gaussian function at the peak of the stellar profile and the position angle of the tilted elliptical Gaussian. The Lorentz function may be elongated, but its long axis must be parallel to the x or y axis.
- A "Penny" function has five free parameters. In this case, the Lorentz function may also be tilted in a different direction from the Gaussian.

5.5.5 Using DAOPHOT on SALTICAM Data

The first step in data reduction is to calibrate data using the IRAF/SALT package in the case of multi-extension FITS files from the SALT telescope. Calibration of simulated SALTICAM data is done using the "**salticam**" task. This task corrects the bias and the flat field on the image (as explained in section 5.5.2). After performing image calibration, the next step is to extract photometric data using various tasks in DAOPHOT package within IRAF. Correction of aperture photometry may be performed using the **mkapfile** task in the **photcal** package.

The initial step of photometric extraction is to display the image and select a few bright stars in the frame and run **imexam** to obtain the FWHM PSF of these stars. The FWHM PSF will be used to obtain the appropriate values on the parameters that are used in the following tasks: (**datapars, centerpars, findpars, fitskypars** and **photpars**). Some of these parameters are used in the **daofind** task used to detect objects in the frame. The "threshold" parameter in the **findpars** algorithm parameter has to be modified and the task rerun for detection of the omitted objects. This process is repeated until all the objects in the frame are detected. A file containing the information about the coordinates, roundness, sharpness and etc. of those detected objects is created automatically after each run.

University of Cape Town

The **phot** task is used to obtain the initial magnitudes of all the objects detected in the frame by the **daofind task**. The infomation that is obtained is used to compute the PSF model that will be fitted to all the stars in the frame. Once again, a file containing the computed PSF infomation is created automatically after running **phot** task. The next step is to compute the PSF model using the **psf task**. After obtaining the PSF model, it has to be fitted to all the stars in the frame. There are three fitting routines: **peak**, **nstar** and **allstar**. The **peak** task fits the PSF model to the stars individually while the **nstar task** fits the PSF model to a group of stars simultaneously. Lastly, the **allstar** task, fits the PSF model to the detected objects and groups these objects together. After grouping these objects they are subtracted from the frame and a file containing the new magnitudes, the magnitude errors, x and y coordinates, the id, etc... of the objects is created. Because the same aperture sizes are used for the bright and faint stars an aperture correction (the correction for the finite size of the aperture) should be applied to account for the flux that falls outside the aperture. The aperture correction is computed from a plot of magnitude against the aperture size (i.e. growth curve). It is determined using the **mkapfile** task in the **photcal** package.

University of Cape Town

Part II

Tests and Applications

University of Cape Town

Chapter 6

Characterisation of the SALTICAM CCD Bias

University of Cape Town

6.1 Introduction

In this chapter, results and tests that were carried out on the SALTICAM CCDs are presented. SALTICAM will be used to collect data with high accuracy, so it is very important to investigate factors that may affect the accuracy. Frames of different readout speeds and different binning factors are required for this investigation. Further, it is very important to check the stability of the detector. Prior to the second major use of SALTICAM by the engineers, we spent several days examining the performance of the SALTICAM CCDs.

We first investigate the bias stability over a substantial period of time in 1×1 binning and both readout modes (fast and slow readout modes, respectively). The results of these investigations are given in Sections 6.2 to 6.4. We then looked at the bias (prescan and image regions) as a function of position, in three different binning modes (1×1, 4×4 and 9×9) and both readout modes. The results of this investigation are given in Section 6.5. We only managed to obtain bias frames using the BRIGHT gain setting. This was due to problems experienced with the SALTICAM electronics beyond our control. Our aim was to investigate variations of the bias level on the SALTICAM CCDs. For this thesis, emphasis was placed on the variations of bias level, measured on the prescan region and on the image region, as a function of time. In addition, measurements of the operating temperature of the CCDs and other components (SDSU, cold box, cold end and the heater) were obtained as functions of time. The variation of bias level with temperature was investigated.

Prescan Area	X_1	X_2	Y_1	Y_2
1 (A)	12	44	987	3075
2 (B)	2104	2136	987	3075
3 (C)	2160	2192	987	3075
4 (D)	4252	4284	987	3075

Table 6.1: The coordinates (X_1, Y_1) and (X_2, Y_2) of diagonally opposite corners of windows created on the prescan region of the bias frame in 1×1 binning mode.

6.2 The Intensity of the Bias Frame as a Function of Time

When a CCD is read out with essentially a zero exposure time, one obtains a frame that has a non-zero average value due to the bias offset. This bias offset must be subtracted from every image before any arithmetic manipulation of the data. Since the bias offset estimate can also be obtained from the prescan region (as explained in the previous chapters), one can compare the bias offset values on both the imaging and the prescan regions which should be the same. The variation of bias level with time is also an important factor.

We begin with an investigation of the variation of bias between the prescan and the image regions. We started by creating one window on each image and prescan region of the bias frames. These windows were created to avoid bad/hot pixels and other effects on the frames. The mean bias level obtained within these windows is then plotted against time, to determine the stability of the bias level in the image and the prescan regions, respectively.

6.2.1 Windows Created on the Bias Frame

Tables 6.1 and 6.2 show the coordinates of diagonally opposite corners of windows that were created in the prescan and image regions using the SCAM software (X is measured along rows and Y along the columns). SALTICAM has two CCD chips, each chip is read out by two amplifiers (one on each side of the CCD chip) as shown in Figure 6.1. Due to faulty electronics of the SALTICAM camera, the first channel (labelled A in Figure 6.1) of the SALTICAM CCDs was very noisy and could not be used for this experiment.

University of Cape Town

Image Area	X_1	X_2	Y_1	Y_2
1 (A)	456	848	483	3627
2 (B)	1300	1692	483	3627
3 (C)	2604	2996	483	3627
4 (D)	3448	3840	483	3627

Table 6.2: The coordinates (X_1, Y_1) and (X_2, Y_2) of diagonally opposite corners of windows created on the image region of the bias frame in 1×1 binning mode.

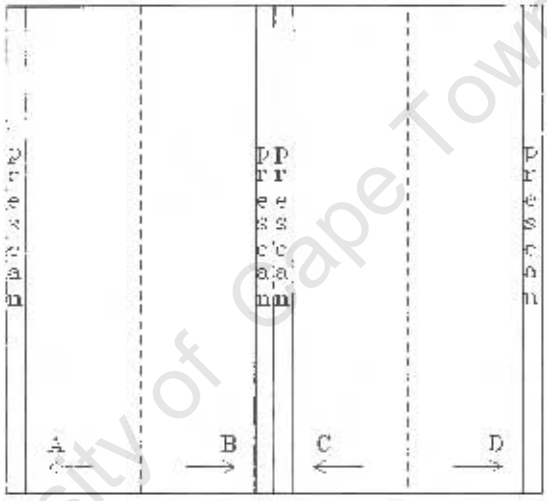

Figure 6.1: A schematic diagram showing the SALTICAM CCDs. The labels A,B,C and D show the amplifier in each channel and the arrows show the readout direction of each amplifier. The prescan regions are clearly identified.

University of Cape Town

6.2.2 Results and Discussion

The bias frames used for this work were obtained using a 1×1 binning factor and both slow and fast readout modes. For the fast and slow readout modes, the bias frames were obtained for 9 hours and 14 hours, respectively. The statistical parameters (calculating the mean, standard deviation, minimum, and the maximum) of each bias frame were computed using the PIP software (developed by Dr. Luis Balona). We started by creating two files, one containing the coordinates of the windows (defined in Section 6.2.1 above) and the other containing the names of the bias frames, and computed the mean bias level (using PIP) on each window. The standard errors for the measurements were calculated using $\sigma_{\bar{x}} = \sigma_x/\sqrt{N}$, where σ_x is the standard deviation per pixel and N is the number of independent pixels in the window. The

error bars shown are 100σ error bars to ensure visibility. Times after 0^h UT have had 24 hours added in Figures 6.2 and 6.3 to produce a monotonically increasing scale for plotting the data. The figures show a significant variation of bias with time.

Fast Readout Speed

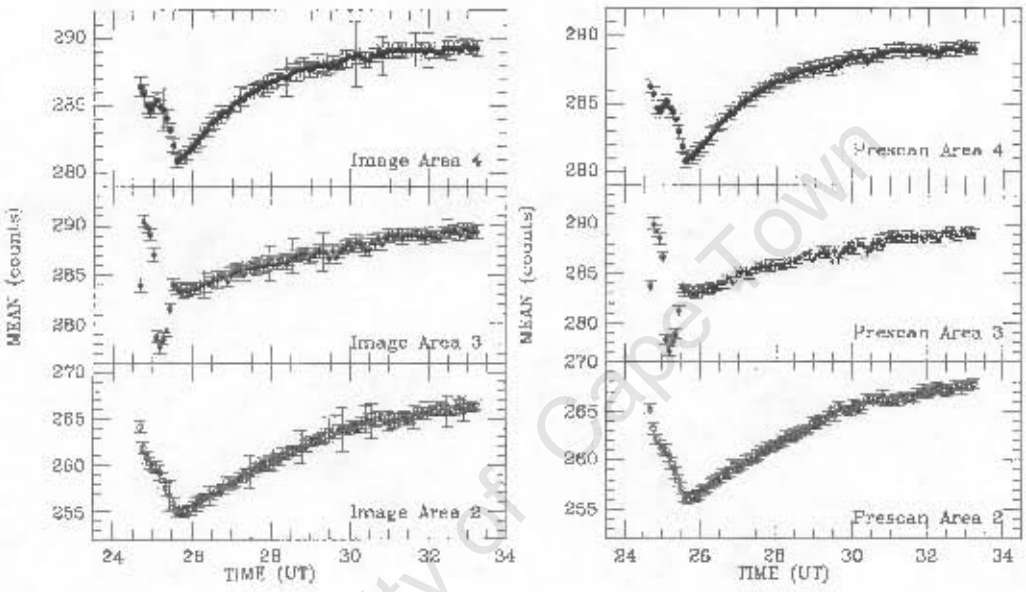

Figure 6.2: Mean bias level (ADU counts) plotted against time (UT). The biases measured from the image region and the prescan region of the CCDs are shown in the left and right panels respectively. The readout speed of the camera was set to **fast readout mode**. The error bars shown are 100σ error bars to ensure visibility.

In Figure 6.2 the mean bias level obtained using fast readout is plotted against time. All image and prescan areas show a similar pattern; the bias level drops rapidly in the first hour and followed by a gradual rise. Between the different image (and prescan) areas (compare areas 2, 3 and 4), there is a difference in the absolute bias level. Note, however, that this is an inherent setting of the CCD. The actual bias level setting is set by a SALT technician and so offsets can occur between the readout sections.

University of Cape Town

Slow Readout Speed

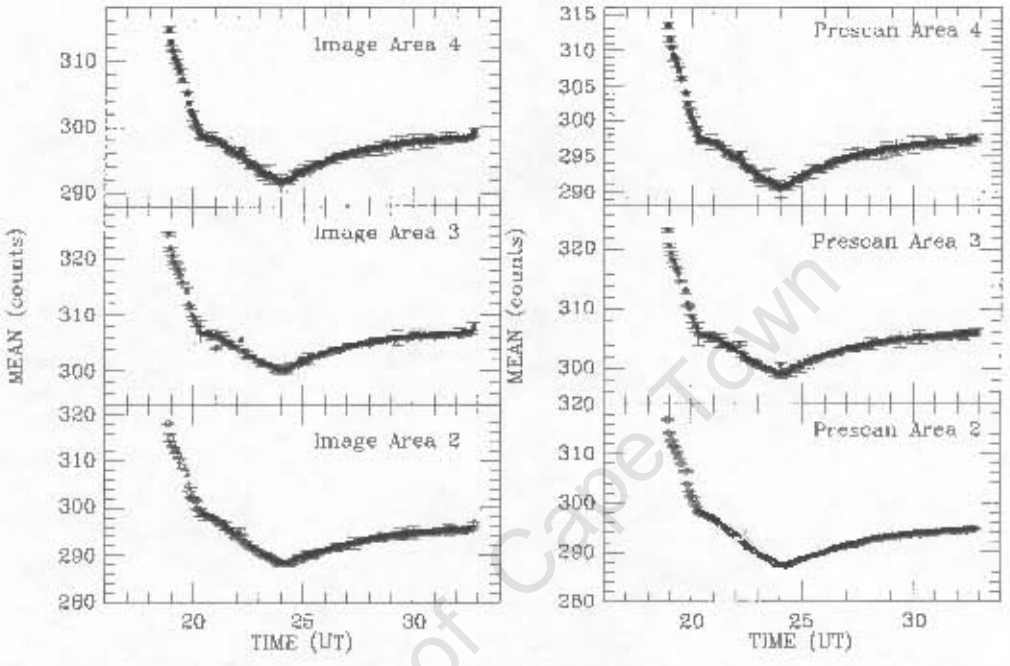

Figure 6.3: Mean bias level (ADU counts) plotted against time (UT). The biases measured from the image region and the prescan region of the CCDs are shown on the left and right panels respectively. The readout speed of the camera was set to **slow readout mode**. The error bars shown are 100σ error bars to ensure visibility.

Figure 6.3 shows plots of the bias level obtained with slow readout mode (in both the image and the prescan regions) plotted against time. As before with the data obtained in the fast readout mode (see Figure 6.2), the bias variation as a function of time looks nearly identical across all the image and prescan areas. A rapid decline (lasting $\sim$ 1 hour), is followed by a slower decline and eventually by a gradual increase in the bias level.

The cause of the temporal variations of the bias level will be looked at in detail in the following two sections, where we explore the time variability of various components of the CCD (Section 6.3) and investigate a correlation between bias level and temperature (Section 6.4).

University of Cape Town

6.3 CCD Temperatures as a Function of Time

Data for the operating temperatures of the CCD were obtained for both fast and slow readout modes. Figures 6.4 and 6.5 show the data of the different temperatures plotted against time, one notices that the data look quantised. This is not due to a round-off error, but intrinsic to the data recorded. Note as well that the temperature steps are not uniform. For example the CCD temperature measured (and plotted in the lower panel of Figure 6.5) is 149.19, 149.29, 149.39, 149.49 and 149.58 Kelvin, here the latter step is 0.09 Kelvin and not 0.1 Kelvin as for the others. These data were used to investigate the effect of temperature on the bias level. In this section the temperature of the CCD (denoted by CCD in the graphs), the cold end temperature (C_End), the cold box temperature (C_Box), the SDSU Controller temperature (SDSU), and the heater temperature were plotted against the time (UT).

- Cold End temperature

  The Cold End temperature is the temperature of a plate on top of the cryotiger, measured in Kelvin. The cryotiger is the device that is used to cool the SALTICAM CCDs to a required temperature, in order to reduce the thermal noise in the CCD.

- Cold Box temperature

  The cold box temperature is the temperature of the housing of the CCDs, measured in degrees Celsius, (°C).

- CCD temperature

  The CCD temperature is the temperature at which the CCD operates, measured in Kelvin.

- SDSU Controller temperature

  This is the temperature of the San Diego State University (SDSU) controller, measured in degrees Celsius, (°C). The SDSU is connected to SALTICAM and a computer. After the SALTICAM CCD has finished clocking, it takes the readout signal to the SDSU and the SDSU takes the signal to the computer.

- Heater temperature

  The CCDs are placed on a cold plate which is cooled below operating temperature by the cryotiger. A heater element and a sensor on the cold plate regulates the CCD temperature precisely.

The heater temperature data was discarded since it was noisy. The plots of the cold box and cold end have the similar shape as the SDSU temperature plots. Plots of the bias level with time (Figures 6.2 and 6.3) have a pattern similar to plots of the temperature with time, indicating a strong correlation of the bias with temperature.

University of Cape Town

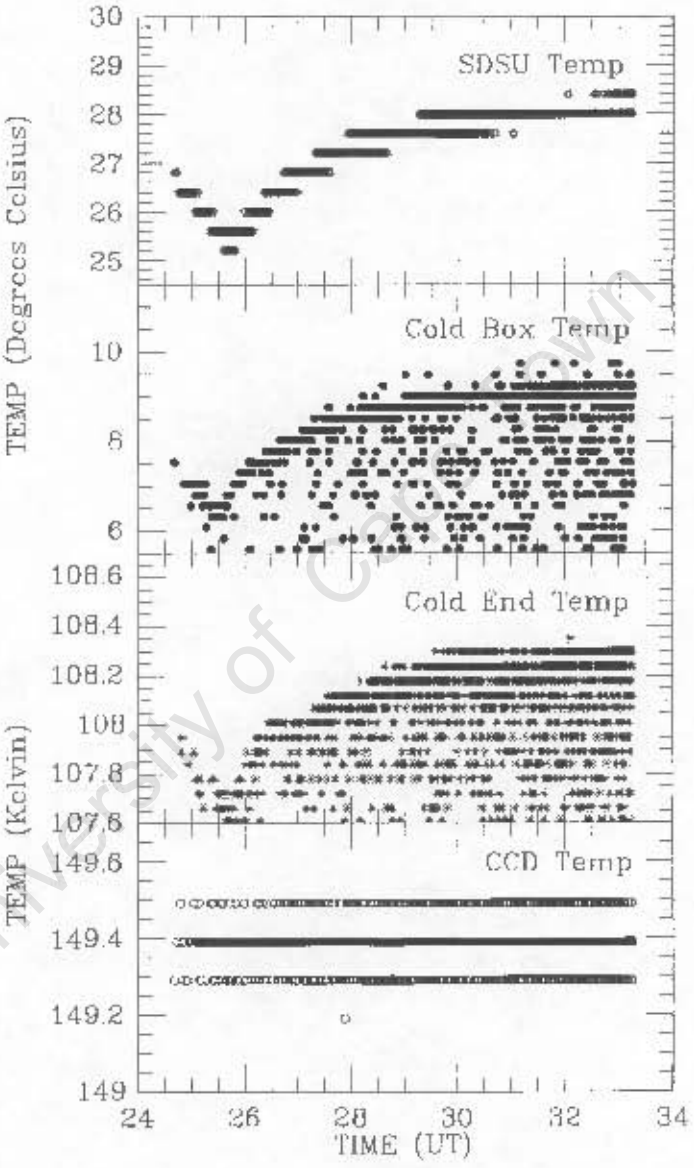

Figure 6.4: Plots of the temperature of the SDSU, Cold Box (both in degrees Celsius), Cold End and CCD (both in Kelvin) (from the top panel to the bottom panel as shown in the figure) against time (UT). These data were obtained at the same time as data of the bias level. **Fast readout mode** was used.

University of California, Irvine

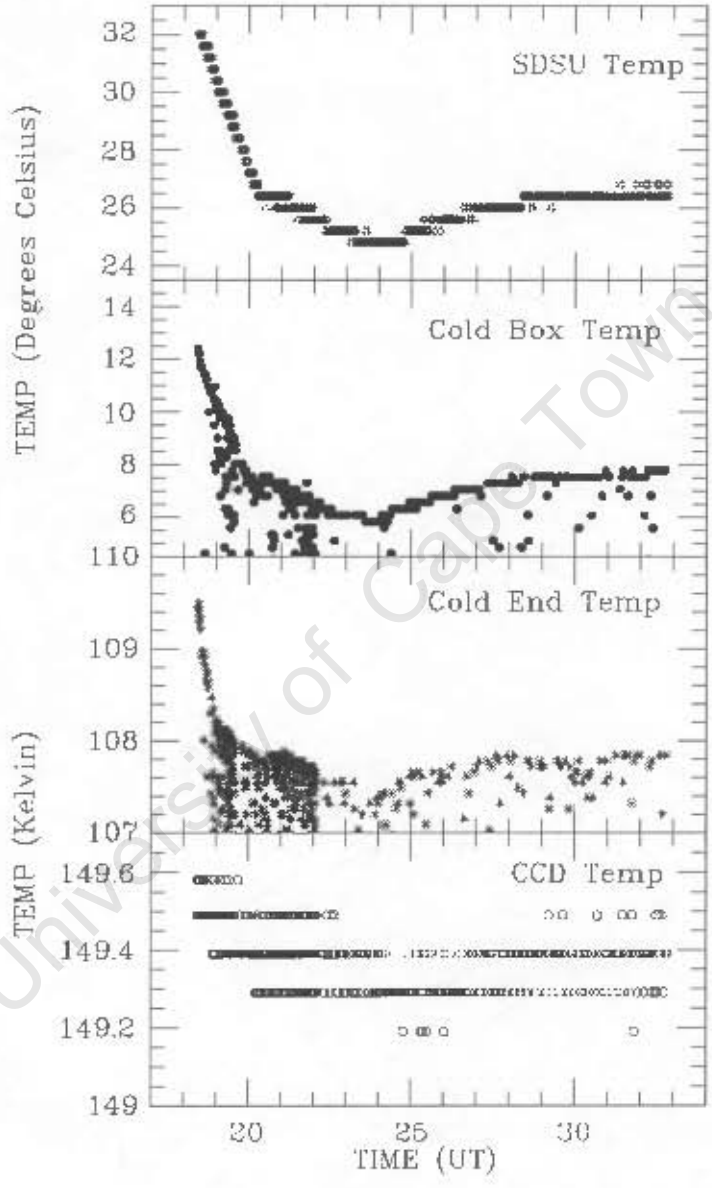

Figure 6.5: Plots of the temperature of the the SDSU, Cold Box (both in degrees Celsius), Cold End and CCD (both in Kelvin)(from the top panel to the bottom panel as shown in the figure) against time (UT). These data were obtained at the same time as data of the bias level. **Slow readout mode** was used.

University of Cape Town

6.4 Correlation of Bias Level with Temperature

In this section the comparison of the smoothed SDSU temperature with bias level is presented. Figures 6.6 and 6.7 show the similarity between the plots of the temperature of the SDSU with bias level. Since the SDSU temperature is less noisy and has a better defined shape than the others it was selected as the data set to determine the relationship between the temperature and the bias level. A small MATLAB code (refer to Appendix E) was used to bin the data (using a binning factor of 15 minutes with each binning containing 15 data points) to reduce the scatter of the data. Figures 6.6 and 6.7 show that the SDSU temperature and the bias level are strongly correlated.

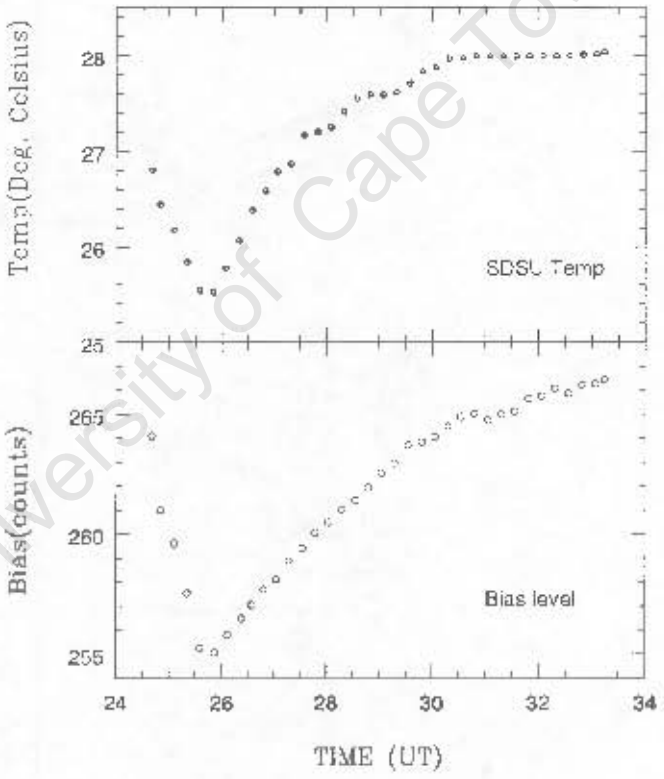

Figure 6.6: The top panel shows the time-dependence of the SDSU temperature (Celsius) while the bottom panel shows the time-dependence of the bias level (ADU counts). This is for **fast readout mode**. Note the similarity in the shape of both curves indicating the strong correlation between the bias level and the temperature.

University of Cape Town

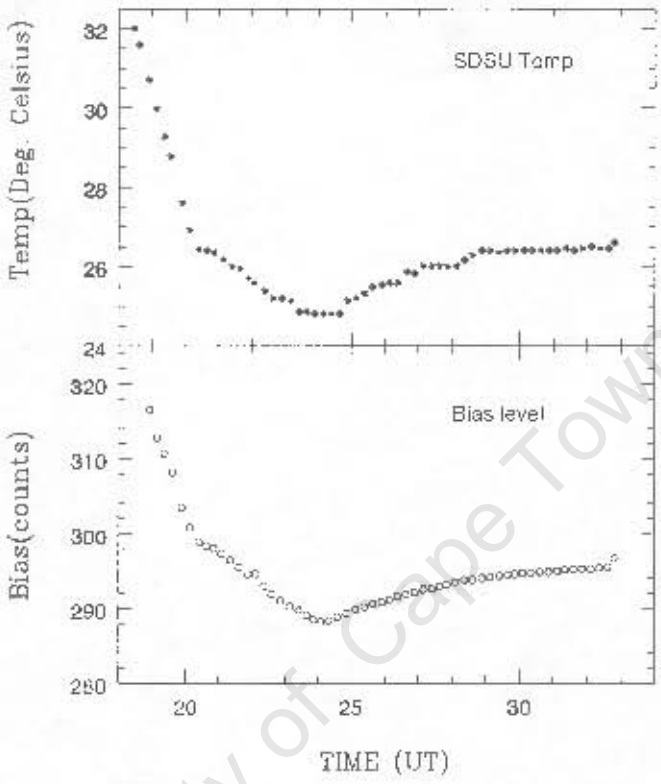

Figure 6.7: The top panel shows the time-dependence of the SDSU temperature (Celsius) while the bottom panel shows the time-dependence of the bias level (ADU counts). This is for **slow readout mode**. Note the similarity in the shape of both curves indicating the strong correlation between the bias level and the temperature.

To obtain the relationship between bias level and SDSU temperature, we plotted the two against each other. This is shown in Figures 6.8 and 6.9 (both fast readout mode) and Figure 6.10 (slow readout mode). In those figures the different symbols represent different relations when the temperature is declining and when it is increasing. After plotting the SDSU temperature against the bias level a polynomial was fitted to the curve. The package used to fit a polynomial uses the method of least squares (explained in the Appendix B) and produces values of the coefficients and the standard error. These polynomial coefficients can be used to interpolate the bias level and SDSU temperature at a give time. In this way, the correlation between bias level and temperature can be determined.

University of Cape Town

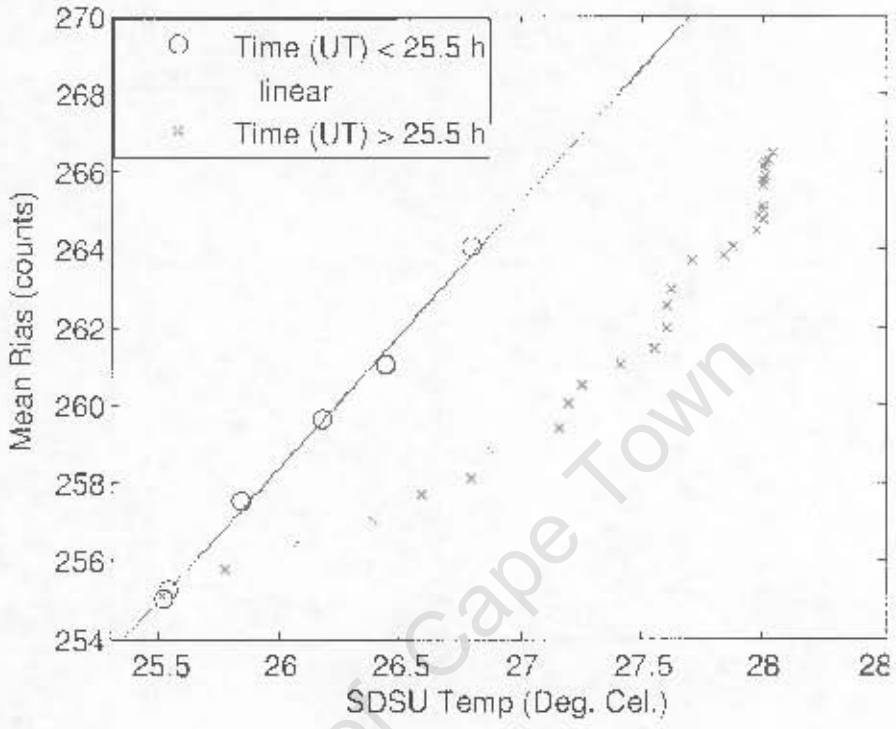

Figure 6.8: The bias level plotted against the SDSU temperature for the **fast readout mode**. The best linear fit to the data of the declining temperature. The values of the coefficients are shown in Table 6.3

6.4.1 Results and Discussion

Fast Readout mode

Figures 6.8 and 6.9 show that a polynomial of first order (i.e. $y = a_0 + a_1 x$) and a third order polynomial (i.e. $y = a_0 + a_1 x + a_2 x^2 + a_3 x^3$ best fit the data, where y is the mean bias level and x is the SDSU temperature (the second order polynomial didn't give best fit to the data). For other data sets, (see also slow readout mode) the best fits are linear however for Figure 6.9 the best fit is a polynomial for reasons not well understood. The figures represent different relations when the temperature is declining (open circle in Figure 6.8) and when it is increasing (crosses in Figure 6.9). Table 6.3 shows the values of the best coefficients (a_0, a_1 and a_2), standard errors and the norm of residuals (the norm of residual is the measure of the goodness of the fit) of polynomials fitted to the data.

University of Cape Town

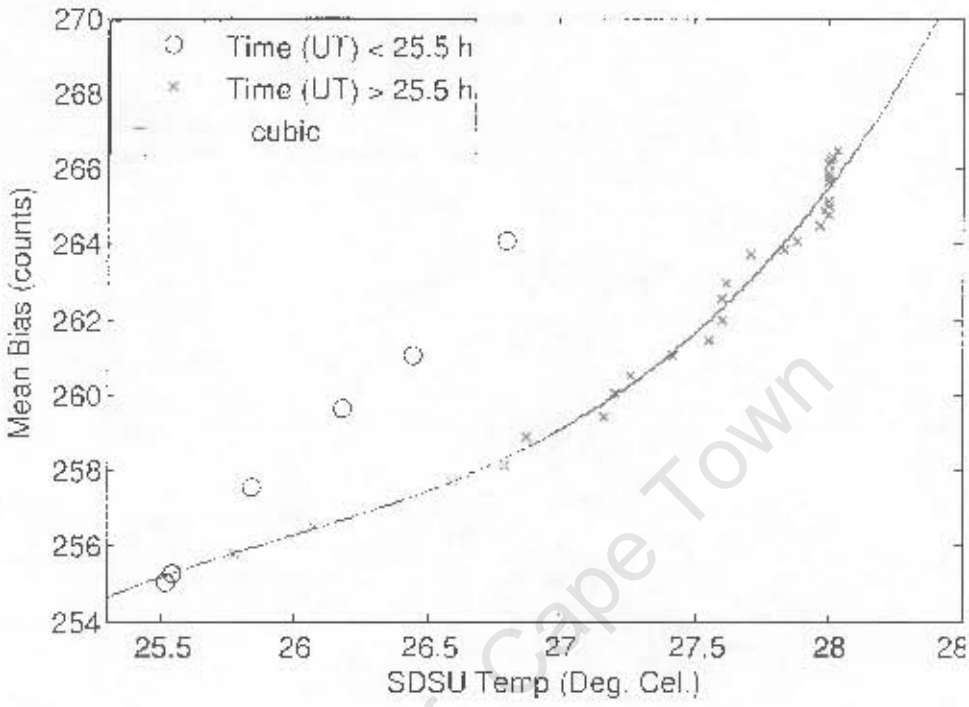

Figure 6.9: The bias level plotted against the SDSU temperature for the **fast readout mode**. The best cubic fit to the data of the increasing temperature. The values of the coefficients are shown in Table 6.3

Slow readout mode

A similar investigation to the fast readout mode an investigation was made on the results of slow readout mode. The relations for increasing and declining temperature (and the bias) are plotted. Figures 6.10 and 6.11 show that the relationship between bias level and temperature in the slow readout mode is a polynomial of first order (i.e. $y = a_0 + a_1 x$) where y is the mean bias level and x is the SDSU temperature. These relations have different gradients for different temperature (rapid and gradual decline and increase). In Figure 6.11, three different regions of variations are identified. Region A (rapid decline of temperature/bias), B (slow decline) and C (increase). Figure 6.10 shows the fit to the correlation of the temperature and bias for rapid decline. This relation is similar to the fit of the correlation for the increase(C in Figure 6.11). The slow decline (B) is different to A and C. This could be because because of a possible hysteresis effect during this transition phase and is worth investigating in detail in future studies. Table 6.4 contains the values of the coefficients, standard errors and the norm of residuals of the linear relations.

University of Cape Town

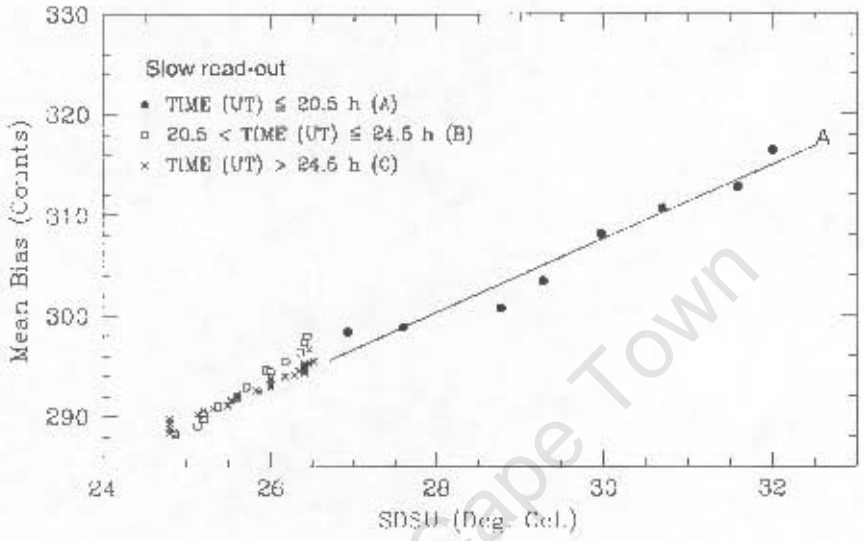

Figure 6.10: The bias level plotted against the SDSU temperature for the **slow readout mode**. The plot shows three different cases of the temperature represented by different points. The line (marked by A) represents the best fit to the data of the initial rapid decline in temperature. The values of the coefficients are shown in Table 6.4

University of Cape Town

Best fit	Coefficients	Values of Coeff.	Norm of residuals
Linear	a_0	81.86 ± 8.43	0.54
	a_1	6.8 ± 0.28	
Cubic	a_0	-1E004	2.29
	a_1	1.2E003	
	a_2	-46	
	a_3	0.59	

Table 6.3: The values of the coefficients and the Norm of residuals of the best fit to the data (**Fast readout mode**).

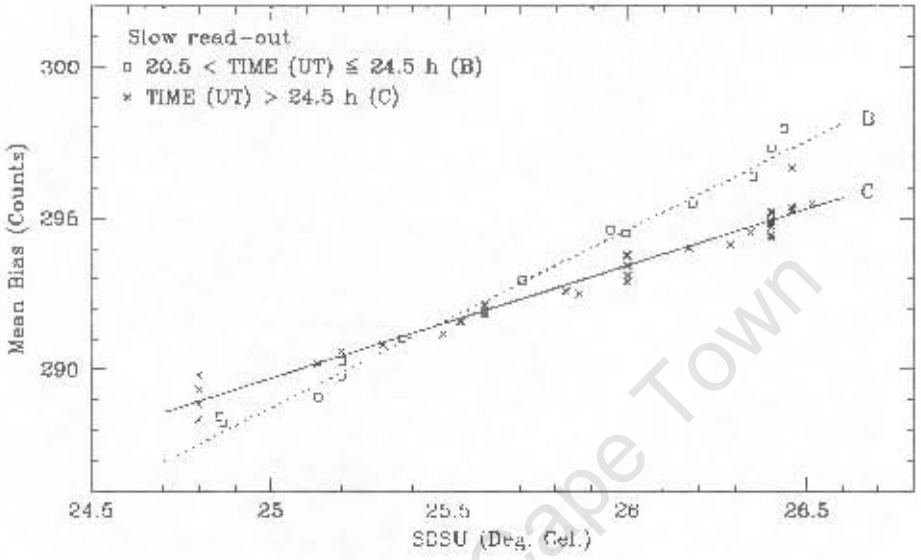

Figure 6.11: The plots show a zoom in section in Figure 6.10. The lines (marked by B and C) represent the best fit to the data, where B is for the gradually declining temperature and C is for the increasing temperature. The values of the coefficients are shown in Table 6.4

University of Cape Town

Line	Coefficients	Values of Coeff.	Norm of residuals
A	a_0	197.66 ± 9.88	1.39
	a_1	3.67 ± 0.33	
B	a_0	141.48 ± 4.82	0.38
	a_1	5.89 ± 0.19	
C	a_0	196.23 ± 3.26	0.41
	a_1	3.74 ± 0.13	

Table 6.4: The values of the the coefficients and the Norm of residuals of the best fit to the plots A,B and C (**Slow readout mode**).

6.5 Investigation of bias variation in individual CCD Channels

This section presents an investigation of how the bias level varies within each image and prescan region of the CCDs. We also discuss how the bias level on the image region changes with the bias level on the prescan region. The expectation is that the mean bias level should be the same in both regions and should cancel when one region is subtracted from the other. Knowing how the bias level changes on the image region and prescan region will help one to understand factors that can affect the accuracy of the data. The prescan region can give a good estimate of the bias level, but it is important to investigate its stability.

For this section, 30 bias frames were obtained (i.e. 10 frames per binning factor, 5 per readout mode, slow and fast, respectively) using the BRIGHT gain setting. To investigate potential variations, four windows on each image and prescan region of the frame were created and statistics (e.g the mean, standard deviations, median, maximum and the minimum) within these windows was obtained using the PIP software as explained in the previous section. The standard error of the measurement were calculated using the error propagation rule, see Taylor (1997).

6.5.1 Results using a 1×1 binning

As previously explained it is not advisable to use the entire image region to find the mean bias level, because there can be bad/hot pixels in the CCD. To avoid these bad pixels, one needs to create windows on the image and prescan regions and measure the bias level within these windows. Table 6.5 shows the coordinates of the multiple windows created in each individual image and the prescan regions of the frame. Note that each window that is created on the image region has an adjacent window that corresponds to it on the prescan region. The error bars shown in the plots are 100σ error bars to ensure visibility.

University of Cape Town

Image region					Prescan region			
CCD 1 (A) channel 1	X_1	X_2	Y_1	Y_2	X_1	X_2	Y_1	Y_2
1	250	850	131	979	10	42	131	979
2	250	850	1131	1979	10	42	1131	1979
3	250	850	2115	2947	10	42	2115	2947
4	250	850	3131	3939	10	42	3131	3939
CCD 1 (B) channel 2	X_1	X_2	Y_1	Y_2	X_1	X_2	Y_1	Y_2
1	1300	1890	131	979	2106	2138	131	979
2	1300	1890	1131	1979	2106	2138	1131	1979
3	1300	1890	2115	2947	2106	2138	2115	2947
4	1300	1890	3131	3939	2106	2138	3131	3939
CCD 2 (C) channel 3	X_1	X_2	Y_1	Y_2	X_1	X_2	Y_1	Y_2
1	2400	3000	131	979	2158	2190	131	979
2	2400	3000	1131	1979	2158	2190	1131	1979
3	2400	3000	2115	2947	2158	2190	2115	2947
4	2400	3000	3131	3939	2158	2190	3131	3939
CCD 2 (D) channel 4	X_1	X_2	Y_1	Y_2	X_1	X_2	Y_1	Y_2
1	3400	4040	131	979	4254	4286	131	979
2	3400	4040	1131	1979	4254	4286	1131	1979
3	3400	4040	2115	2947	4254	4286	2115	2947
4	3400	4040	3131	3939	4254	4286	3131	3939

Table 6.5: Coordinates (X_1, Y_1) and (X_2, Y_2) of diagonally opposite corners of the windows created on both the image and prescan regions of the CCD.

6.5.2 Results and Discussion

The mean bias level obtained within the windows created on the prescan regions were subtracted from the mean bias level obtained within the adjacent windows on the image regions. The results are plotted against time to investigate how the difference in the bias level between prescan and image region varies. As expected from the previous analysis (Section 6.2 to 6.4) there is no substantial change in the bias level over this short period $\sim$ 1.5 minutes. Figures 6.12 and 6.13 confirm the temporal stability of the difference in bias (image - overscan) for the four different readout windows for the data obtained in slow readout mode. In these figures the difference between the bias measured for the image and as measured from prescan is shown, i.e. difference mean bias = image region - prescan region. The error bars correspond to 100σ, where σ of the data taken in the fast readout is different to σ of the data taken in slow readout mode.

Results of the fast readout mode

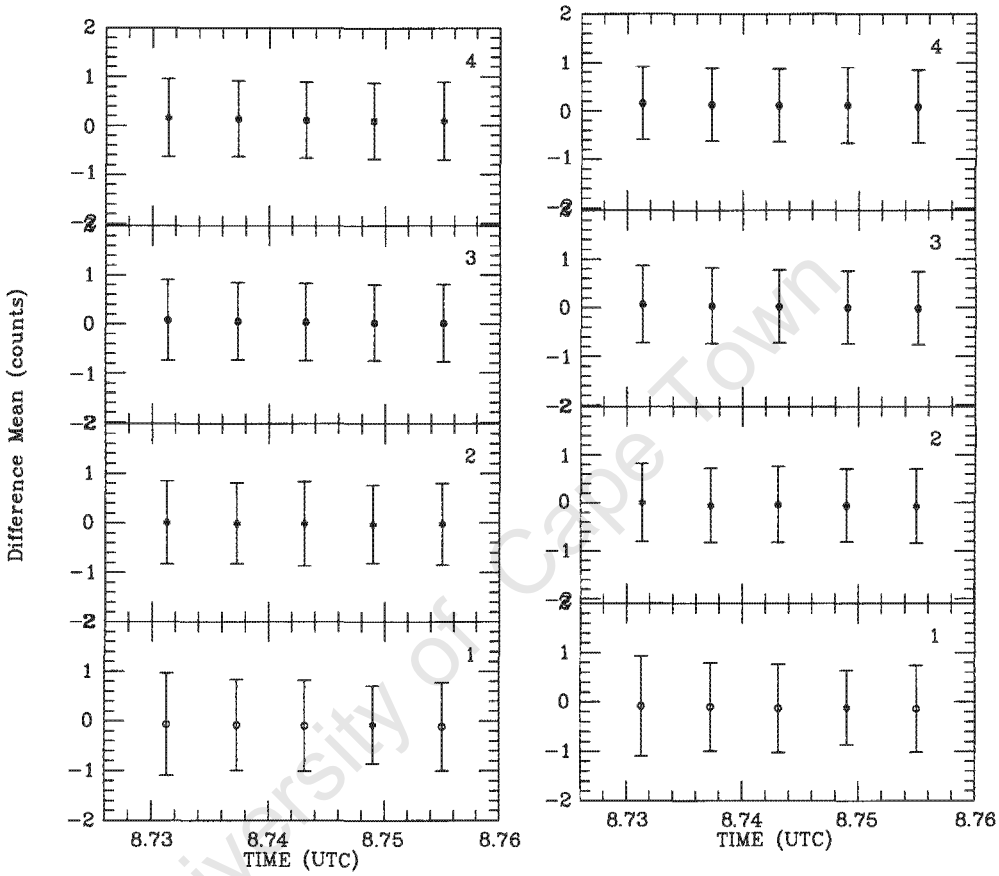

Figure 6.12: The difference in the mean bias level measured in the prescan and image regions (ADU counts) plotted against time (UT) for the first and the second channels of the **first CCD** (channel 1 and 2), respectively, for **fast readout mode**. The numbers 1, 2, 3 and 4 indicate the windows created in each individual image and the prescan region of the CCD (see Table 6.5). The error bars shown are 100σ error bars to ensure visibility.

University of Cape Town

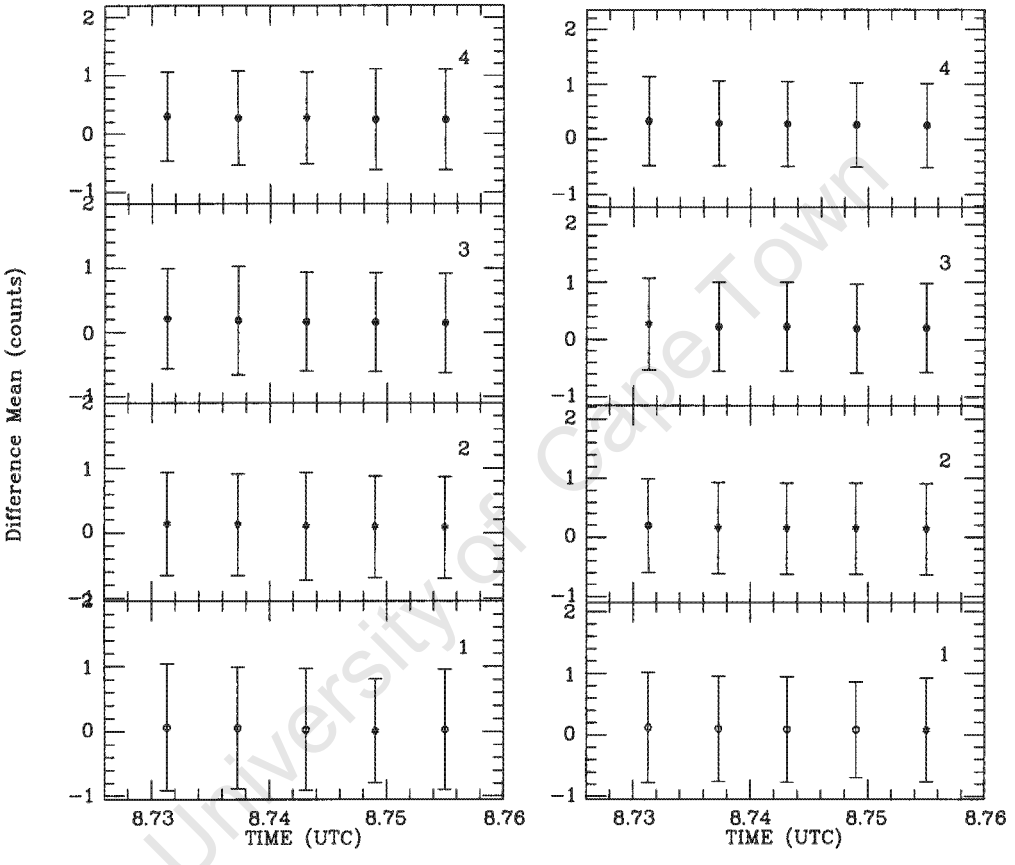

Figure 6.13: The difference in the mean bias level measured in the prescan and image regions (ADU counts) plotted against time (UT) for the first and the second channels of the **second CCD** (channel 3 and 4), respectively, for **fast readout mode**. The numbers 1, 2, 3 and 4 indicate the windows created in each individual image and the prescan region of the CCD (see Table 6.5). The error bars shown are 100σ error bars to ensure visibility.

University of Cape Town

Results of the slow readout mode

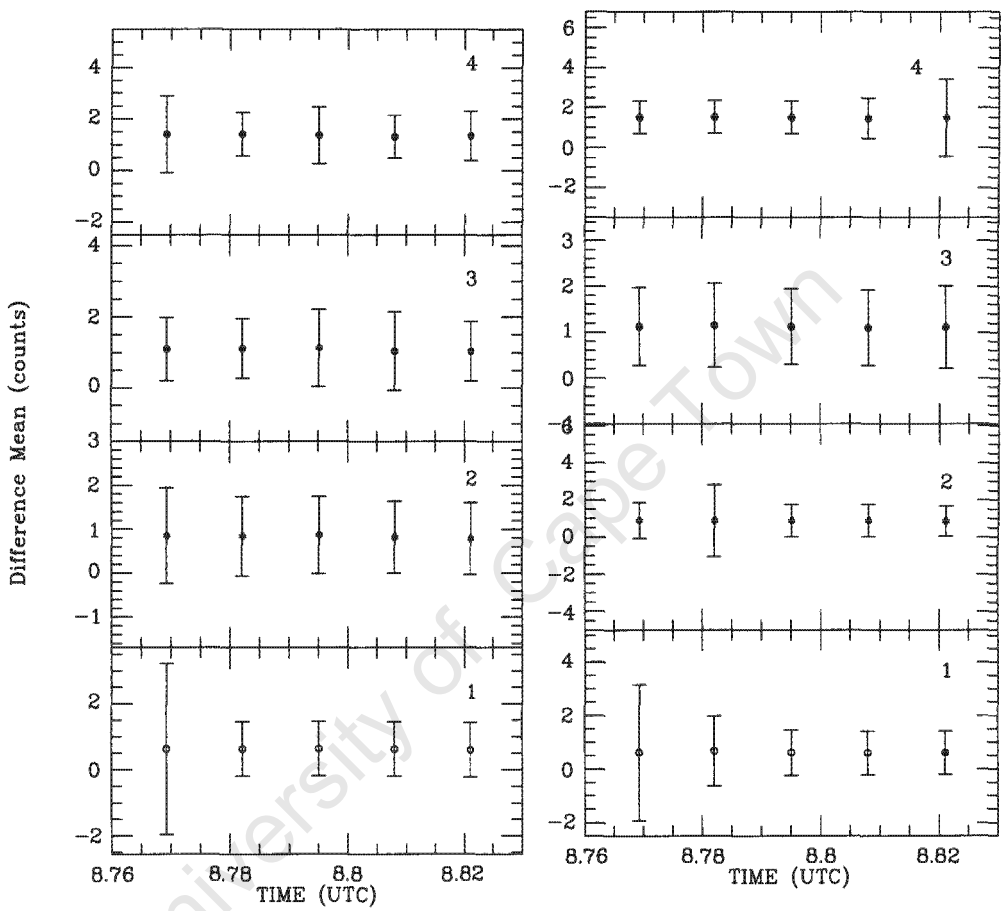

Figure 6.14: The difference in the mean bias level measured in the prescan and image regions (ADU counts) plotted against time (UT) for the first and the second channels of the **first CCD** (channel 1 and 2), respectively, for **slow readout mode**. The numbers 1, 2, 3 and 4 indicate the windows created in each individual image and the prescan region of the CCD (see Table 6.5). The error bars shown are 100σ error bars to ensure visibility.

University of Cape Town

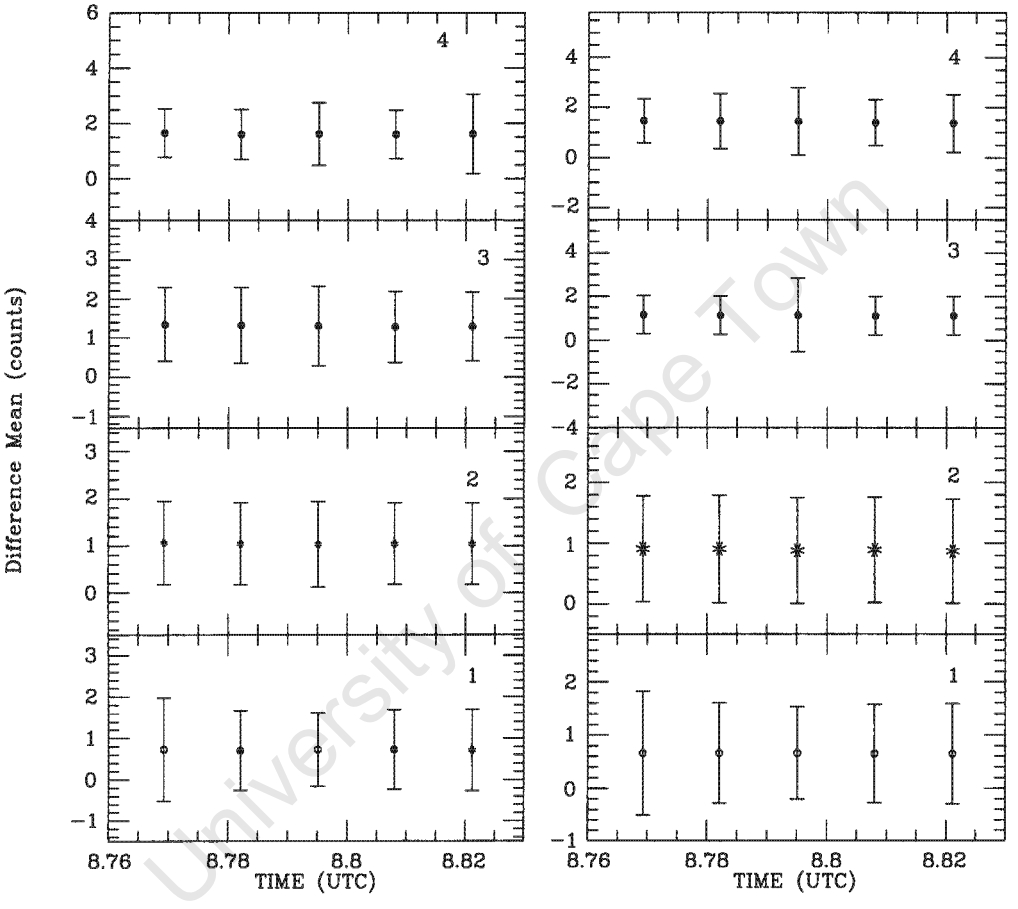

Figure 6.15: The difference in the mean bias level measured in the prescan and image regions (ADU counts) plotted against time (UT) for the first and the second channels of the **second CCD** (channel 3 and 4), respectively, for the **slow readout mode**. The numbers 1, 2, 3 and 4 indicate the windows created in each individual image and the prescan region of the CCD (see Table 6.5). The error bars shown are 100σ error bars to ensure visibility.

University of Cape Town

Discussion

Figures 6.12 to 6.15 show plots of the difference in the mean bias level on the image region and the prescan region against time. We have plotted the difference in the mean bias level on the image region and the prescan region at different areas of the CCD (windows 1 to 4, see Table 6.5). If the difference is positive then it implies that the bias level on the image area is higher than on the prescan region; if the difference is negative the bias level on the image region is lower than that on the prescan region.

We need to understand why there is a difference in bias level between the prescan and image regions in the first place. It is clear that the difference persists in both fast and slow readout modes. This is an important problem which needs further investigation as it means that the prescan region cannot be used to remove the bias. One needs to know whether it is the prescan bias or the image bias which correctly represents the true bias. Figure 6.16 shows the spatial correlation of the bias difference; there is a clear gradient in the mean bias level difference from top to bottom.

University of Cape Town

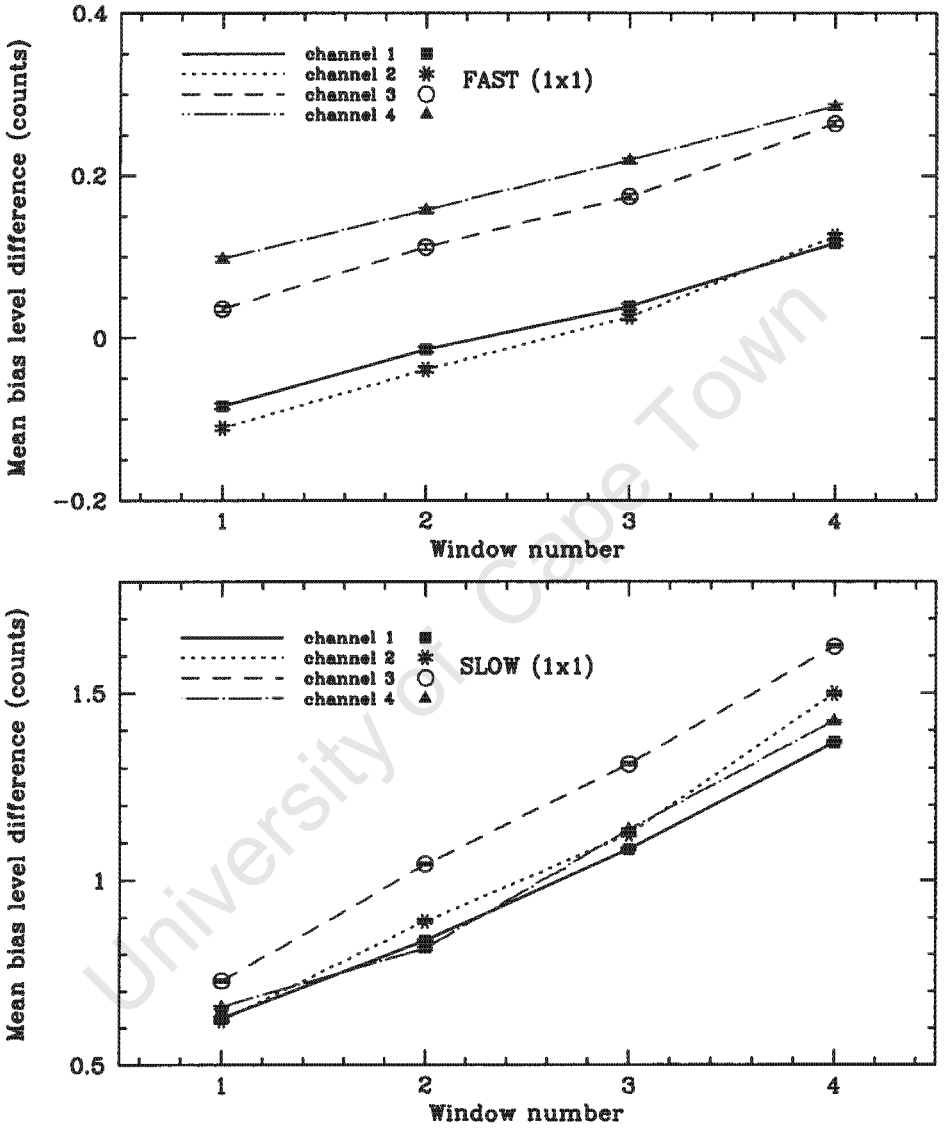

Figure 6.16: Plots of the mean bias level difference (in Figures 6.12 to 6.15) averaged over the four windows created in every channel of the four frames (y-axis) plotted against the window number (x-axis). These plots show that there is a spatial variation of bias level difference (image − prescan) from top to bottom in each channels (i.e. from windows 1 to 4, corresponding to measured y-position on the CCD).

University of Cape Town

6.5.3 Results using a 4×4 Binning Factor

In 4×4 binning, four columns and four rows are combined to form what is called a "superpixel". Binning is used to reduce the noise and to increase the signal-to-noise. The frames were obtained with the gain set to BRIGHT. Windows were created on the frames to do statistical analysis. Table 6.6 contains the coordinates of the windows created on the image and prescan regions.

	Image region				Prescan region			
CCD 1 (A) channel 1	X_1	X_2	Y_1	Y_2	X_1	X_2	Y_1	Y_2
1	72	188	39	245	2	8	39	245
2	72	188	275	467	2	8	275	467
3	72	188	519	725	2	8	519	725
4	72	188	765	955	2	8	765	955
CCD 1 (B) channel 2	X_1	X_2	Y_1	Y_2	X_1	X_2	Y_1	Y_2
1	350	466	39	245	530	536	39	245
2	350	466	275	467	530	536	275	467
3	350	466	519	725	530	536	519	725
4	350	466	765	955	530	536	765	955
CCD 2 (C) channel 3	X_1	X_2	Y_1	Y_2	X_1	X_2	Y_1	Y_2
1	610	726	39	245	540	546	39	245
2	610	726	519	725	540	546	519	725
3	610	726	275	467	540	546	275	467
4	610	726	765	955	540	546	765	955
CCD 2 (D) channel 4	X_1	X_2	Y_1	Y_2	X_1	X_2	Y_1	Y_2
1	888	1004	39	245	1068	1074	39	245
2	888	1004	275	467	1068	1074	275	467
3	888	1004	519	725	1068	1074	519	725
4	888	1004	765	955	1068	1074	765	955

Table 6.6: Coordinates $(X_1, Y1)$ and (X_2, Y_2) of diagonally opposite corners of the windows created on both the image and prescan regions of the CCD.

University of Cape Town

6.5.4 Results and Discussion

As previously performed for the 1×1 binning, a statistical analysis was performed in the windows specified by the coordinates in Table 6.6 (for 4×4) using the PIP software. The mean bias level on the prescan region was subtracted from the mean bias level on the image region. There were no variations of the bias as a function of time over a short period, as expected.

The results obtained using 4×4 binning, conform to those obtained using 1×1 binning, and indicate that the puzzling differences in bias level between prescan and image regions are not isolated to 1×1 binning. As observed in the 1×1 binning, the bias level did not show any variations as function of time in a short period.

As also observed in the 1×1 binning plots, the difference mean bias level on top panel (window 1) is lower than the difference mean bias level on bottom panel (window 4) in the 4×4 binning plots. Figure 6.17 shows spatial correlation of the bias difference. This is further evidence that mean bias level has a gradient from top to bottom (windows 1-4 in the figures). The other observation that was made is that the mean bias level on the prescan region is always lower than the mean bias level on the image region for both the fast and slow readout modes.

University of Cape Town

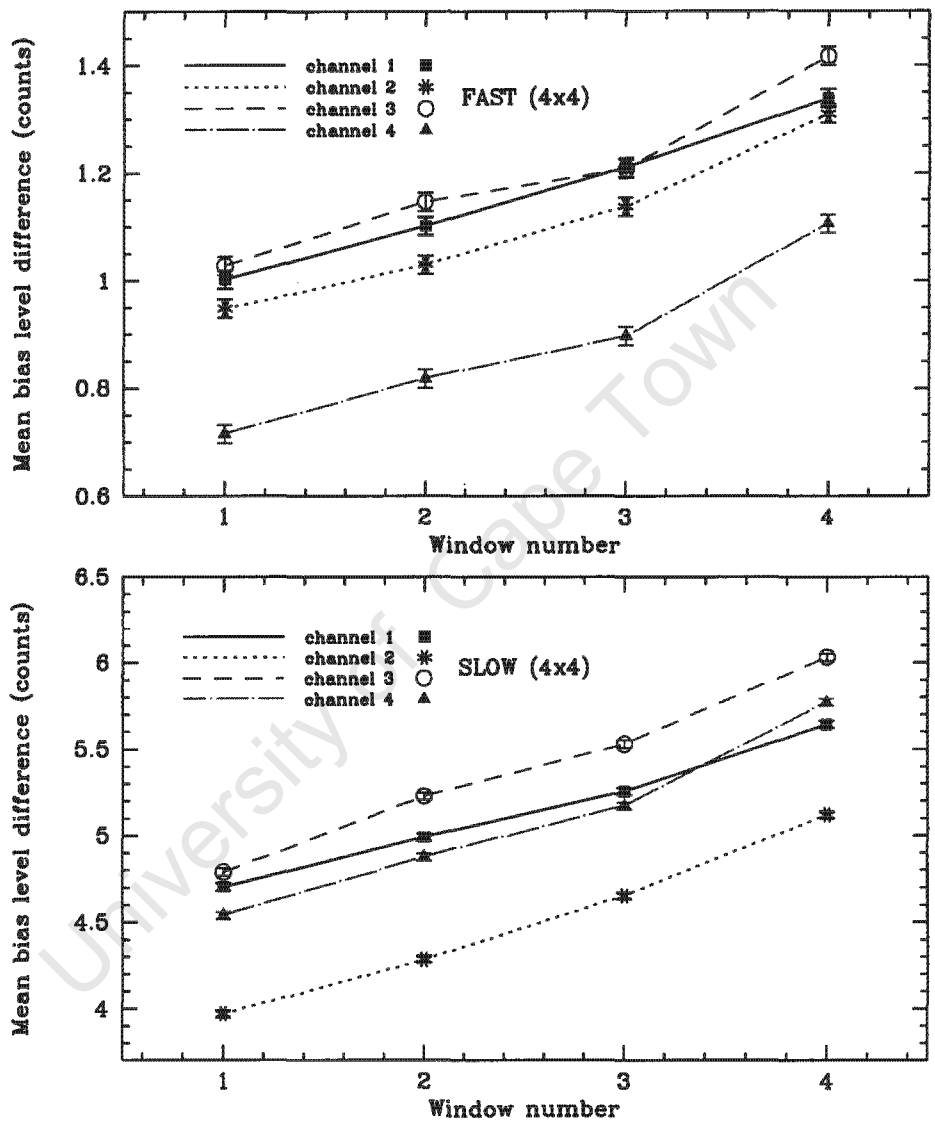

Figure 6.17: Plots of the mean bias level differences averaged over the four windows created in every channel of the four frames (y-axis) plotted against the window number (x-axis). These plots show that there is a spatial variation of bias level difference (image − prescan) from top to bottom in each channel (i.e. from windows 1 to 4, corresponding to y-position on the CCD).

University of Cape Town

6.5.5 Results using a 9×9 Binning Factor

As a final experiment in our investigation of the bias difference between image and prescan we present results using 9×9 binning. Table 6.7 shows the coordinates of the windows created in the prescan and the image regions of each channel.

Image region					Prescan region			
CCD 1 (A) channel 1	X_1	X_2	Y_1	Y_2	X_1	X_2	Y_1	Y_2
1	32	74	27	112	10	42	15	109
2	32	74	135	218	10	42	125	220
3	32	74	249	337	10	42	235	327
4	32	74	353	434	10	42	347	437
CCD 1 (B) channel 2	X_1	X_2	Y_1	Y_2	X_1	X_2	Y_1	Y_2
1	166	208	27	112	2106	2138	15	109
2	166	208	135	218	2106	2138	125	220
3	166	208	249	337	2106	2138	235	327
4	166	208	353	434	2106	2138	347	437
CCD 2 (C) channel 3	X_1	X_2	Y_1	Y_2	X_1	X_2	Y_1	Y_2
1	272	314	27	112	2158	2190	15	109
2	272	314	135	218	2158	2190	125	220
3	272	315	249	337	2158	2190	235	327
4	272	314	353	434	2158	2190	347	437
CCD 2 (D) channel 4	X_1	X_2	Y_1	Y_2	X_1	X_2	Y_1	Y_2
1	406	448	27	112	4254	4286	15	109
2	406	448	135	218	4254	4286	125	220
3	406	448	249	337	4254	4286	235	327
4	406	448	353	434	4254	4286	347	437

Table 6.7: Coordinates of diagonally opposite corners of the windows created on both the image and prescan regions of the CCD using 9×9 binning.

University of Cape Town

Results and Discussion

As observed in the previous sections the bias level did not show any significant variation as a function of time over a short period. Figure 6.18 shows, once again, a spatial correlation of the bias difference. The bias difference is positive, indicating that the mean bias level on the prescan region is always lower than the mean bias level on the image region (for both the fast and slow readout modes). These results conform to those obtained using 1×1 and 4×4, once again indicating clear differences in bias level between prescan and image regions, where the amount of bias difference varies per binning (compare the scales on Figures 6.16, 6.17 and 6.18).

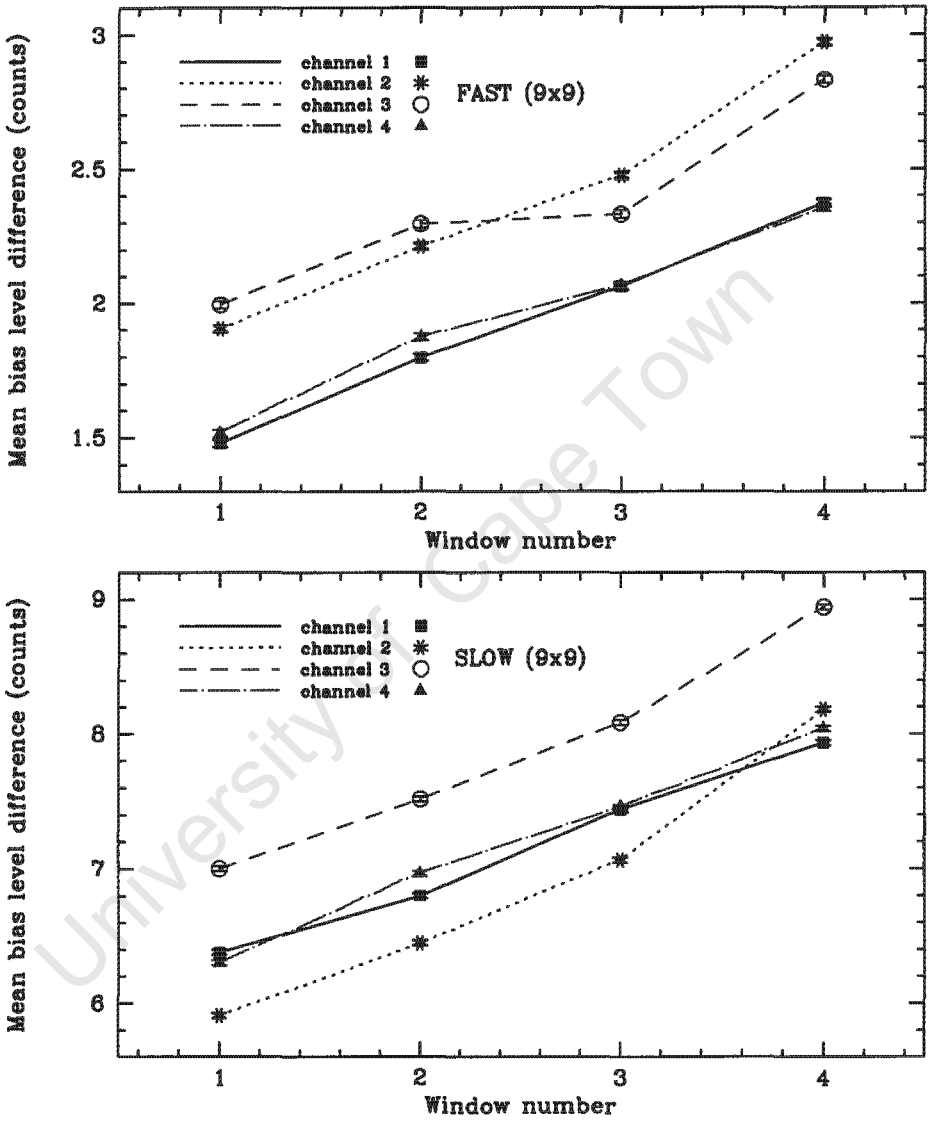

Figure 6.18: Plots of the mean bias level difference averaged over the four windows created in every channel of the four frames (y-axis) plotted against the window number (x-axis). These plots show that there is a spatial variation of the bias level difference (image − prescan) from top to bottom in each channel (i.e. from windows 1 to 4, corresponding to y-position on the CCD).

University of Cape Town

6.5.6 Analysis of contribution of the bias

In this subsection we are analysing the individual contribution of the image and prescan regions to the bias level of the CCD. In the previous sections we only looked at the bias difference. Variations of the bias difference can be due to variations in the image region, the prescan region, or a combination of both. For this analysis, we only investigate the behaviour of the first channel of the first CCD (CCD 1A = channel 1), as the overall variation seems similar for each of the channels. The three binnings (1×1, 4×4 and 9×9) are investigated.

In each of the different windows (see tables 6.5, 6.6 and 6.7 in pages 59, 66 and 69 respectively) in the first channel (image and prescan region), the mean of the bias of the five data frames was determined. Occasionally, only four frames were averaged, when the mean bias level was influenced by a cosmic ray. Also, it was noted that when changing readout mode (slow to fast, or vice versa), the bias level both in the prescan and image region takes some time to settle to a constant level (although the difference stays constant, see Figures 6.12 and 6.13). The first frame obtained after changing readout mode was not used in the determination of the mean bias because of this effect.

In Fig. 6.19 we show the variation of the mean bias level in the image region (filled circles) and the prescan region (crosses) in the lower boxes, and the difference bias level (filled squares, upper box), for each of the binnings used (1×1: upper panels, 4×4: middle panels, 9×9: lower panels) for the fast readout mode. The standard deviation of the mean bias level is 0.4, 1.8 and 1.4 counts, for 1×1, 4×4 and 9×9 binning respectively (same for image and prescan region). Both the bias and prescan bias levels decline as a function of increasing y-position on the CCD. It appears that this decline is not linear (most noticably in the 1×1 binning), although the variation (with y-position) of the bias diffeerence (image - prescan) is linear. With increasing binning, the difference between the bias in the image region and the prescan region clearly increases. This was seen before in Figs. 6.16, 6.17 and 6.18.

Fig. 6.20 shows the same for the slow readout mode. In this readout mode, the standard deviation of the mean bias level is 1.1, 0.2, and 3.4 counts, for 1×1, 4×4 and 9×9 binning respectively (same for image and prescan region). A slightly different behaviour is seen in the slow readout mode. A linear increase of the bias in the image region (4×4 and 9×9 binning) matched by a (linear) decrease of the bias level in the prescan region (as a function of the y-position of the CCD) gives rise to a clear linear increase in the bias difference. The level of this difference increases with binning, and is larger than in the fast readout mode. Comparing the mean level of the bias difference (averaged per channel) between the two readout modes, shows an increasing difference between fast and slow readout as a function of increasing binning (Table 6.8).

University of Cape Town

Binning	Channel 1	Channel 2	Channel 3	Channel 4
1×1	0.96	1.01	1.03	0.82
4×4	3.99	3.4	4.2	4.22
9×9	5.21	4.51	5.52	5.24

Table 6.8: The offset of the averaged bias difference (averaged per channel) between the slow and fast readout modes (slow - fast) for different binning factors.

6.6 Conclusion

The purpose of the first experiment was to examine the variation of the bias level with time in both the overscan and the image regions and to determine the relationship of the bias level and the temperature of the components (i.e. the Cold End, Cold Box, SDSU and the heater). It was found that the bias level in the SALTICAM CCDs varies with time. This is shown by Figure 6.2 [page 47] for fast readout mode and for the slow readout mode this can be seen in Figure 6.3 [page 48].

It was also found that the bias level and the temperature of the SDSU are strongly correlated. This is shown by Figures 6.10 [page 56], 6.11 [page 57], 6.8 [page 54] and 6.9 [page 55] that as the bias level increases (decreases) the SDSU temperature increases (decreases) as well. It is therefore concluded, that the SDSU temperature needs to be stabilised to give constant bias level.

The objective of the second experiment was to investigate the difference in the bias level on the image and the prescan regions and to examine the spatial variation on the image and the prescan regions of the CCDs for both the fast and slow readout modes. Figures 6.16 [page 65], 6.17 [page 68] and 6.18 [page 70] show that the bias level on both the prescan and the image region is not constant along a column, but showing clear spatial variation. The bias level in window 1 is lower than in window 4 on every channel of both CCDs.

The plots on Figures from 6.12 to 6.15, [refer to pages from page 60 to 63] shows that there is difference in the bias level between the prescan region and the image region. This is quite a serious problem, the bias level on the prescan still needs to be correct for more accurate data acquisition. In all cases the bias level from the image region is larger than that from prescan region. Figures 6.19 and 6.20 show which part of the CCD contributes to the difference between the image area and the overscan. One possible explanation for the differences between the bias level in the prescan and image regions could be light leakage on to the CCD image region, because light will affect the image region, but not the prescan region. Also, we note that the difference in bias level increase with binning, see Table 6.8.

University of Cape Town

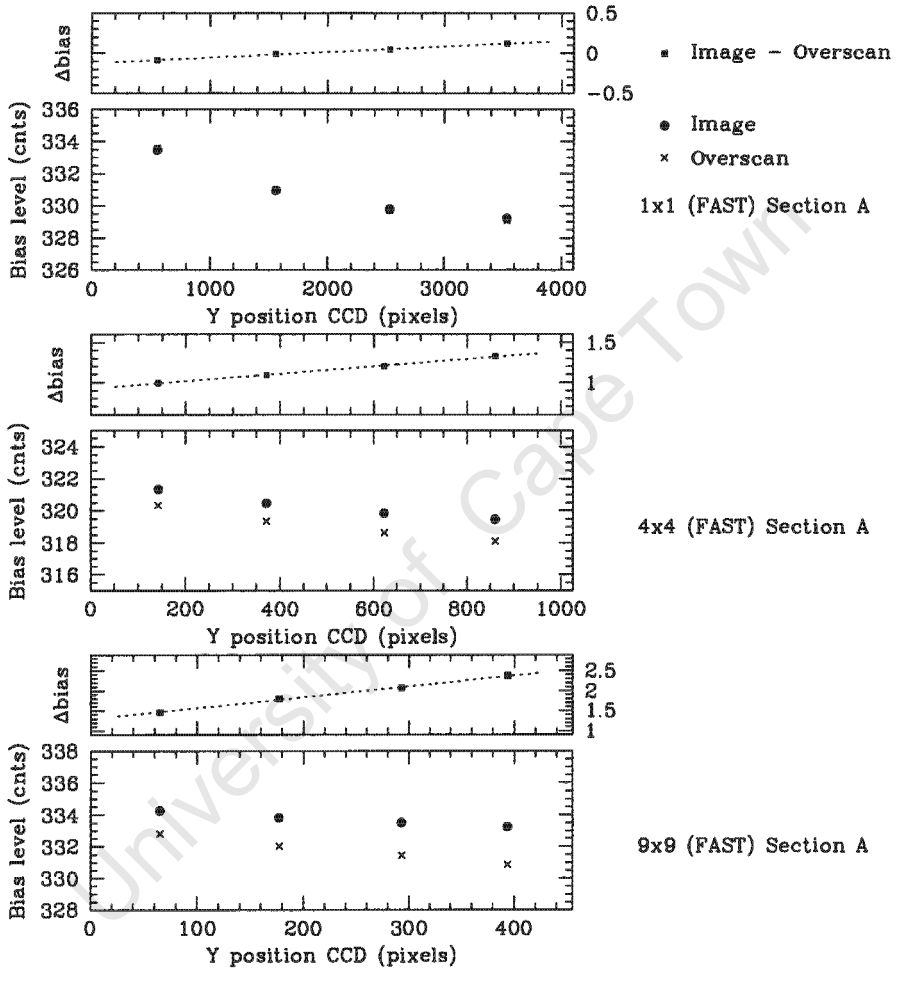

Figure 6.19: The spatial variation along the first readout section (A, i.e. channel 1) of the first CCD for different binning factors (top: 1×1, middle: 4×4, bottom: 9×9). For each binning the difference (shown by filled squares) and the individual values (image region: filled circles, overscan image: crosses) were plotted against position on the CCD. These plots are for the **fast readout mode**.

University of Cape Town

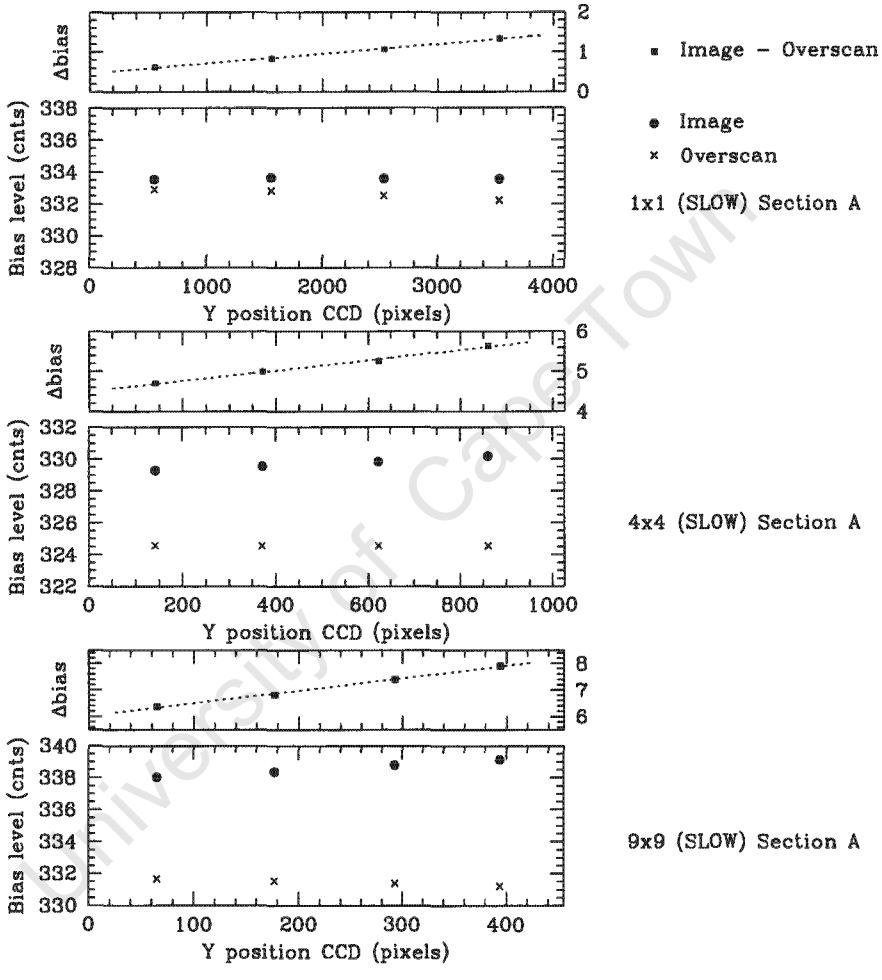

Figure 6.20: The spatial variation along the first readout section (A, i.e channel 1) of the first CCD for different binning factors (top: 1×1, middle: 4×4, bottom: 9×9). For each binning the difference (shown by filled squares) and the individual values (image region: filled circles, overscan image: crosses) were plotted against position on the CCD. These plots are for the **slow readout mode**.

University of Cape Town

Chapter 7

The Effect of Aperture Size on Photometry

University of Cape Town

7.1 Introduction

In this final chapter an investigation of the effect of aperture size on photometry is presented using artificial frames. These artificial frames contained stars with known intensities and positions. They were generated using a program developed by my supervisor (Dr. L. A. Balona), see Figure 7.1. This program is capable of generating calibration frames (i.e. bias, dark and flat-field frames), stellar image frames, spectrum frames and the photon transfer frames for testing purposes. The program reads the Point Spread Function (PSF) profile from a file that contains the PSF data. It allows the user to choose the number of CCDs, the prescan factors and numbers of amplifiers that one wants to use for a particular test. The user can choose the number of frame to be generated, the mean sky level and number of cosmic rays in the frames.

For this thesis, the stars in the generated frames were chosen in order of their brightness. The stellar frames were sparse and no noise was added during the generation of the artificial frames. Even though the absence of noise in the artificial frames might limit a comparison with real data (which do have noise), it does not impact on the current investigation where we solely investigate multi-aperture versus psf-fitted photometry for bright and faint stars. In comparison with real data, our errors might seem somewhat small. We used uncrowded fields because the crowded-field is discussed in Schechter et. al (1993). The sky background was set to 50 ADU/pixel. Photometry information from these artificial frames was extracted using the IRAF/DAOPHOT package which has several tasks embedded to perform both aperture and point spread function fitted photometry. Different aperture sizes (i.e. radius of 3, 5, 8, 11, 14, 17 and 21 pixels) were used to measure the intensities of these stars in order to investigate how the intensity changes with aperture size. A

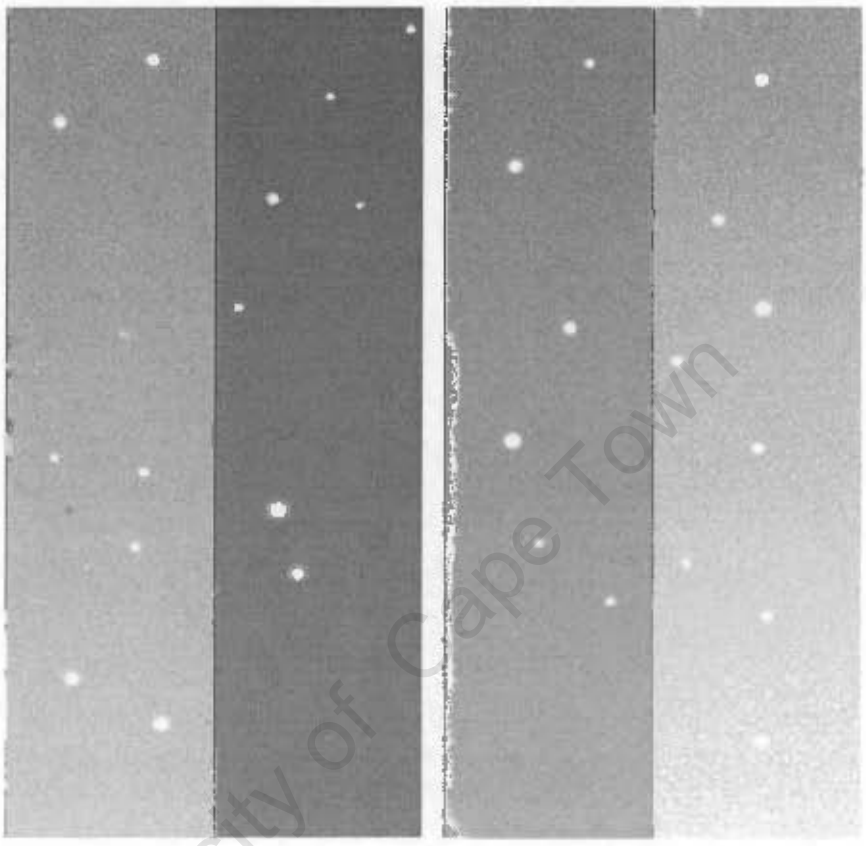

Figure 7.1: This is an artificial SALTICAM image generated using a program developed by Dr. L.A. Balona. This frame shows all the stars that were used in the experiments performed in this chapter

University of Cape Town

sky annulus with a radius of 25 pixels and a width of 12 pixels was used for every aperture size. As explained in a previous chapter, Chapter 5, the total intensity within the aperture is a contribution from both the star and the background sky. After obtaining the magnitudes, the measured magnitudes were compared with both the true magnitudes of those stars and the profile fitting results.

Since the stars in the frame were generated with known intensities, I_a, the known magnitudes are simply given by

$$m_a = -2.5 \log(I_a), \tag{7.1}$$

where m_a is the magnitude of star and I_a is the known intensity of the star above the sky. These known magnitudes were measured relative to that of the brightest star in this investigation (star 2, channel 2, $m = -11.482$ mag).

Input Parameter	
PSF	Gaussian
FWHM	5.1 pixels
Sky	50 ADU/pixel
Noise	No
Stars/CCD	6 to 7
Range of Mag.	-11.482 to -5.637

Table 7.1: The parameters used to generate the image that was used for this work.

7.2 Results and Discussions

7.2.1 Aperture Magnitude vs True magnitude

The information about the Full Width at Half Maximum (FWHM) of the PSF was obtained using the **imexam** task, and pressing "r" or "h" keys on the keyboard for the radial profile or the histogram respectively. The FWHM PSF of the brightest, isolated stars was found to be ~5 pixels. This value was used to determine the algorithm parameters, amongst other things the sky annulus and the initial aperture size for performing the initial photometric extraction.

The **phot** task was used to measure the multi-aperture magnitudes of these stars. After performing multi-aperture photometry, the **mkapfile** task was used to compute the aperture correction. The aperture correction[1] helps in obtaining good S/N and helps in crowded field. This aperture correction, which is always negative, (see Figure 7.2) is added to the magnitude obtained using a smaller aperture to get the estimate of the total instrumental magnitude. All the aperture magnitudes quoted in all the tables in this chapter and used in the comparison with the "input" magnitudes and PSF-fitting magnitudes are aperture-corrected. The aperture-corrected magnitudes were compared with the input values by computing the differences of the two magnitudes, in the sense of measured-input. All the magnitudes are calculated relative to the brightest star in the sample (star2 of channel 2), see Tables 7.2 and 7.3. A FORTRAN code was used to perform the calculations of the magnitudes and the magnitude differences (see Appendix F).

Tables 7.4 and 7.5 show the values of the difference in the magnitudes for each aperture size used. The negative values show that the measured magnitude values are brighter than that of the true magnitudes. Overestimating the sky background value affects the measurement of the magnitude, as a result of using larger sky annuli and apertures. If the sky correction value is bigger, it minimises the goodness of the estimate of the intensity. The deviations of the measured magnitudes from the true

[1]If one has a frame with several faint and bright stars, we measure the bright stars using a small aperture (say radius = 1 FWHM) and also with a bigger aperture (say 4 FWHM). The ratio of light in the small to large aperture, is called the aperture correction.

University of Cape Town

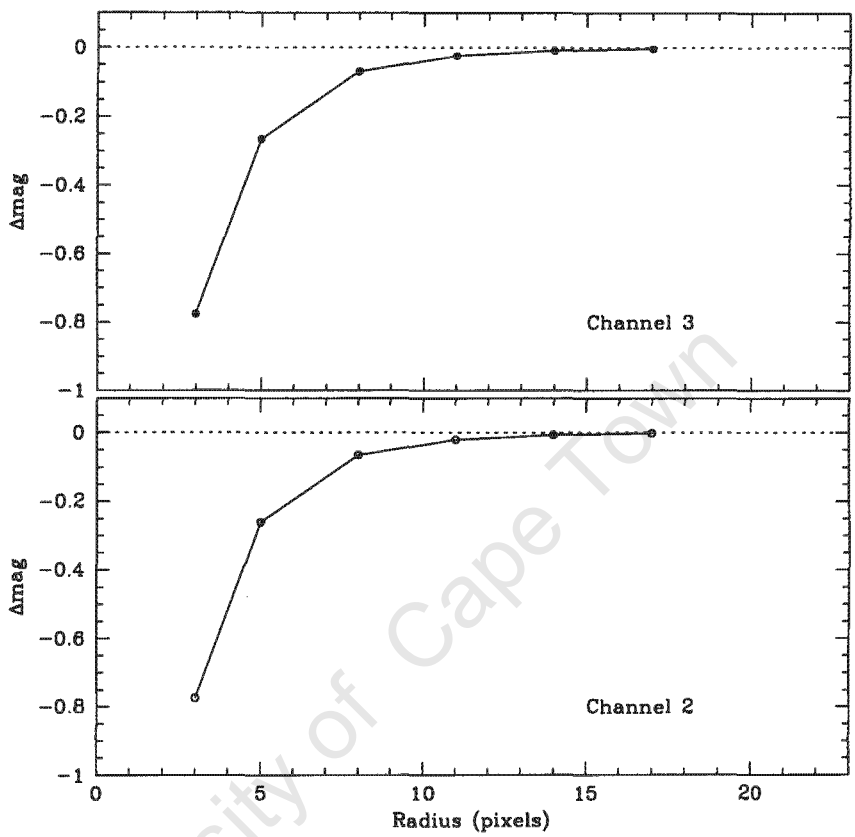

Figure 7.2: These plots show the curves of growth(aperture-correction) for channels 2 (bottom panel) and channel 3 (top panel).

magnitudes were plotted against the aperture sizes in Figure 7.3. These differences in the magnitude values show that the bigger apertures have large errors than the smaller apertures (see Tables 7.4 and 7.5), however this is not always the case. In some cases small apertures can be too small to let a significant fraction of light through, so that photometric errors will be dominated by Poisson statistics. Figure 7.4 shows the difference in the averaged aperture magnitude and the input magnitude for each of the stars. The errors increase dramatically towards the fainter magnitudes and significant deviations start to occur.

University of Cape Town

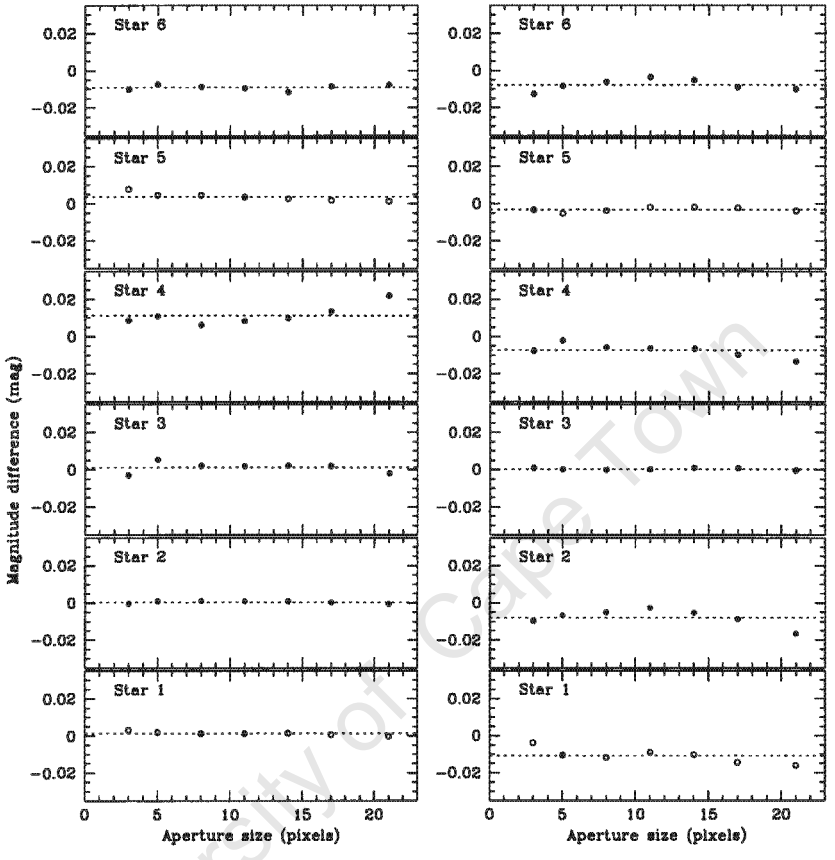

Figure 7.3: These plots show the deviation of the measured magnitude from the true magnitude in channels two (left panel) and three (right panel).

University of Cape Town

Aper Size	Star 1	Star 2	Star 3	Star4	Star 5	Star 6
3.	1.296	0.0	3.442	4.982	2.638	4.103
5.	1.294	0.0	3.449	4.983	2.634	4.105
8.	1.293	0.0	3.446	4.978	2.633	4.103
11.	1.293	0.0	3.446	4.980	2.633	4.103
14.	1.294	0.0	3.446	4.982	2.632	4.101
17.	1.293	0.0	3.447	4.986	2.632	4.104
21.	1.293	0.0	3.444	4.996	2.632	4.106
True mags	-10.189	-11.482	-8.037	-6.509	-8.852	-7.369

Table 7.2: The measured magnitudes of stars in channel two and a row containing the true magnitudes of these stars. All magnitudes are calculated relative to the brightest star in channel 2, Star 2.

Aper Size	Star 1	Star 2	Star 3	Star4	Star 5	Star 6
3.	4.573	4.645	1.744	3.02	2.833	4.314
5.	4.566	4.646	1.742	3.025	2.83	4.317
8.	4.564	4.648	1.742	3.021	2.831	4.319
11.	4.567	4.65	1.742	3.021	2.833	4.322
14.	4.566	4.648	1.743	3.02	2.833	4.320
17.	4.562	4.645	1.744	3.018	2.834	4.317
21.	4.562	4.638	1.743	3.015	2.833	4.317
True mags	-6.905	-6.828	-9.739	-8.454	-8.646	-7.156
Profile mags	-6.915	-6.836	-9.739	-8.458	-8.651	-7.161

Table 7.3: The measured magnitudes of stars in channel three and a row containing the true magnitudes of these stars. All magnitudes are calculated relative to the brightest star in channel 2, Star 2.

University of Cape Town

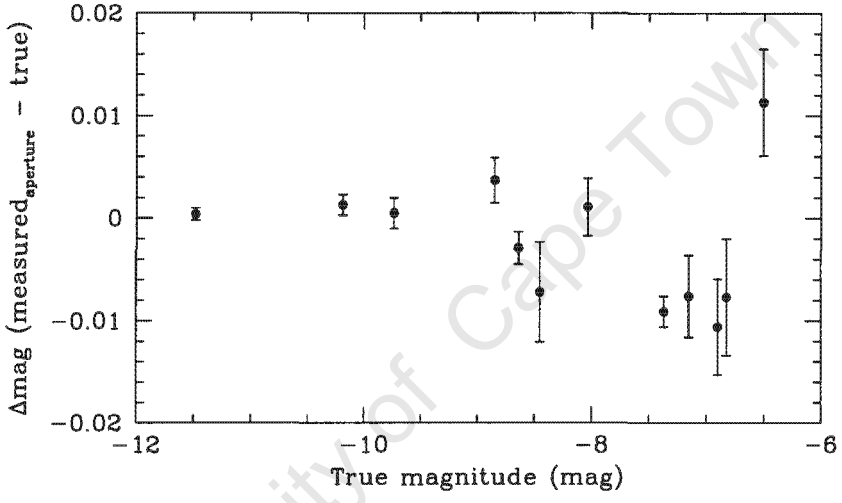

University of Cape Town

Figure 7.4: The difference of the averaged-aperture magnitudes and the 'true' magnitude as a function of brightness of the star. Significant deviations occur for faint stars.

7.2.2 Aperture Magnitude vs Profile Fitting Magnitude

The **pstselect** task was used to select stars that were used for computing the PSF model for all stars in the frame. These stars were then used in the **psf** task to compute the PSF model that is fitted to all stars in the frame. The PSF model that was used was a Gaussian. This PSF model is fitted to the stars and subtracted from the frame using the **allstar** task. At the end of the run, the task also outputs the best fit magnitudes for all the stars. If the subtracted stars are not visible or there is no evidence of where they were, then this means that the PSF model fits the data well. But if the subtracted stars are still visible, then the PSF model is not a good model for the data and has to be recomputed using different set of stars.

Aper Size	Star 1	Star 2	Star 3	Star4	Star 5	Star 6
3.	0.003	0.000	-0.003	0.009	0.008	-0.01
5.	0.002	0.001	0.005	0.011	0.005	-0.007
8.	0.001	0.001	0.002	0.006	0.004	-0.009
11.	0.001	0.001	0.002	0.008	0.003	-0.009
14.	0.002	0.001	0.002	0.01	0.003	-0.012
17.	0.001	0.000	0.002	0.013	0.002	0.008
21.	0.000	-0.001	-0.002	0.022	0.001	0.008
Mean Difference	0.000	0.001	0.001	0.011	0.004	-0.009

Table 7.4: The magnitude difference between the aperture-corrected magnitude and the true magnitude of the star in channel two (i.e. the true magnitude is subtracted from the measured magnitude).

Aper Size	Star 1	Star 2	Star 3	Star4	Star 5	Star 6
3.	-0.004	-0.01	0.01	-0.008	-0.004	-0.013
5.	-0.011	-0.007	0.00	-0.002	-0.005	-0.008
8.	-0.012	-0.005	0.00	-0.006	-0.004	-0.006
11.	-0.009	-0.003	0.00	-0.006	-0.002	-0.004
14.	-0.01	-0.005	0.001	-0.007	-0.002	-0.005
17.	-0.014	-0.009	0.001	-0.010	-0.002	-0.009
21.	-0.016	-0.017	0.00	-0.013	-0.004	-0.01
Mean Difference	-0.011	-0.008	0.000	-0.007	-0.003	-0.008

Table 7.5: The magnitude difference between the aperture-corrected magnitude and the true magnitude of the star in channel three (i.e. the true magnitude is subtracted from the measured magnitude).

The best fit magnitudes of the stars are calculated relative to the brightest star used in this investigation. The profile fitting magnitudes were subtracted from the aperture magnitudes to investigate the deviation of the aperture magnitudes from the profile fitting magnitudes. Tables 7.6 and 7.7 contain the difference between the profile fitting magnitudes and the aperture magnitudes of the selected stars. The negative values in Tables 7.6 and 7.7 tell us that the aperture magnitudes are brighter than the profile fitting magnitudes. Positive values show that the aperture magnitudes are fainter than the profile fitting magnitudes. Differences can occur because there are some defects in modeling the PSF caused by the centering. The magnitude differences are plotted against the aperture sizes (see Figure 7.5) to investigate the distribution of the deviations. Figure 7.6 shows the difference in the averaged aperture magnitude and the psf-fitted magnitude. Compared to Figure 7.4, the difference at fainter magnitudes deviates far less significantly.

University of Cape Town

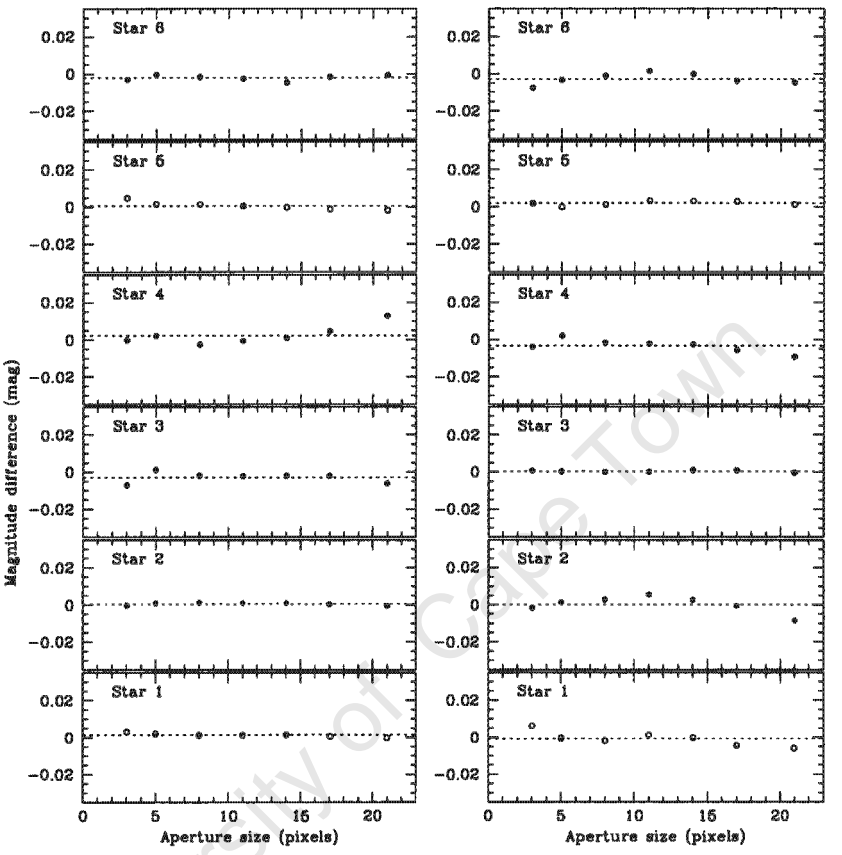

University of Cape Town

Figure 7.5: These plots show the deviation of the aperture magnitude from the profile fitting magnitude in channels two and three respectively.

Aper Size	Star 1	Star 2	Star 3	Star4	Star 5	Star 6
3.	0.003	0.000	-0.007	0.000	0.005	-0.003
5.	0.002	0.001	0.001	0.002	0.002	-0.000
8.	0.001	0.001	-0.002	-0.003	0.001	-0.002
11.	0.001	0.001	-0.002	-0.001	0.000	-0.002
14.	0.002	0.001	-0.002	0.001	0.000	-0.005
17.	0.001	0.000	-0.002	0.004	-0.001	-0.002
21.	0.000	-0.001	-0.006	0.013	-0.002	-0.001
Mean Difference	0.001	0.000	-0.003	0.002	0.001	-0.002
Profile mags	-10.189	-11.482	-8.033	-6.5	-8.849	-7.376

Table 7.6: This table shows the values of the difference between the aperture magnitudes and the profile fitting magnitudes of the stars in channel two (i.e. the profile magnitude is subtracted from the measured magnitude).

Aper Size	Star 1	Star 2	Star 3	Star4	Star 5	Star 6
3.	0.006	-0.002	0.001	-0.004	0.002	-0.008
5.	-0.001	0.001	0.000	0.002	0.000	-0.003
8.	-0.002	0.003	0.000	-0.002	0.001	-0.001
11.	-0.001	0.005	0.000	-0.002	0.003	0.001
14.	0.000	0.003	0.001	-0.003	0.003	0.000
17.	-0.004	-0.001	0.001	-0.006	0.003	-0.004
21.	-0.006	-0.009	0.000	-0.009	0.001	-0.005
Mean Difference	-0.001	0.000	0.000	-0.003	0.002	-0.003
Profile mags	-6.915	-6.836	-9.739	-8.458	-8.651	-7.161

Table 7.7: This table shows the values of the difference between the aperture magnitudes and the profile fitting magnitudes of the stars in channel three (i.e. the profile magnitude is subtracted from the measured magnitude).

University of Cape Town

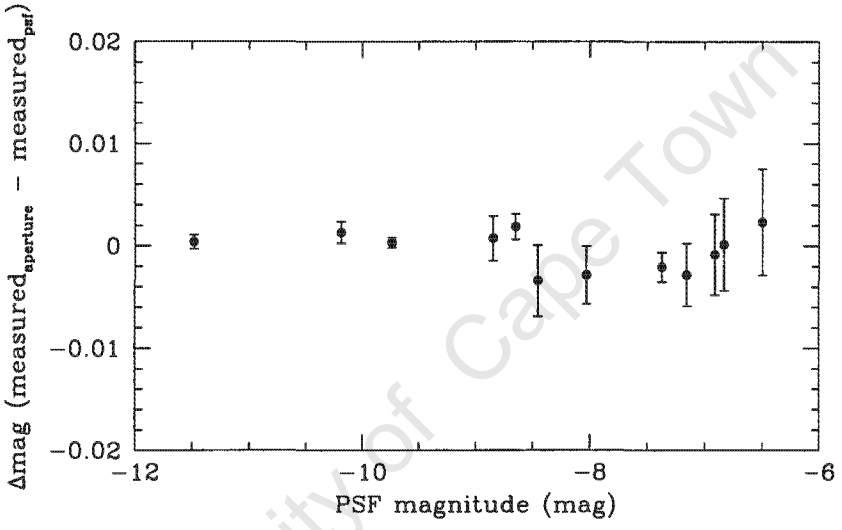

University of Cape Town

Figure 7.6: The difference of the averaged-aperture magnitude and the 'psf-fitted' magnitude as a function of brightness of the star. A much better agreement is found over all brightnesses compared to Figure 7.4.

7.2.3 Comparing the Profile Fitting and the True magnitude

Tables 7.8 and 7.9 show the differences between the true and the profile fitting magnitudes of the stars in the channels 2 and 3 respectively. Negative differences show that the profile magnitudes are brighter than true magnitudes and positive differences show that profile fitting magnitudes are fainter than the true magnitudes. This is as a result of imperfect computation of the PSF model.

	Star 1	Star 2	Star 3	Star4	Star 5	Star 6
Profile mags	-10.189	-11.482	-8.033	-6.5	-8.849	-7.376
True mags	-10.189	-11.482	-8.037	-6.509	-8.852	-7.369
Difference mag	0.00	0.0	0.004	0.009	0.003	-0.007

Table 7.8: The difference between the profile and the true magnitudes of the stars in channel two.

	Star 1	Star 2	Star 3	Star4	Star 5	Star 6
Profile mags	-6.915	-6.836	-9.739	-8.458	-8.651	-7.161
True mags	-6.905	-6.828	-9.739	-8.454	-8.646	-7.156
Difference mag	-0.01	-0.008	0.0	-0.004	-0.005	-0.011

Table 7.9: The difference between the profile and the true magnitudes of the stars in channel three.

7.2.4 The Error Associated with Magnitude Measurement

For a given star brightness, the uncertainty associated with the magnitude measurement within an aperture can be calculated from the signal-to-noise (S/N). The magnitude uncertainty is

$$\begin{aligned} \Delta m &\approx 2.5 \log\left(\frac{S+N}{S}\right) \\ &\approx 2.5(0.43429) \ln\left(\frac{S+N}{S}\right) \\ &\approx 2.5(0.43429)\left(\frac{N}{S}\right) \\ &\approx 1.0857\left(\frac{S}{N}\right)^{-1} \end{aligned} \tag{7.2}$$

$$\sigma_{Mag.error} = \frac{1.0857\sqrt{(S/G) + N\sigma_B^2 + (N^2\sigma_B^2/N_A)}}{S}, \tag{7.3}$$

where the factor 1.0857 is given by $(2.5/\ln(10))$; S is the total flux (in electrons) from the star within the chosen aperture of size N. G is the CCD gain (in electrons per ADU) and σ_B is the standard deviation of the sky background measurement within the sky annulus N_A (see Equation 5.5). The approximation from second step to the third step of Equation 7.2 can only be done under high signal-to-noise (S/N) consideration. The third step is obtained using natural logarithm series ($\ln(1+x) = x - \frac{1}{2}x^2 + \frac{1}{3}x^3$, with $x \ll 1$, in our case $x = N/S$). From Equation 7.3, it can be seen that as the aperture size increases the value of the magnitude error increase for faint stars.

University of Cape Town

Tables 7.10 and 7.11 show the magnitude errors in the aperture magnitudes of stars in channels two and three respectively. All the magnitude errors are calculated relative to the brightest star in each channel (see propagation of uncertainty in Taylor 1997). The magnitude errors of both stars 4 and 6 in Table 7.10 are larger than those of stars 1, 3 and 5, because stars 4 and 6 are fainter than the other stars. Looking at the magnitude errors in Tables 7.10 and 7.11, they are larger for some of the smaller apertures and get smaller for bigger apertures, since there is more intensity in smaller apertures. For some fainter stars, at bigger apertures the magnitude errors become the same as that of the smaller apertures. This is because the sky intensity is comparable to the intensity of the star.

Aper Size	Star 1	Star 2	Star 3	Star4	Star 5	Star 6
3.	0.003	0.0	0.007	0.014	0.005	0.010
5.	0.003	0.0	0.006	0.012	0.004	0.008
8.	0.003	0.0	0.006	0.012	0.004	0.008
11.	0.003	0.0	0.006	0.013	0.004	0.008
14.	0.003	0.0	0.006	0.015	0.004	0.009
17.	0.003	0.0	0.006	0.017	0.004	0.009
21.	0.003	0.0	0.006	0.021	0.005	0.010

Table 7.10: This table shows the values of the magnitude errors of the stars in channel two. All the errors are calculated relative to the bright star.

Aper Size	Star 1	Star 2	Star 3	Star4	Star 5	Star 6
3.	0.009	0.011	0.0	0.011	0.011	0.011
5.	0.007	0.009	0.0	0.009	0.009	0.009
8.	0.007	0.009	0.0	0.009	0.009	0.008
11.	0.007	0.009	0.0	0.009	0.009	0.008
14.	0.007	0.009	0.0	0.009	0.009	0.009
17.	0.007	0.009	0.0	0.010	0.009	0.009
21.	0.008	0.010	0.0	0.010	0.010	0.009

Table 7.11: This table shows the values of the magnitude errors of the stars in channel three. All the errors are calculated relative to the bright star.

University of Cape Town

7.3 Conclusion

For faint stars larger apertures do not give good results because of a large sky contribution, thus making the errors large (see Figure 7.4 and 7.6). When using bigger apertures, the statistical fluctuations are higher and the signal-to-noise is small. Small photometric errors are obtained using small apertures, whereas large apertures can have large photometric errors when the total number of stellar photons in the aperture becomes comparable with the total number of background photons in the aperture.

Small apertures are dominated by errors from the Poisson statistics. Since a small signal is measured, the other sources of noise in the S/N equation carry less weight. The contribution from the star can be increased (decreased) by underestimating (overestimating) the sky background. A measurement error for the background intensity as small as just 1 electron per pixel can by itself produce large photometric uncertainties at large aperture radii. The background sky is normally larger than the star intensity in the aperture for faint stars.

It is clear that profile fitting gives better results than aperture photometry for faint stars (see Figure 7.6, and Tables 7.6 and 7.7). The difference between the true and the profile fitting magnitudes are smaller than that of the true and aperture photometry magnitudes. This can be seen in the magnitude difference of stars 4 and 6 in Tables 7.4 and 7.6 and stars 1 and 2 in Tables 7.5 and 7.7. Profile fitting has the ability to minimise the noise by weighting the fitting. It is more sensitive to varying PSF and pixel-centering, than aperture photometry. When dealing with faint stars it is best to use profile fitting for accurate photometry (Suchkov and Casertano 1997).

Aperture photometry gives good results for bright stars, as can be clearly seen in Figures 7.3 and 7.5 (stars 1 and 5 in channel 2). These plots shows that for smaller apertures we get a higher intensity than for large apertures. Some of the results presented in Tables 7.10 and 7.11 agree with the theoretical expectation given by Equation 7.3, however for an aperture size of 3 pixel, the errors are larger than in an aperture size of 5 pixel. This expectation is that for a given brightness, the magnitude error is larger for smaller aperture and vice versa.

In summary, aperture photometry gives good results for bright stars and well exposed images, while profile fitting is the best when undertaking accurate photometry of faint stars.

University of Cape Town

Conclusions and Recommendations

In this project, the aim was to study and understand the use of CCDs in astronomy. I used the SALTICAM imaging camera on SALT for this purpose. I first summarized the theory behind the practical use of CCDs, then applied this knowledge to resolve a particular problem experienced with SALTICAM. This problem was the observation that the bias levels were unstable and drifted during the night. In a series of experiments performed at the SAAO in Sutherland, I found that the drift in the bias level was strongly correlated with the temperature of the SDSU controller, housing the electronics. This relationship was found to be linear in most of the data, and cubic in one instance. With this information, the solution to the problem became apparent; the SDSU temperature needs to be tightly controlled to stabilize the bias level.

Since SALTICAM will be used to obtain accurate photometry of stellar fields, it is necessary to have a good understanding of how photometric information can be extracted from a CCD image. To this effect, I investigated the theory of aperture photometry. I performed a series of simulations where an image was created with artificial stars of known brightnesses. Extraction of aperture magnitudes of these stars using different aperture sizes confirmed that the simulations did indeed correspond to the theoretical predictions. This information led to a better understanding of the possible problems that might confront the extraction of photometric information from real SALTICAM data.

The effect of aperture size in photometry was investigated using artificial stellar frames. The experiments perfomed confirmed the theoretical expectations that best magnitude measurements are obtained using small apertures, whereas bigger apertures have higher statistical fluctuations reducing the signal-to-noise ratio. Bigger apertures do not work effectively for faint stars, since most of the contributions will be from the background sky. Hence increasing the aperture size reduces the signal-to-noise ratio, since the statistical fluctuations increase. The other important factor to consider during aperture photometry is the background sky determination. If the background sky is overestimated or underestimated the noise level will increase or decrease affecting the measure of the magnitude. The choice of aperture size in photometry is very important, since additional contributions from the neighbouring stars has to be avoided. The profile fitting technique has the ability to reduce noise and to deal with fainter stars than aperture photometry.

University of Cape Town

The work in this thesis therefore leads to a recommendation that the SDSU temperature needs to be tightly controlled to stabilize the bias level. It is also recommended that aperture photometry be perfomed with small aperture size of about $\sim$ 1.5 times the FMHW. For faint stars profile fitting technique is recommended for performing photometry whereas for bright stars aperture photometry is recommended.

University of Cape Town

Appendix A

Calculating the Readout Noise and the Gain of SALTICAM

University of Cape Town

Two consecutive bias frames were subtracted from each other to check for the spatial variations in the bias level due to the imperfection in the external electronics. The expectation would be that the two bias frames would experience the same variations, which would cancel when one frame was subtracted from the other. The standard deviation, σ, of the difference frame was obtained using the PIP software. To get the readout noise one divides the standard deviation by $\sqrt{2}$ (that is if $\sigma_A = \sigma_B$). The equation of the readout noise is given by Equation 2.8 in page 13. The readout noise must be given in electrons, we can only measure it in ADU.

$X1$	$Y1$	$X2$	$Y2$	Mean	Standard Deviation
10	8	110	108	0.01	3.56
194	156	294	256	0.01	3.57
390	386	490	486	0.03	3.57

Table A.1: The values of the coordinates of the points where we measured the mean and the standard deviation on the difference image.

The average of the standard deviation = 3.56, and the readout noise in ADU is

$$\sigma = \frac{3.56}{\sqrt{2}}$$
$$= 2.52\ ADU$$

To be able to express the readout noise in electrons we need to calculate the gain of the CCD, λ (defined in Equation 2.7 in page 9) given in electrons/ADU. We have to measure variance σ_z^2 as a function of the mean counts N. Several flat field frames were obtained with two at each signal level. Two frames obtained at the same signal level were subtracted from each other. The standard deviation at three different

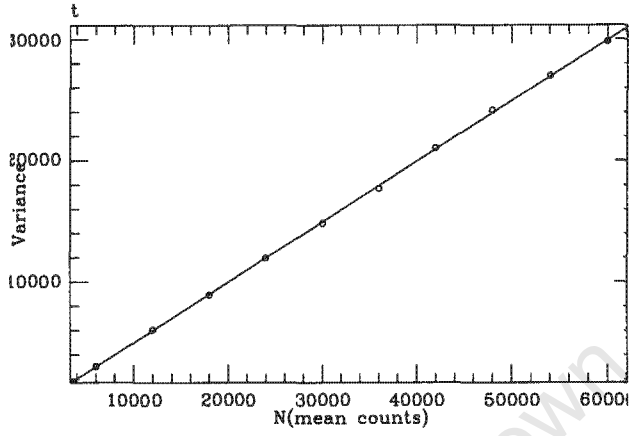

Figure A.1: The mean bias level is plotted against the variance. A first order polynomial is fitted to the data to obtain the slope of the curve.

points on each difference frame were measured. We calculated the average of the standard deviation and squared the average of the standard deviation of each image and divided by 2; by squaring the standard deviation we get the variance. We used the same coordinates as above, which led to the following output:

N (mean counts)	Variance
6000.3	3045.9
11999.59	6070.92
18000.92	8949.88
23999.86	11981.52
30001.98	14850.54
35999.18	17703.97
41998.65	21035.06
47999.55	24123.06
53999.97	26981.65
59998.14	29794.85

Table A.2: The values of the measured mean counts and the variance at those points on the difference image.

University of Cape Town

Coefficients	Values of Coeff.	Standard error
a_0	20.14	92.1
a_1	0.498	0.0025

Table A.3: The values of the coefficient of the polynomial fitted to the data plotted above in Figure A.1.

The equation of first order polynomial is $y = a_0 + a_1 x$, where a_0 is the x-intercept and a_1 is the slope of the curve. The values of the coefficients tabulated in table A.3 were obtained using the least-squared method (explained in Appendix B). Since, Equation 2.7 is the equation of a straight line, the slope will be the inverse of the gain, λ given by

$$slope = \frac{1}{\lambda},$$

substituting the value of the slope (a_1) one gets

$$\lambda = (0.498)^{-1} = 2.008$$

we can expressed the readout noise in electrons,

$$\begin{aligned} \sigma_{R_e} &= \lambda \sigma_{R_{adu}} \\ &= (2.008)(2.52) \\ &= 5.06 \; electrons \end{aligned}$$

University of Cape Town

Appendix B

The Least Squares Method

University of Cape Town

Least squares is a mathematical way of finding the best-fit curve to a set of data points (Bevington and Robinson 1992). This is done by minimizing the sum of the squares of the offsets of the points from the curve. The outlying points can have small effect on the fit. This fitting technique can be generalized from a best-fit line to a polynomial. Least squares proceeds by fitting the sum of the squares of the deviations R^2 of n set of data points. We have the equation of the

$$y_i = f(x_i) + \varepsilon_i,$$

where ε is the uncertainty associated with the measurement of y. Then

$$\varepsilon_i = y_i - f(x_i),$$

and

$$R^2 = \varepsilon_i^2 = \sum_{i=1}^{n} [y_i - f(x_i)]^2.$$

We have to minimize the sum of the squares of the deviations to get the best fit line. The condition of R^2 to be minimum is that

$$(R^2)' = 0$$

for a linear fit

$$f(x_i) = a + bx_i,$$

we have

$$\varepsilon_i^2 = \sum_{i=1}^{n} [y_i - (a + bx_i)]^2.$$

We differentiate with respect to the constant(a and b) to get

$$-2 \sum_{i=1}^{n} [y_i - (a + bx_i)] = 0$$

and

$$-2\sum_{i=1}^{n}[y_i-(a+bx_i)]x_i=0.$$

then we have two equations with two unknowns (the constants a and b). We get

$$na+b\sum_{i=1}^{n}x_i=\sum_{i=1}^{n}y_i$$

and

$$a\sum_{i=1}^{n}x_i+b\sum_{i=1}^{n}y_i=\sum_{i=1}^{n}y_ix_i,$$

and we can use the "matrix" to solve the two equations for the two unknowns. let

$$\sum_{i=1}^{n}=\sum$$

$$\begin{bmatrix} n & \sum x_i \\ \sum x_i & \sum x_i^2 \end{bmatrix}\begin{bmatrix} a \\ b \end{bmatrix}=\begin{bmatrix} \sum y_i \\ \sum y_ix_i \end{bmatrix}$$

so

$$\begin{bmatrix} a \\ b \end{bmatrix}=\begin{bmatrix} n & \sum x_i \\ \sum x_i & \sum x_i^2 \end{bmatrix}^{-1}\begin{bmatrix} \sum y_i \\ \sum y_ix_i \end{bmatrix}$$

then the 2×2 matrix inverse is given by

$$\begin{bmatrix} n & \sum x_i \\ \sum nx_i & \sum x_i^2 \end{bmatrix}^{-1}=\frac{1}{n\sum x_i^2-(\sum x_i)^2}\begin{bmatrix} \sum x_i^2 & -\sum x_i \\ -\sum x_i & n \end{bmatrix}$$

then after we have done some matrix algebra we get

$$\begin{bmatrix} a \\ b \end{bmatrix}=\frac{1}{n\sum x_i^2-(\sum x_i)^2}\begin{bmatrix} \sum x_i^2\sum_y-\sum x_i\sum x_iy_i \\ n\sum x_iy_i-\sum x_i\sum_y \end{bmatrix}$$

our constants will be given by the following

$$a=\frac{\sum x_i^2\sum_y-\sum x_i\sum x_iy_i}{n\sum x_i^2-(\sum x_i)^2},$$

but we know that $\overline{y}=\frac{1}{n}\sum y_i$ same for x then

$$a=\frac{\overline{y}(\sum x_i^2)-\overline{x}\sum x_iy_i}{\sum x_i^2-n(\overline{x}^2)}$$

$$b=\frac{n\sum x_iy_i-\sum x_i\sum_y}{n\sum x_i^2-(\sum x_i)^2}$$

$$=\frac{\sum x_iy_i-\overline{xy}}{\sum x_i^2-n(\overline{x}^2)},$$

University of Cape Town

we can rewrite them in a simpler form by defining the sums of the squares to be

$$S_{xx} = \sum (x_i - \overline{x})^2 = (\sum x_i^2) - n\overline{x}.$$

We will use the same notation for S_{yy}

$$S_{xy} = \sum (x_i - \overline{x})(y_i - \overline{y}) = (\sum x_i y_i) - n\overline{x}\overline{y}.$$

These can be written as

$$\sigma_x^2 = \frac{S_{xx}}{n}$$

$$\sigma_y^2 = \frac{S_{yy}}{n}$$

$$cov(x, y) = \sigma_{xy}^2 = \frac{S_{xy}}{n},$$

where $cov(x, y)$ is the covariance.Then

$$b = \frac{cov(x, y)}{\sigma_i^2},$$

and we can give a in terms of b

$$a = \overline{y} - b\overline{x}.$$

When it comes to fitting a polynomial to the data points

$$y_i = a_0 + a_1 x_i + a_2 x_i^2 + \ldots$$

we will have more than two constants to solve depending on the degree of our polynomial. Even the size of the matrix will change. The quality of the least squares fit is given by the correlation coefficient. That is defined by

$$r^2 = \frac{S_{xy}^2}{S_{xx} S_{yy}}.$$

University of Cape Town

Appendix C

Examples of Coordinates Transformation

University of Cape Town

The SALTICAM camera has a mosaic of two 2k×4k CCD chips to make 4k×4k, each CCD has two amplifiers that readout 1k×4k. The controller system can flip the readout order, or bin the pixels during the readout process and even select the region of interest. So in our first case we decided to bin using the 4×4 binning mode and flip the readout order, then get the coordinates. For the second case we decided to bin using the 4×4, flip the readout order and then choose the region of interest.

Case A

We choose amplifier A as the origin, the arrows shows the readout direction. All the coordinates y-axis does not change when we transform, the coordinate on the x-axis are the ones changing. We flip the readout order, and then we bin using the 4×4 binning mode.

```
Amplifier
    A              B                    C                    D
As = Cx       As = 2049 - Cx       As = Cx         As = 2049 - Cx
Ap = Cy       Ap = Cx              Ap = Cy         Ap = Cy
Il = Cx/4     Il = Cx/4 - 218.125  Il = Cx/4       Il = Cx/4 - 218.125
Ic = Cy/4     Ic = Cy/4            Ic = Cy/4       Ic = Cy/4
Dx = Cx       Dx = Cx              Dx = Cx + 2148  Dx = Cx + 2148
Dy = Cy       Dy = Cy              Dy = Cy         Dy = Cy
```

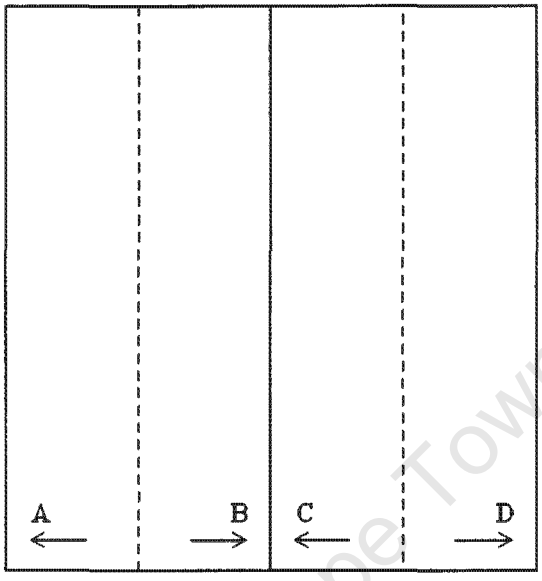

Figure C.1: Mosiac of 4k×4k with two 2k×4k CCDs, with each CCD having two amplifiers.

University of Cape Town

AMPLIFIER	A	B	C	D
CCDSEC	[1:1074,1:4102]	[1075:2148,1:4102]	[1:1074,1:4102]	[1075:2148,1:4102]
AMPSEC	[1:1074,1:4102]	[1074:1,1:4102]	[1:1074,1:4102]	[1074:1,1:4102]
DATASEC	[1:269,1:1026]	[51:319,1:1026]	[1:269,1:1026]	[51:319,1:1026]
DETSEC	[1:1074,1:4102]	[1075:2148,1:4102]	[2149:3222,1:4102]	[3223:4296,1:4102]
NSUM	4 4	4 4	4 4	4 4
LTM1_1	0.25	0.25	0.25	0.25
LTM2_2	0.25	0.25	0.25	0.25
LTV1	0.375	-218.125	0.375	-218.125
LTV2	0.375	0.375	0.375	0.375
ATM1_1	1	-1	1	-1
ATM2_2	1	1	1	1
ATV1	0	2148	0	2148
ATV2	0	0	0	0
DTM1_1	1	1	1	1
DTM2_2	1	1	1	1
DTV1	0	0	2148	2148
DTV2	0	0	0	0

Case B

We created a region of interest (ROI) with the binning of 4×4. The controller flips the readout order. The region of interest is given by 500 to 3800 by 1000 to 3000. There are 50 pixels of the overscan which are on the right of amplifiers B and D and on the left of amplifiers A and C . Amplifier A is still the origin and the arrows show the readout direction.

```
Amplifier
   A                    B                    C                    D
As = Cx              As = 2049 - Cx       As = Cx              As = 2049 - Cx
Ap = Cy              Ap = Cx              Ap = Cy              Ap = Cy
Il = Cx/4 - 124.375  Il = Cx/4 - 218.125  Il = Cx/4           Il = Cx/4 - 218.125
Ic = Cy/4-249.375    Ic = Cy/4-249.375    Ic = Cy/4-249.375    Ic = Cy/4-249.375
Dx = Cx              Dx = Cx              Dx = Cx + 2148       Dx = Cx + 2148
Dy = Cy              Dy = Cy              Dy = Cy              Dy = Cy
```

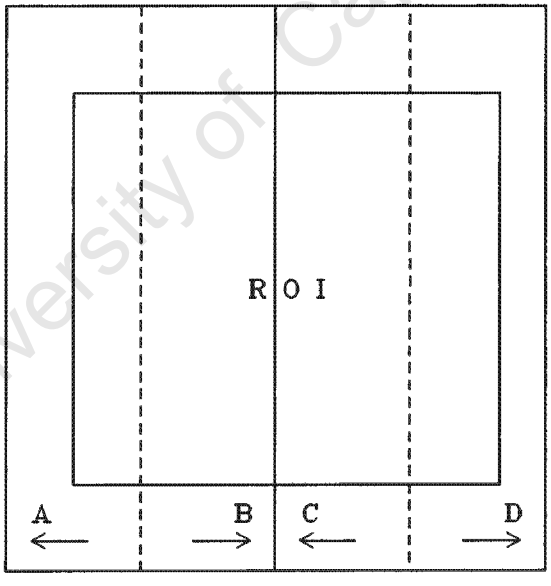

University of Cape Town

Figure C.2: A region of interest (ROI) is specified in the CCD.

AMPLIFIER	1	2	3	4
CCDSEC	[500:1074,1000:3000]	[1075:2148,1000:3000]	[1:1074,1000:3000]	[1075:1652,1000:3000]
AMPSEC	[500:1074,1000:3000]	[1074:1,1000:3000]	[1:1074,1000:3000]	[1074:496,1000:3000]
DATASEC	[1:144,1:500]	[51:319,1:500]	[1:269,1:500]	[51:195,1:500]
DETSEC	[500:1074,1000:3000]	[1075:2148,1000:3000]	[2149:3222,1000:3000]	[3223:4296,1000:3000]
NSUM	4 4	4 4	4 4	4 4
LTM1_1	0.25	0.25	0.25	0.25
LTM2_2	0.25	0.25	0.25	0.25
LTV1	-124.375	-218.125	0.375	-218.125
LTV2	-249.375	-249.375	-249.375	-249.375
ATM1_1	1	-1	1	-1
ATM2_2	1	1	1	1
ATV1	0	2148	0	2148
ATV2	0	0	0	0
DTM1_1	1	1	1	1
DTM2_2	1	1	1	1
DTV1	0	0	2148	2148
DTV2	0	0	0	0

University of Cape Town

Appendix D

Example of FITS Primary and Extension Data Header

University of Cape Town

```
Primary data header
................................................................
SIMPLE   =                    T / file does conform to FITS standard
BITPIX   =                   16 / number of bits per data pixel
NAXIS    =                    2 / number of data axes
NAXIS1   =                 4296 / length of data axis 1
NAXIS2   =                 4102 / length of data axis 2
EXTEND   =                    T / FITS dataset may contain extensions
COMMENT   FITS (Flexible Image Transport System) format is defined in 'Astronomy
COMMENT   and Astrophysics', volume 376, page 359; bibcode: 2001A&A...376...359H
OBJECT   = 'BIAS     '           / Object name
RA       = '00:00:00.00'         / RA of object
DEC      = '00:00:00.00'         / Dec of object
OBJEPOCH =                2000. / Epoch of object RA, Dec
EQUINOX  =                2000. / Equinox telescope pointing
DATE-OBS = '2004-08-25'          / Date of observation
UTC-OBS  = '06:11:19'            / UTC start of observation
TIME-OBS = '06:11:19'            / UTC start of observation
EXPTIME  =     1093414280.41454 / Exposure time
DETSIZE  = '[1:4296,1:4102]'    / Detector size
BSCALE   =    0.178937728937729 / Val=BSCALE*pix+BZERO
BZERO    =                5862. / Val=BSCALE*pix+BZERO
FILTER   = 'V        '           / Filter name
FILPOS   =                   1 / Filter position
NCCDS    =                   2 / Number of CCDs in detector
CCDSUM   = '1 1      '           / On chip summation
GAIN     =                1.36 / Nominal CCD gain
ROSPEED  = 'SLOW     '           / CCD readout speed
```

```
TELNORTH =                    0. / Direction of North
PROPMOT  =                    0. / Proper motion (arsec/yr)
POSANG   =                    0. / Position angle (degrees)
TELRA    = '09:09:09.99'         / RA of telescope
TELDEC   = '-09:09:09.99'        / Dec of telescope
TELEPOCH =                 2000. / Equinox of telescope RA, Dec
HA       = '09:09:09.99'         / HA of telescope
TELALT   =                   39. / Altitude of telescope
TELAZ    =                    9. / Azimuth of telescope
CCDTEM   =     149.389439105228 / CCD temperature (K)
DEWTEM   =     7.54029999999999 / Cold box temperature (C)
AMPTEM   =                 26.8 / SDSU controller temperature (C)
CENTEM   =     102.841561423651 / Cold end temperature (C)
DEWPRE   = 6.05708757093697E-10 / Dewar pressure
END

Image extension header
.....................................................
XTENSION = 'IMAGE  '             / IMAGE extension
BITPIX   =                   16 / number of bits per pixel
NAXIS    =                    2 / number of data axes
NAXIS1   =                 4296 / lenght of data pixel 1
NAXIS2   =                 4102 / lenght of data pixel 2
PCOUNTS  =                    0 / parameter per group
GCOUNTS  =                    1 / number of group
...
END
```

University of Cape Town

Appendix E

MatLab code for binning data

The objective was to write a code that could bin the data of the bias and temperature. The same code was modified and used to bin time.

```
function bin

load bistats21_fast.mat   % matrix called "bistats21"
load temp_fast.mat % matrix called "data"

time = bistats21_fast(:,1);
time_temp = temp_fast(:,1);
C = bistats21_fast(:,2);
time_bias = bistats21_fast(:,7);

T = temp_fast(:,5);   % temperatures in celcius
time_temp_bin = temp_fast(:,7);

t0 = 24.45;
t02 = 24.45;   % bin min for temp
delt = 0.25;
nbin = zeros(1,100);

% bias mean calculation
for i=1:length(C)
    j=floor((time(i)-t0)./delt)+1;
    nbin(j)=nbin(j)+1;
    Count(j,nbin(j))=C(i);
end

for i=1:length(time_bias)
```

University of Cape Town

```
    j=floor((time(i)-t0)./delt)+1;
    nbin(j)=nbin(j)+1;
    t_b(j,nbin(j))=time_bias(i);
end

Count;
t_b;
nbin
j=j

for k=1:j
   den = nbin(k)
   Cmean(k)= sum(Count(k,:))/den
end

for k=1:j
   den = nbin(k)
   t_bmean(k)= sum(t_b(k,:))/den
end

x=1:j;
cm = 2*Cmean
tbm = 2*t_bmean
Countsdata=[tbm',cm']
%plot(tbm,cm,'.')

% temp mean calculation

nbin = zeros(1,100);
for i=1:length(T)
    j = floor((time_temp(i)-t02)./delt)+1;
    nbin(j)=nbin(j)+1;
    Tbin(j,nbin(j))=T(i);
end

for i=1:length(time_temp_bin)
    j = floor((time_temp(i)-t02)./delt)+1;
    nbin(j)=nbin(j)+1;
    ttb(j,nbin(j))=time_temp_bin(i);
end

for k=1:j
```

University of Cape Town

```
   den = nbin(k);
   Tmean(k)= sum(Tbin(k,:))/den;
end

for k=1:j
   den = nbin(k);
   ttbmean(k)= sum(ttb(k,:))/den;
end

Tmean2 = Tmean(1:j)
ttbmean2 = ttbmean(1:j)
x=1:j;
tmean = 2*Tmean
ttbin =  2*ttbmean
Tempdata=[ttbin',tmean']
plot(ttbin,tmean,'.')
%plot(tmean,Cmean,'.')

%TB = [Tmean2',Cmean']
```

University of Cape Town

Appendix F

FORTRAN Code for calculating magnitude differences

University of Cape Town

Objective:
The objective was to write a code that could calculate the magnitude of the known intensities, relative magnitudes and magnitude differences between the known and aperture magnitudes.

Code:

```
      integer i, j, k, l, n
      parameter (k=7)
      real m32(k),m42(k),m52(k),m62(k),m72(k),s(k),delta12(k),
     &     delta32(k),delta42(k),delta52(k),delta62(k),delta72(k),
     &     diff12(k),diff32(k),diff42(k),diff52(k),diff62(k),
     &     diff72(k),m12(k),s1(k),s2(k),s3(k),s4(k), s5(k),s6(k),
     &     s7(k),s8(k),mstar1(k),mbright2(k),mstar3(k),mstar4(k),
     &     mstar5(k),mstar6(k)
c
      parameter (a=-0.263)
c
      open (unit=1, FILE="intensities.dat", STATUS="UNKNOWN")
      read(1,*)
      open (unit=2, FILE="mbright.dat", STATUS="UNKNOWN")
      write(2,*)
c
      do i=1,k
      read(1,*)s1(i),s2(i),s3(i),s4(i),s5(i),s6(i),s7(i),s8(i)
c
c
```

```
       mstar1(i)= -2.5 * log10(s2(i))
       mbright2(i)= -2.5 * log10(s3(i))
       mstar3(i)= -2.5 * log10(s4(i))
       mstar4(i)= -2.5 * log10(s5(i))
       mstar5(i)= -2.5 * log10(s6(i))
       mstar6(i)= -2.5 * log10(s7(i))
c       mstar7(i)= -2.5 * log10(s8(i))
c
       write(2,*) s1(i),mstar1(i),mbright2(i),mstar3(i),
     &      mstar4(i),mstar5(i),mstar6(i)
c
       enddo
c
       close(1)
c
       close(2)
c
*************************************************************************
*      Opening a file called ratio.dat. This file contains measured     *
*      intensities of stars 1 to 9. This intensities are measured       *
*      using IRAF/DAOPHOT.                                              *
*************************************************************************
c
       open (unit=1, file="intensities.dat", status="unknown")
c       read(1,*)
c
*************************************************************************
*      Creating a file that will write the output data(ratios) into     *
*************************************************************************
c
       open (unit=3, file="ratios.dat", status="unknown")
       write(3,*)
       write(3,"(6X,A)") 'The ratios of the stars from 1 - 9'
       write(3,"(6X,A)") '================================='
c      rewind(unit=1)
*************************************************************************
*      Read the file containing the intensities of the stars.           *
*************************************************************************
c
       do j=1,k
       read(1,*) s1(j),s2(j),s3(j),s4(j),s5(j),s6(j),s7(j),s8(j)
```

University of Cape Town

```
c
*************************************************************************
*      Then we have to calculate the log of the ratio's of the          *
*      intensities of each star with star 9. By the way star 9 is       *
*      the brightest star in the field.                                 *
*************************************************************************
c
       delta12(j)= -2.5 * log10(s2(j)/s3(j))
c       delta22(j)= -2.5 * log10(s3(j)/s3(j))
       delta32(j)= -2.5 * log10(s4(j)/s3(j))
       delta42(j)= -2.5 * log10(s5(j)/s3(j))
       delta52(j)= -2.5 * log10(s6(j)/s3(j))
       delta62(j)= -2.5 * log10(s7(j)/s3(j))
c       delta72(j)= -2.5 * log10(s8(j)/s3(j))
c
*************************************************************************
*      Printing the calculated ratio's and the value of the aperture    *
*      size into a file in UNIT=4.                                      *
*************************************************************************
c
       write(3,*) s1(j),delta12(j),delta32(j),delta42(j),
     &            delta52(j),delta62(j)
c
       enddo
c
       close(3)
c
c
*************************************************************************
*      Opening a file containing the intensities of star 1 - 8 and      *
*      the other file containing the magnitude of star 9.               *
*************************************************************************
c
       open (unit=3, file="ratios.dat", status="unknown")
       read(3,*)
       read(3,*)
       read(3,*)
c
       open (unit=2, file="mbright.dat", status="unknown")
       read(2,*)
c
       open (unit=4, file="relativemag.dat", status="unknown")
```

University of Cape Town

```
       write(4,*)
       write(4,"(6X,A)") 'The magnitudes of the stars relative to star9'
       write(4,"(6X,A)") '++++++++++++++++++++++++++++++++++++++++++++++'
c
*****************************************************************************
*      Calculating the relative magnitudes of the stars relative to         *
*      the brightest star, star9.                                           *
*****************************************************************************
c
       do l=1,k
          read(3,*) s(l),delta12(l),delta32(l),delta42(l),
     &         delta52(l),delta62(l)
          read(2,*) s1(l),mstar1(l),mbright2(l),mstar3(l),
     &      mstar4(l),mstar5(l),mstar6(l)
c
          m12(l)= mbright2(l) + delta12(l)
c          m22(l)= mbright9(l) + delta29(l)
          m32(l)= mbright2(l) + delta32(l)
          m42(l)= mbright2(l) + delta42(l)
          m52(l)= mbright2(l) + delta52(l)
          m62(l)= mbright2(l) + delta62(l)
c
          write(4,*) s(l),m12(l),m32(l),m42(l),m52(l),m62(l)

c
       enddo
c
       close(2)
c
       close(3)
c
       close(4)

*****************************************************************************
*     Calculating the magnitude difference (between the brightest star      *
*     and the other stars), the output should be the same as the            *
*     output in the file called "ratios.dat". This makes the output         *
*     in the file called "relativemag.dat" to be the same as the            *
*     output in the mbright to be the same.                                 *
*****************************************************************************
c
       open (unit=4, file="relativemag.dat", status="unknown")
```

University of Cape Town

```
      read(4,*)
      read(4,*)
      read(4,*)
c
      open (unit=2, file="mbright.dat", status="unknown")
c
      open (unit=5, file="differences.dat", status="unknown")
      write(5,*)
      write(5,"(6X,A)") 'The difference of star 9 and the other stars'
      write(5,"(6X,A)") '++++++++++++++++++++++++++++++++++++++++++++'
c
      do n=1,k
         read(2,*)s1(i),mstar1(n),mbright2(n),mstar3(n),
     &      mstar4(n),mstar5(n),mstar6(n)
c
         read(4,*)s(n),m12(n),m32(n),m42(n),m52(n),
     &         m62(n)
c
         diff12(n) = -mbright2(n) + m12(n)
c         diff29(n) = -mbright9(n) + m29(n)
         diff32(n) = -mbright2(n) + m32(n)
         diff42(n) = -mbright2(n) + m42(n)
         diff52(n) = -mbright2(n) + m52(n)
         diff62(n) = -mbright2(n) + m62(n)
c
         write(5,*) s(n), diff12(n),diff32(n),diff42(n),diff52(n),
     &         diff62(n)
c
      enddo
c
      close(2)
c
      close(4)
c
      close(5)
c
      end
```

University of Cape Town

Bibliography

[1] Bevington R. Philip and Robinson D. Keith; Data Reduction and Error Analysis for the Physical Sciences; *The Textbook*; Mass. McGraw-Hill, Boston, 1992

[2] Buonanna R. and Iannicola G.; Stellar Photometry with Big Pixels; PASP **101**, (1989) 294–301

[3] Chromey F. R. and Hasselbracher D. A.; The Flat Sky: Calibration and Background Uniformity in Wide-Field Astronomical Images; PASP **108**, (1996) 949–994

[4] Corlan R.; http://astro.corlan.net/gcx/html/node7.html, 2004

[5] Davenhall A. C., Privett G. J., Taylor M. B.; The 2-D CCD Data Reduction Cookbook; SL; 1999

[6] Davis L. E.; A Reference Guide to the IRAF/DAOPHOT Package; National Optics Astronomy Observatory, 1994

[7] Dolphin A. E.; WFPC2 Stellar Photometry with HSTphot; PASP **112**, (2000) 1383–1396

[8] Gudehus D. H. and Hegyi D. J.; The Design And Construction of a Charge-Coupled Device Imaging System; The Astronomical Journal, Vol. **90**, number 1, (1985) 130–137

[9] Hanisch R. J., Farris A., Greisen E. W., Pence W. D., Schlesinger B. M., Teuben P. J., Thompson R. W., Warnock III A.; Definition of the Flexible Image Transport System (FITS); A&A **376**, (2001) 359–380

[10] Howell S. B.; Handbook of CCD Astronomy; *The Textbook*; Cambridge University Press, 2000

[11] Howell S. B.; Two-Dimensional Aperture Photometry: Signal-To-Noise of Point Source Observations and Optimal Data-Extraction Techniques; PASP**101**, (1989) 616–622

University of Cape Town

[12] Mackay C. D.; Charge-Coupled Devices in Astronomy; Ann. Rev. A&A **24**, (1986) 255–283

[13] McLean I. S.; Electronic and Computer Aided Astronomy: from eye to electronic sensors; *The Textbook*; Ellis Horwood of Space Science and Technology Series in Astronomy., John wiley & Sons, Chichester, 1989

[14] Moffat A. F. J.; A Theoretical Investigation of Focal Stellar Images in the Photographic Emulsion and Application to Photographic Photometry; A&A **3**, (1969) 455–461

[15] Napiwotzki R., Schönberner D., and Wenske V.; On the determination of effective temperature and surface gravity of B, A, and F stars using Strömgren *uvbyβ* photometry; A&A **268**, (1993) 653–666

[16] Naylor T.; An Optimal Extraction Algorithm for Imaging Photometry; Mon. Not. R. Astron. Soc. **296**, (1998) 339–346

[17] Newberry M. V.; Signal-To-Noise consideration for sky-subtracted CCD data; PASP**103**, (1991) 122–130

[18] O'Donoghue D.; SALTICAM: The Southern African Large Telescope Imaging Camera, Version 2.0, 2000

[19] O'Donoghue D., Bauermeister E., Carter D. B., Evans G. P., Koorts W. P., O'Connor J., Osman F., van der Merwe S., Bigelow B. C.;
SALTICAM: A $0.5M Acquisition Camera: Every Big Telescope Should Have One, in Instrument Design and Performance for Optical/Infrared Ground-based Telescopes; Masanori Iye, Alan F. M. Moorwood editors; Proc. SPIE **4841**, (2003) 465–476

[20] Penny A. J. and Dickens R. J.; CCD Photometry of the globular cluster NGC 6752; Mon. Not. R. astr. Soc. **220**, (1986) 845–867

[21] Penny A.J. and Leese R.; Stellar Photometry with CCD Sub-Pixel Sensitivity Variation; ASP Conf. Series, George H. Jacoby and Jeannette Barnes, eds; Vol.**101**, (1986) 29–32

[22] Ponz J. D., Thompson R. W. and Muñoz J. R.; The FITS image extension; A&AS **105**, (1994) 53–55

[23] Schechter P. L., Mateo M. and Saha A.; DoPhot, A CCD Photometry Program: Description and Tests; PASP **195**, (1993) 1342–1353

[24] Sterken C. and Manfroid J.; Astronomical Photometry: A Guide; *The Textbook* Kluwer Academics Publishers, Dordrecht/ Boston/ London, 1992

University of Cape Town

[25] Stetson P.; DAOPHOT: A Computer Program for Crowded-Field Stellar Photometry; PASP **99**, (1987) 191–222

[26] Strömgren B.; Problems of Internal Constitution and Kinematics of Main Sequence Stars; QJRAS **4**, (1963) 8–37

[27] Suchkov A. and Casertano S.; Aperture Corrections for WFPC2 Stellar Photometry; HST Calibration Workshop; 1997

[28] Taylor R. John; An Introduction to Error analysis: The Study of Uncertainties in Physical Science; *The Textbook*, Second Edition; University Science Books, 1997

[29] Valdes F.; NOAO Image Data Structure Definitions; http://iraf.noao.edu/projects/ccdmosaic/imagedef/imagedef.html; 2000

[30] Wells D. C., Greisen E. W. and Harten R. H.; FITS : A Flexible Image Transport System; A&AS **44**, (1981) 363–370

University of Cape Town